12-19-2013

Sickle Cell Disease Erythrocyte Stiffness and Cytoadhesion Investigated via Atomic Force Microscopy

Jamie L. Maciaszek
University of Connecticut - Storrs, jamie.maciaszek@gmail.com

Sickle Cell Disease Erythrocyte Stiffness and Cytoadhesion Investigated via Atomic Force Microscopy

Jamie Lynn Maciaszek, PhD

University of Connecticut, 2013

The biomechanical properties of red blood cells (RBCs), including increased stiffness and abnormal cytoadherence, are integral components in the cascade of events resulting to vasoocclusive episodes (VOEs) in sickle cell disease (SCD). VOEs are the main cause of morbidity in SCD and sickle cell trait (SCT). Using experimental techniques based on atomic force microscopy (AFM), we studied the stiffness and adhesion of RBCs from SCD patients and from subjects with SCT. We found that SCD and SCT RBCs are three-fold stiffer than normal RBCs. Further, a ten-fold increase in the stiffness of sickled RBCs was measured upon deoxygenation. In an effort to rectify the increased stiffness of sickle RBCs, mice were fed a diet supplemented with docosahexanoic acid (DHA), an omega-3 fatty acid. A decrease in RBC stiffness was measured suggesting therapeutic benefits of DHA. Cytoadherence of RBCs to subendothelial laminin via the basal cell adhesion molecule/Lutheran (BCAM/Lu) is implicated in vasculopathy, a common condition in SCD patients. We established the *in vitro* technique of single-molecule force spectroscopy (SMFS) which enables detection of single BCAM/Lu proteins on the RBC surface via measurement of the unbinding force with laminin. It was shown that epinephrine, acting through the cyclic adenosine monophosphate (cAMP) signaling pathway, increases the population of active BCAM/Lu receptors on SCT RBCs, suggesting a role in exercise-induced VOEs. The sensitivity of the SMFS system was validated in a neuronal system to quantitatively map SK channels and then employed to investigate the effects of cAMP pathway targeting on BCAM/Lu receptor expression on normal and SCD RBCs. We illustrated

that A-kinase anchoring proteins are crucial for BCAM/Lu receptor activation. To examine the relevance of results based on SMFS in the cytoadhesion of entire RBCs, single-cell force spectroscopy (SCFS) was established to measure the adhesion of whole cells with a functionalized substrate. We established a correspondence between the SMFS and SCFS results. Both techniques were able to detect significant changes in the adhesive response of RBCs to cAMP pathway modulation and variability was measured amongst human subjects, suggesting that RBCs maintain diverse intracellular levels of tonic protein kinase A.

Sickle Cell Disease Erythrocyte Stiffness and Cytoadhesion Investigated via Atomic Force Microscopy

Jamie Lynn Maciaszek

B.S., Lehigh University, 2009

M.S., University of Connecticut, 2012

A Dissertation

Submitted in Partial Fulfillment of the

Requirements for the Degree of

Doctor of Philosophy

at the

University of Connecticut

2013

APPROVAL PAGE

Doctor of Philosophy Dissertation

Sickle Cell Disease Erythrocyte Stiffness and Cytoadhesion Investigated via Atomic Force Microscopy

Presented by

Jamie Lynn Maciaszek, B.S., M.S.

Major Advisor _____
George Lykotrafitis

Associate Advisor _____
Anastasios V. Tzingounis

Associate Advisor _____
Biree Andemariam

Associate Advisor _____
Tai-Hsi Fan

Associate Advisor _____
Wei Sun

University of Connecticut

2013

Acknowledgment

It is amazing how quickly the past four and a half years have flown by, years filled with some of my greatest memories as well as some of the toughest challenges. The completion of my doctoral degree has been an extremely enriching experience, both personally and professionally. All of this would not have been possible without the guidance and help of several individuals who contributed and extended their valuable assistance in the completion of this research, and more importantly have provided me support throughout these years.

First and foremost, it is with immense gratitude that I acknowledge the invaluable support and mentorship of my Major Advisor, Dr. George Lykotrafitis. I am sincerely appreciative of his unparalleled guidance and unwavering belief in me and in my growth as a researcher over the past four years.

I would like to thank Dr. Biree Andemariam at the University of Connecticut Health Center for providing me with her expertise on sickle cell disease. I am very grateful to Dr. Anastasios Tzingounis for his expertise on pathway signaling and valuable perspective on my experimental results. I would also like to thank my associate advisors Dr. Wei Sun and Dr. Tai-Hsi Fan for their mentorship and support on my fellowship applications and dissertation studies. Thank you to my fellow Cell Mechanics Lab members for their support, assistance, and always being there to listen. I would also like to appreciatively acknowledge the Departments of Biomedical Engineering and Mechanical Engineering for their continued support of my research. I am also very grateful for the financial support of the American Heart Association Founder's Affiliate Predoctoral Fellowship (11PRE7280009).

Thanks are due to many others, particularly Drs. Nancy Wandersee and Madelyn Hanson of the Blood Center of Wisconsin for collaborating with us on the murine erythrocyte stiffness project. I have greatly learned from their knowledge of sickle cell disease and experimental planning

which will certainly benefit me in my career. In addition, I would like to thank Harriet Zawistowski of the Clinical Research Center at the University of Connecticut Health Center who took the time recruit and enroll subjects for the study. I would also like to thank Dr. William Zempsky and James Santanelli at Connecticut Children's Medical Center for providing me with blood samples to fulfill my American Heart Association predoctoral fellowship study.

Last but certainly not least, I would like to thank my family and friends, who have provided me with encouragement, support, and an infinite amount of necessary laughter. I am blessed to have such wonderful friends in my life, and would like to especially thank my BFFs – Rachel, Shana, Gina, and Jill – for countless phone calls, text messages, and keeping me grounded. **Most importantly**, to my mom, dad, and brother: I am forever grateful for your unwavering support and commitment to my accomplishments. Thank you for your unconditional love through the many challenges that I have encountered. This journey would not have been possible without you. I love you.

Table of Contents

List of Figures

List of Tables

Chapter 1. Introduction

1.1. Sickle cell disease

Sickle cell disease (SCD) is a multisystem disease characterized by extreme pain and episodes of acute illness resulting from microvascular infarction [1-3]. The genotype for homozygous SCD results in early mortality and high morbidity, while the heterozygous sickle cell trait (SCT) occasionally can be associated with collapse and sudden death during physical exertion [1-4]. SCD occurs in over 100,000 individuals in the United States [4] and over 3 million individuals worldwide [5-6]. Over 70% of sufferers live in Africa, where little is known about the disease [1, 4, 7-8]. The number of SCD cases is expected to increase about 30% by 2050, making it a significant global health issue [5]. SCT occurs in approximately 300 million people worldwide, with the highest prevalence of approximately 30% to 40% in sub-Saharan Africa where it offers protection against severe malaria [9]. Recurrent vasoocclusive episodes (VOEs) and inflammation result in progressive damage to most organs, including the brain, kidneys, lungs, bones, and cardiovascular system, which becomes apparent with increasing age [1]. One of the main problems of SCD in children is the increased occurrence of stroke [10-12], with overt stroke estimated to occur in 11% of individuals under the age of 20, often resulting in permanent neurological and cognitive impairment [11-19]. Silent cerebral infarcts, a relatively newly recognized complication of SCD, occur in 22% of neurologically asymptomatic children and correlate with neurophysiologic dysfunction and predisposition of overt stroke [12, 19-27].

SCD is an inherited blood disorder caused by a single point mutation in one of the genes encoding hemoglobin [28-34]. Hemoglobin (Hb) is formed by four polypeptide chains, two of type α and two of type β. In abnormal sickle hemoglobin (HbS), the normal sequence of *Val-His-Leu-Thr-Pro-Glu-Glu-Lys* is changed to *Val-His-Leu-Thr-Pro-Val-Glu-Lys*, with the amino acid valine substituting for glutamic acid at the β6 site. The replacement of two charged groups with

two hydrophobic groups leads to polymerization of deoxygenated Hb and to the formation of long stiff rodlike fibers [33, 35-36], which force RBCs to assume a wide variety of irregular shapes [37]. Other factors such as lowered pH, RBC dehydration and hyperthermia are also known to prompt sickling [38]. The genetics and underlying biophysics of the disease related to HbS have been extensively studied [1, 33, 35, 37, 39-42], however little remains known about the onset and progression of VOEs, specifically cell-cell interactions and blood cell adhesion events which are thought to be an integral component of VOEs. Therefore, clinical management of SCD is still basic and, although some evidence lends support to the use of blood transfusion and hydroxyurea in some circumstances, no drugs have been developed that specifically target the pathophysiology of the disease.

SCT is marked by the presence of both HbS and HbA [43]. HbS comprises approximately 20-46% of the total hemoglobin content in RBCs from persons with SCT [44], with most individuals having 40-42% [45]. SCT has a very significant social impact because approximately it occurs in approximately 300 million people worldwide and three million people in the United States, making it 40 to 50 times more prevalent than SCD [46]. In comparison to the homozygous SCD, the heterozygous SCT is traditionally regarded as a benign condition [28, 47-48]. During strenuous exercise, individuals can develop a syndrome resembling SCD with VOEs resulting from changes in the RBC morphology, viscoelasticity, and adhesion [38, 49-54]. These VOEs can lead to organ damage and ischemic pain, and are occasionally associated with significant morbidity and mortality, specifically in the case of physical training [55]. VOEs can also develop in other extreme conditions such as hypoxia, acidosis, dehydration, hyperosmolarity, or elevated erythrocyte 2,3-diphosphoglycerate (DPG) [46, 49-50, 56]. SCT is exclusively associated with rare but often fatal renal medullary cancer. Other complications associated with SCT include increased urinary tract infections in women, gross hematuria, complications of hyphema, splenic

infarction with altitude hypoxia or exercise, and life-threatening complications of exercise, exertional heat illness (exertional rhabdomyolysis, heat stroke, or renal failure) or idiopathic sudden death [46, 53, 57].

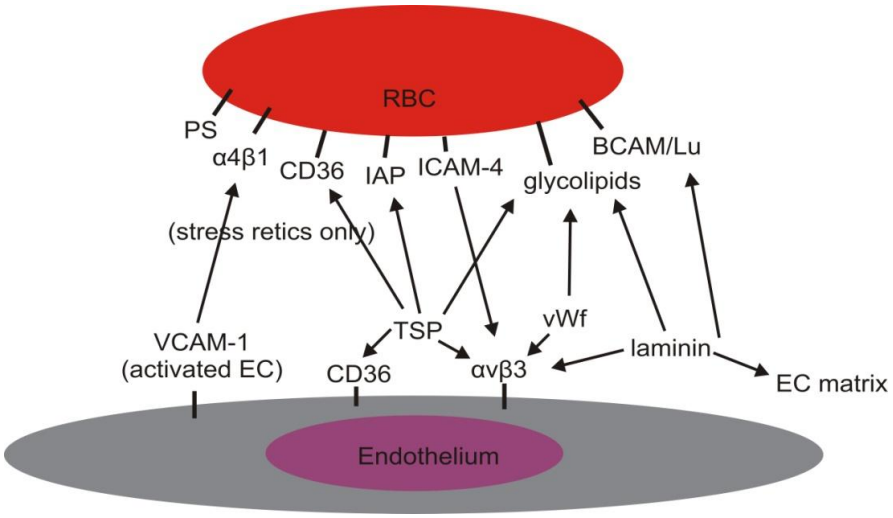

Figure 1.1.1. Human red blood cell surface adhesion receptors. These receptors mediate adhesion on healthy and pathological RBCs.

Healthy RBCs have a diameter of approximately 8-10 μm and a height of 2.5 μm. They are very deformable and have the ability to deform to diameters as small as 1-3 μm to traverse narrow capillaries and blood vessels during their approximately three-month life cycle [58]. Healthy erythrocytes contain only soluble adult hemoglobin (HbA), a globular protein totaling 25-30% of the cell, which transports oxygen from the lungs to tissues [33, 59]. These cells have a characteristic biconcave shape which increases the surface area to facilitate the diffusion of O_2 and CO_2 into and out of the cell [59-60]. This biconcave morphology is also associated with the high compliance of the erythrocytes [61]. Although RBCs are generally considered to be relatively inactive due to their lack of a nucleus and organelles, they express several surface adhesion receptors (Figure 1.1.1) which modulate cellular physiology and function [62]. Many of these receptors mediate cell-cell interactions, or adhesion, on both healthy and pathological

RBCs. Membrane proteins known to be involved in mediating the interaction between RBCs and the endothelium include: basal cell adhesion molecule and its isoform Lutheran (BCAM/Lu), a high-affinity laminin receptor; ICAM-4 (LW glycoprotein), a receptor for a number of integrins; CD47, a thrombospondin (TSP) receptor, as shown in Figure 1.1.2 [63].

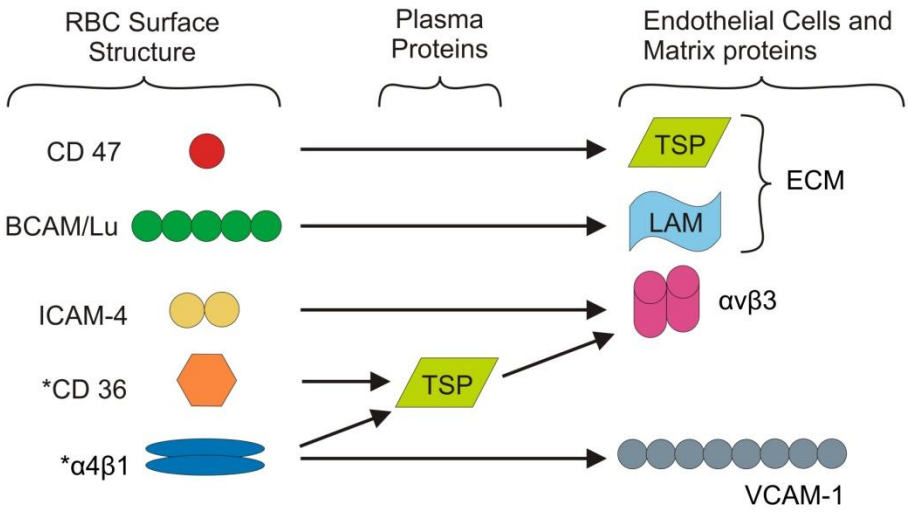

Figure 1.1.2. Red blood cell surface adhesion receptors for endothelial ligands.

A cascade of events results in the onset and progression of painful VOEs, the hallmark of SCD, which result from the blockage of small vessels in many different organs [31, 64-67]. The development of vascular obstruction in SCD is complicated and likely involves many different abnormalities of both circulating blood and the blood vessel wall (Figure 1.1.3). Endothelial cell activation, cytoadherence, inflammation, and coagulation activation contribute to blood flow obstruction and play a critical role in the pathophysiology of VOEs [64, 66, 68]. The pathogenesis of complications in SCD begins with loss of RBC deformability and increased cytoadherence of the RBCs. Loss of deformability and increased RBC rigidity occurs because Hb fibers form noncovalent cross-links and create a gel. This gives RBCs their irregular shapes and also alters their viscoelastic behavior and increases their cytoadherence [36, 69-70]. The

abnormal morphologic, adhesive, and elastic properties of sickle RBCs then causes obstruction of the microvasculature which ultimately results in stroke, VOEs, and organ damage. Importantly, cytoadherence of RBCs to the vascular endothelium and subendothelial matrix is thought to be a major contributor to and possibly the primary cause of vasculopathy in SCD [12, 64, 71].

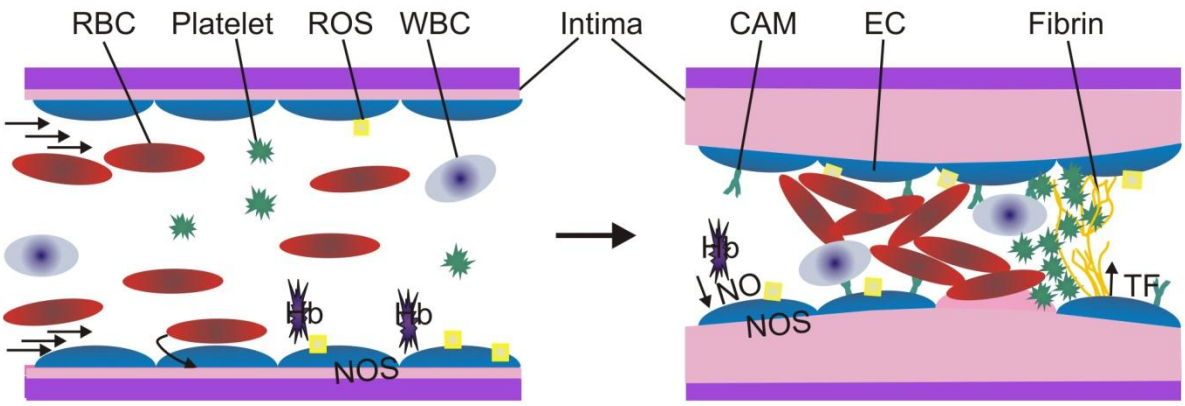

Figure 1.1.3. Vasculopathy of sickle cell disease. The combination of abnormal cytoadherence of the sickle RBC, the over-activity of the blood clotting system, and vessel wall damage contribute importantly to blood vessel occlusion and crises in SCD. There are many other factors involved in SCD vasculopathy including: sickle RBC adhesion, abnormal shear, increased inflammation, oxidative endothelial cell damage (ROS), an increase in serum free Hb, dysregulation of the nitric oxide pathway (NO/NOS), increases in cell adhesion molecule (CAM) and tissue factor (TF) expression, loss of vasoregulation, intimal hyperplasia, platelet and leukocyte adhesion, propagation of fibrin clot, and entrapment of rigid sickle RBCs.

On healthy and pathological RBCs, the activation of adhesion receptors can be modulated by hormones such as epinephrine [30, 72], pharmaceutical drugs such as hydroxyurea [73], and other biochemical stimuli. Hydroxyurea (HU) is currently the only pharmacologic treatment to reduce the frequency of VOEs, yet only two-thirds of patients respond favorably to the drug [74]. Hydroxyurea stimulates an increase in fetal hemoglobin (HbF) [75-76], however clinical improvement following HU treatment has been observed prior to measureable increases in HbF,

suggesting the critical role of other mechanisms such as altered RBC signaling [73, 77-78].

Quantitative understanding of RBC cytoadherence mediated by the second messenger cyclic adenosine monophosphate (cAMP) is necessary to fully elucidate the mechanism of RBC adhesion and signaling, and to guide advances in SCD pharmacotherapy. The current work will focus in part on subcellular targeting of the cAMP-dependent protein kinase A (PKA), a tetrameric holoenzyme consisting of two catalytic and two regulatory subunits [79]. Because SCD patients have extensive endothelial damage [80] and elevated plasma levels of laminin [81], RBC adhesion studies have focused on the specific interaction between BCAM/Lu and the α5 chain of laminin (LAMA5), a component of the subendothelial matrix [82-83]. Importantly, by using a flow adhesion assay, Hines et al [72] previously demonstrated that the interaction between BCAM/Lu and laminin is mediated by cAMP, an upstream effector of the PKA pathway [84]. In RBCs, stimulation of the β2-adrenergic receptor (β2-AR) [85-86] activates the G-protein coupled receptor Gαs, which stimulates adenylyl cyclase (AC) [87]. AC then catalyzes the conversion of adenosine triphosphate (ATP) to cAMP, which results in PKA activation and resultant BCAM/Lu-laminin adhesion (Figure 1.1.4). It was previously reported that levels of cAMP are significantly higher in sickle RBCs than RBCs from healthy subjects [72-73]. Contrary to the established mechanism of the PKA pathway, studies have also shown that healthy RBCs have little response to stimulation by epinephrine or forskolin [72]. Further, it is currently unknown if scaffold or anchoring proteins, such as A-kinase anchoring proteins (AKAPs), which compartmentalize PKA [88], play a role in BCAM/Lu receptor activation. Subsequent chapters of this work will investigated these subcellular targets and their specific effects on the population of active BCAM/Lu receptors. In addition, we will investigate the effect of epinephrine on the population of active BCAM/Lu and ICAM-4 receptors on normal and SCT erythrocytes.

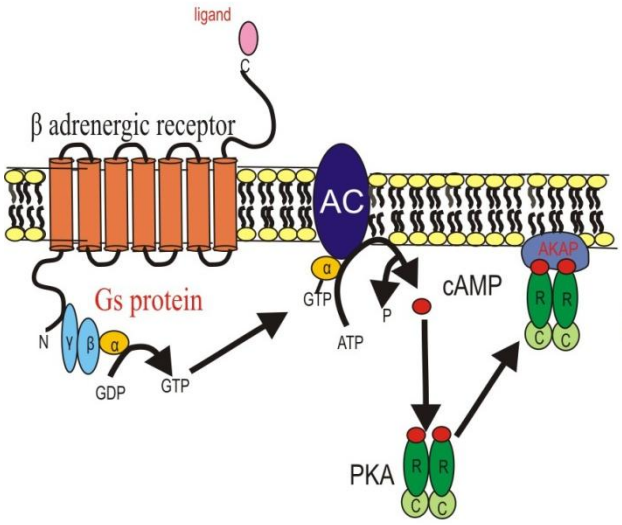

Figure 1.1.4. Beta adrenergic pathway. The beta adrenergic pathway is a cAMP-dependent signaling pathway which modulates the activation of adhesion receptors on human RBCs.

1.2. Objectives

The objectives for subsequent chapters are outlined below.

Chapter 2. Atomic Force Microscopy

Atomic force microscopy (AFM) is appropriate for measuring the biomechanical and adhesive properties of living cells due to its high force sensitivity and its ability to measure local and overall properties of individual cells under physiological conditions. This chapter aims to describe the principles of AFM with respect to biological applications.

Chapter 3. Microelasticity of Red Blood Cells in Sickle Cell Disease

A systematic force-displacement curve analysis is reported on the quantification of material stiffness via AFM using two theoretical models derived from the Hertz model. We determined the model for a four-sided pyramidal indenter to be the best fit for our application as compared to the model for a parabolic indenter. This analysis was applied to red blood cells from patients

with sickle cell disease to determine the Young's modulus of these cells in the oxygenated and deoxygenated state. Our findings conclude that deoxygenation and therapeutic treatment have a significant impact on the stiffness. This analysis presents a new approach to addressing medical disorders.

Chapter 4. Sickle Cell Trait Human Erythrocytes Show a Significant Increase in their Stiffness Compared to Erythrocytes from Healthy Individuals

The force-displacement curve analysis established in Chapter 3 was employed to measure the stiffness of abnormal human RBCs from patients with the genotype for SCT. The determined Young's modulus was compared with measurements of erythrocytes from healthy subjects. The results showed that the Young's modulus of SCT erythrocytes was approximately three times higher than in normal cells. Observed differences indicate the effect of the polymerization of hemoglobin S as well as possible changes in the organization of the cell cytoskeleton associated with the sickle cell trait.

Chapter 5. Dietary Supplementation with Docosohexanoic Acid (DHA) Increases Red Blood Cell Membrane Flexibility in Mice with Sickle Cell Disease

In an effort to rectify the increased stiffness of sickle RBCs determined in Chapter 3, mice were fed a diet supplemented with docosahexanoic acid (DHA), an omega-3 fatty acid, and measurements were recorded via AFM. Murine RBCs were examined for: 1) stiffness, as measured by AFM using the force-displacement curve analysis established in Chapter 3; 2) deformability, as measured by ektacytometry; and 3) percent irreversibly sickled RBCs on peripheral blood smears. Using AFM, stiffness is increased and deformability decreased in RBCs from SS mice fed CTRL diet compared to wild-type mice. In contrast, RBCs from SS mice fed DHA diet had markedly decreased stiffness and increased deformability compared to RBCs from SS mice fed CTRL diet. Furthermore, examination of peripheral blood smears revealed

less irreversibly sickled RBCs in SS mice fed DHA diet as compared to CTRL diet. In summary, our findings indicate that DHA supplementation improves RBC flexibility and reduces irreversibly sickled cells in SS mice. These results point to potential therapeutic benefits of dietary omega-3 fatty acids in SCD. changes

Chapter 6. Epinephrine Modulates BCAM/Lu and ICAM-4 Expression on the Sickle Cell Trait Red Blood Cell Membrane

The *in vitro* technique of single-molecule force spectroscopy was established using RBCs from subjects with SCT. We report that epinephrine, a hormone secreted under stress and strenuous exercise, increases both the frequency and strength of adhesion events between BCAM/Lu and subendothelial laminin, and between ICAM-4 and endothelial integrin $\alpha_v\beta_3$, compared to non-stimulated SCT erythrocytes. Increases in adhesion frequency present significant evidence of the role of epinephrine in BCAM/Lu-laminin and ICAM-4-$\alpha_v\beta_3$ bonding, and suggest mechanisms of vaso-occlusion during physical exertion in SCT.

Chapter 7. Topography of Native SK Channels Revealed by Force Nanoscopy in Living Neurons

As a proof of principle, we demonstrate that integration of pharmacology with single molecule AFM allows for the high-resolution mapping of native potassium channels in living neurons. By linking apamin, a toxin that specifically binds to SK channels, to the tip of an AFM cantilever, we are able to detect binding events between the apamin and SK channels. We find that native SK channels from rat hippocampal neurons reside primarily in dendrites as single entities and in pairs. To establish the sensitivity of the assay, we also show that SK channel dendritic distribution is dynamic and under the control of protein kinase A.

Chapter 8. AKAP-Dependent Modulation of BCAM/Lu Adhesion on Normal and Sickle Cell Disease RBCs Revealed by Force Nanoscopy

SMFS was employed to investigate the effects of subcellular cAMP pathway targeting on BCAM/Lu receptor expression on normal and SCD RBCs. Human normal and sickle RBCs adhere with high affinity to laminin via the BCAM/Lu receptor which is implicated in VOEs in SCD and activated through the cAMP signaling pathway. We measured the unbinding force between BCAM/Lu on the RBC and laminin attached to the AFM probe. We showed that the expression of active BCAM/Lu receptors is higher in homozygous sickle RBCs (SS-RBCs) than normal RBCs and that it is critically dependent on the cAMP signaling pathway on both normal and SS-RBCs. Importantly, we illustrated that A-kinase anchoring proteins (AKAPs) are crucial for BCAM/Lu receptor activation. Furthermore, we found that SS-RBCs from hydroxyurea-treated patients show a lower expression of active BCAM/Lu receptors, a lower unbinding force to laminin, and insignificant stimulation by epinephrine as compared to SS-RBCs from untreated patients. These findings may lead to novel anti-adhesive targets for VOEs in SCD.

Chapter 9. Single-Cell Force Spectroscopy as a Technique to Quantify Human Red Blood Cell Adhesion to Subendothelial Laminin

To examine the relevance of results based on SMFS in the cytoadhesion of entire RBCs, single-cell force spectroscopy (SCFS) was established to measure the adhesion of whole cells with a functionalized substrate. Adhesion forces were recorded as RBCs attached to AFM cantilevers were pulled-off of substrates coated with laminin protein. We established a correspondence between the SMFS and SCFS results. In particular, it was found that elevated overall cell adhesion measured via SCFS coincided with a rise in the resultant total force measured on 1 μm^2 areas of the RBC membrane at baseline via SMFS. Both techniques were able to detect significant changes in the adhesive response of RBCs to cAMP pathway modulation and variability was measured amongst human subjects, suggesting that RBCs maintain diverse

intracellular levels of tonic protein kinase A. By using single-cell measurements, we established a powerful new method for the quantitative measurement of the adhesion of single RBCs with specific receptor-mediated binding.

1.3. Rationale

Multiple biological processes contribute to the pathogenesis of vasculopathy in SCD including red cell sickling, inflammation and adhesion biology, coagulation activation, stasis, deficient bioavailability and excessive consumption of NO, excessive oxidation, and reperfusion injury physiology. The biomechanical properties of RBCs, including increased stiffness and abnormal cytoadherence, are integral components in the cascade of events resulting to vasculopathy in SCD and SCT [1, 9, 28]. The hemoglobin biophysics and genetics underlying the disease have been extensively studied, however despite substantial evidence underlining the importance of RBC stiffness and hetero-cellular interactions in the onset and progression of VOEs, the exact mechanism is not known. Thus, clinical management of SCD is still basic and although some evidence supports the use of blood transfusion therapy and hydroxyurea to reduce the frequency of VOEs, no drugs have been developed that specifically target the pathophysiology of the disease. ***Therefore, substantial work must be performed to better understand RBC biophysics in SCD, namely stiffness and adhesion, in an effort to develop better therapeutic methods for the prevention and treatment of VOEs.***

Human normal and sickle RBCs adhere with high affinity to laminin via the BCAM/Lu receptor which is activated through the cAMP signaling pathway. The adhesion of single RBCs and the effect of cAMP signaling at the single-molecule and single-cell level are *central to disease pathology and anti-adhesive drug development*. We established two *in vitro* techniques, based on AFM, to study human RBC adhesion in physiological conditions. The first, SMFS enables

detection of single BCAM/Lu proteins on the RBC surface and measures the exact unbinding force between BCAM/Lu and laminin. The second, SCFS enables quantitative study of RBC adhesion while maintaining the native state of surface receptors. By studying RBC adhesion using SMFS in conjunction with SCFS, we expect a significant impact on identifying potential targets for anti-adhesive drug therapies to prevent and treat VOEs in SCD.

Chapter 2. Atomic Force Microscopy

Atomic force microscopy (AFM; Figure 2.1) [89] has opened a wide range of novel possibilities for imaging and manipulating biological systems in their native environment [90-91]. It allows for measurements of native biological samples in physiological conditions [30, 92-93] while avoiding complex sample preparation procedures and the artifacts connected with such procedures. The mild experimental conditions used in AFM allow for dynamic studies of cellular morphology, elasticity, and molecular interactions at the single-molecule and single-cell level [30, 90, 94]. In particular, functionalization of the AFM cantilever tip with ligands has allowed for mapping the distribution of complementary receptors on model or cellular surfaces [90-91, 94-98] with high resolution.

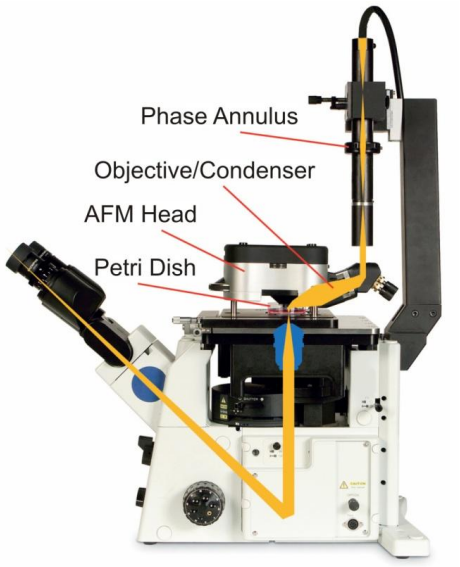

Figure 2.1. Atomic force microscope. Labeled components of the Asylum Research MFP-3D-BIO AFM atop a Zeiss optical inverted microscope. Image edited from Asylum Research MFP-3D-BIO brochure [99].

The AFM works by scanning, in a raster fashion, a very tiny tip mounted at the end of a flexible cantilever in gentle touch with the sample. This relative motion is performed with sub-Angstrom accuracy by a piezoelectric actuator. Interacting with the sample, the cantilever deflects and the

tip-sample interaction can be monitored with high resolution exploiting a laser beam impinging on the back of the cantilever [89, 92]. The beam is reflected towards a split photodetector configuring an optical lever which amplifies cantilever deflections. Connected to the cantilever deflection sensor is a feedback circuit that keeps interactions between the cantilever tip and the sample at a fixed value by controlling the distance between the cantilever tip and the sample. AFM cantilever probes utilized in biological applications are generally composed of thin silicon nitride with a tiny pyramid tip at the end of the probe. Typical spring constants for these AFM cantilevers range from 0.01 N/m to 100 N/m, enabling a minimum force sensitivity of approximately 10^{-11} N.

A typical force-distance curve (Figure 2.2) can be divided into several regions. Starting from the right (region I) the AFM tip is far from the sample and no interaction is detected. Moving towards the left side of the plot (dotted curve), the tip is approaching the sample and no interaction is detected until the cantilever deflects downwards towards the sample as a result of van der Waals forces (region II). At this point, these van der Waals forces cause the cantilever tip to snap into contact with the sample. The 'jump to contact' point corresponds to the position where the gradient of the interaction force exceeds the cantilever spring constant. At each position in the force curve, the cantilever is deflected until the restoring force is equal to the interaction force with the sample, thus causing the system to be always at equilibrium. After the contact, as the tip continues its approach cycle and moves closer to the surface, a positive deflection of the cantilever arises (region III) due to repulsive forces. This is the contact region of the force curve where elastic properties of the sample can be measured [93, 100-103]. The cantilever moves toward the sample until a preset force threshold is reached. At this time, the movement direction is inverted and the cantilever starts moving away from the sample (solid curve). Initially, the behavior of the cantilever during withdrawal equals that described for the approach, but due to adhesion between the functionalized cantilever tip and the sample, the cantilever starts to

deflect negatively (region IV) until the adhesion force is overcome by the cantilever restoring force and the contact breaks. The resulting breakage of contact is referred to as the rupture force and is used to determine the bond magnitude of a protein-protein interaction, or any interaction between a molecule functionalized on the cantilever tip and a receptor on the sample.

In a force-curve cycle the cantilever deflection is measured and can be converted to force using Hooke's law:

$$F = -kd$$

where F is the force, k is the spring constant of the cantilever and d is the cantilever deflection. By using a cantilever with a very small spring constant, a resolution of 10 pN can be obtained in the measurement of forces [92].

The retraction component of the force curve quantifies the exact detachment force, denoting the adhesive force, of the cell-cell or cell-protein interaction [30, 91]. If on the sample surface there is a molecule or a cell and the tip is functionalized in order to expose a partner suitable to specific interaction with it off its surface, the ligand-receptor interaction can be measured by exploiting the detachment force in the retraction portion of the force-distance curve. When the tip and sample are brought into contact, the molecules/cells present on the tip and surface interact and form bonds. Upon cantilever retraction, the bonds previously formed are disrupted and the typical detachment force is measured. To analyze the collected data, usually a distribution of the number of detachment events as a function of the detachment force is obtained. In SMFS, the presence of a detachment force is the indication that a single-molecule interaction is measured, the multiples of the unbinding force being the result of coincident

breakage of several bonds. Moreover, when a retraction curve presents several detachment events, the last one most likely represents a single bond breakage [92, 104]. In SCFS, the detachment forces are characteristic of the breakage of many receptor-ligand bond formations and are typically higher than those recorded in SMFS.

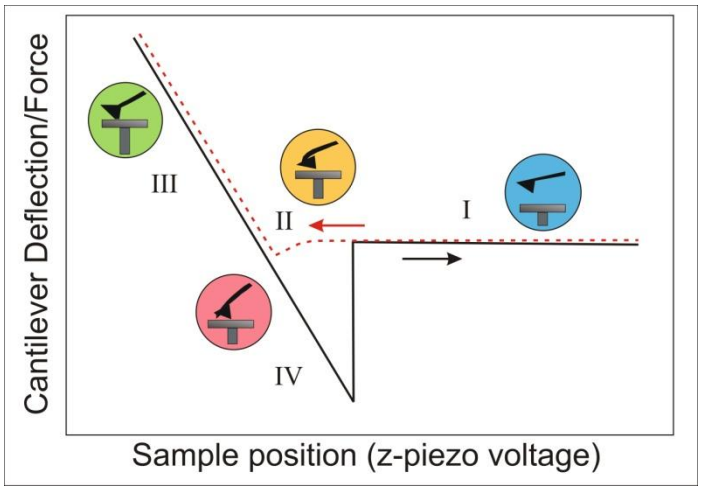

Figure 2.2. Force curve regions. Force curve illustration with the different regions of the approach and withdrawal portions highlighted. Region I demonstrates no interaction between the tip and the sample, region II shows the cantilever deflecting downward towards the sample as a result of van der Waals forces, region III shows the positive deflection of the cantilever due to repulsive forces, and region IV demonstrates the negative deflection of the cantilever tip as a result of adhesion forces between the tip and the sample. The different regions are discussed thoroughly in the text.

Contact problems

The general theory of elasticity has been applied to AFM measurements based on the contact theory of Hertz and Sneddon [105-107]. AFM stiffness measurement is modeled as indentation of an elastic half-space, $z < 0$, by a frictionless rigid punch [108], as shown in Figure 2.3. The profile of the punch is described by the function $f(x, y)$, and $u_z(x, y)$ is the normal deformation of the indented elastic half-space surface. In this case, the half-space represents the indented RBC.

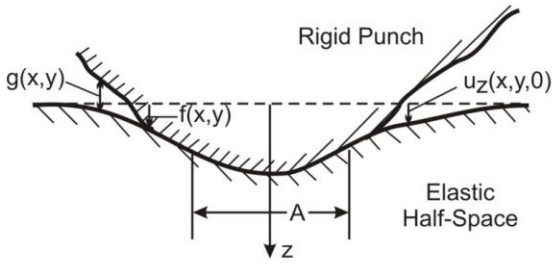

Figure 2.3. The general indentation problem for a smooth, rigid, frictionless punch.

The gap $g(x,y)$ between the punch and the half-space is defined as

$$g(x,y) = u_z(x,y,0) - f(x,y) \geq 0. \quad (1)$$

When the shape of the employed indenter exhibits a two-fold symmetry (e.g. pyramidal or parabolic) then the contact area A preserves the same symmetry as the base of the indenter, with the center of A at the coordinate origin (x = 0, y = 0, z = 0). The contact tractions act normal to the surface and are compressive inside A and zero exactly at the contact perimeter, as well as outside A.

The gap is zero within the contact region A and positive in the separation region $\bar{A}$, since interpenetration of material is prohibited. Therefore, we have two conditions

$$u_z(x,y,0) = f(x,y); \text{ in } A \quad (2)$$

$$u_z(x,y,0) > f(x,y); \text{ in } \bar{A}. \quad (3)$$

The definition of the frictionless contact problem is completed by assuming that the tangential

traction is zero throughout the surface of the half-space,

$$\sigma_{zx} = \sigma_{zy} = 0; \text{ all } x, y, z = 0 \tag{4}$$

and that the contact pressure $p(x,y) = -\sigma_{zz}(x,y,0)$ is zero in the separation region $\bar{A}$ and positive in the contact region A, that is

$$p(x,y) = 0 \text{ in } \bar{A} \tag{5}$$

$$p(x,y) > 0 \text{ in } A. \tag{6}$$

If the contact region A is specified, the equality conditions (2), (4), (5) define a well-posed boundary value problem for the half-plane which has a unique solution. Then the total contact force is obtained by

$$P_z = \iint_A p(x,y)dxdy \tag{7}$$

The inequalities (3) and (6) serve to determine the extent of the contact area for the contact problem, but it has been shown [109] that the value of A, which satisfies (3) and (6), maximizes the total force P_z given by equation (7).

In the case of a spherical indenter, by solving the boundary contact problem as performed by Hertz [106], the following result is obtained,

$$P_z(r_s) = p_0\sqrt{a^2 - r_s^2} \quad (8)$$

where $s = |r| = (r^2 + r_s^2 - 2rr_s cos\theta + {u_z}^2)^{1/2}$ is the distance between source $(r_s, 0,0)$ and observation point (r, θ, u_z); θ is the angular distance and $p_0 = 2E/\pi R(1 - v^2)$, where E is the Young's modulus. The contact radius, a, is given in terms of the applied force, F, and the Poisson's ration, v, of the sample

$$a = \left(\frac{3}{4}\frac{1-v^2}{E}FR\right)^{1/3} \quad (9)$$

Sneddon extended the Hertz model from a spherical indenter to an indenter of arbitrary profile deforming elastic half space [107, 110]. Solutions of the boundary contact problem for other tip geometries with two-fold symmetry generated models for parabolic [111-113] and pyramidal [102, 110, 114-115] indenters. The general solution for force as a function of indentation for a parabolic indenter can be approximated as

$$F_{parabolic} = \frac{4}{3}\sqrt{R}E'{u_z}^{\frac{3}{2}} \quad (10)$$

where E' is the reduced Young's modulus of the tip-sample system defined as

$$\frac{1}{E'} = \frac{1-v^2}{E} \quad (11)$$

The general solution for force as a function of indentation for a pyramidal indenter [102, 114-115] can be approximated as

$$F_{pyramid} = \frac{3E \tan\theta}{4(1-\nu^2)} {u_z}^2 \quad (12)$$

Atomic force microscopy contact problems

In a force curve on a sample indented via AFM, the indentation, u_z, is equal to

$$u_z = d - \delta \quad (13)$$

where δ is the deflection of the cantilever on the rigid substrate and d is the deflection of the cantilever on the indented half-space. In this particular study, δ is the deflection of the cantilever on the poly-l-lysine coated mica substrate and d is the deflection of the cantilever on the indented erythrocyte surface.

Three important assumptions of the Hertz-Sneddon model are the following: (i) the indenter must have a parabolic shape, (ii) the indented sample is assumed to be extremely thick in comparison to the indentation depth, and (iii) there is no adhesive interaction between the sample and the indenter. The first assumption remains a valid one for the case when a spherical tip radius is much larger than the indentation depth ($u_z < 0.3R$) [116]. The second assumption states that elastic models based on Hertz-Sneddon contact mechanics are accurate when the indentation depth is small compared to the thickness of the cell. This corresponds with the well

known fact that the effect of the substrate over which the cells are placed is negligible if the indentation depth is less than 10% of the total thickness of the specimen [117]. In cases where the third assumption is not satisfied, the Johnson-Kendall-Roberts (JKR) model should be employed to incorporate the effect of adhesion [118]. The JKR model considers the effect of contact pressure and adhesion within the area of contact. In the current study, we did not observe a pull-off force, or rupture force, in the experimental force-distance curves. This can be attributed to the fact that our AFM indenter was not functionalized. Therefore, the Hertz-Sneddon model appropriately describes the measurements in the present study.

While in the current work only the elastic behavior of RBCs is studied, RBCs have been found to exhibit viscoelastic behavior under repetitive deformations [119]. The viscoelastic properties of normal RBCs have been studied via magnetic twisting cytometry. Results indicate that G', the storage modulus which represents the Young's modulus, is nearly constant for different frequencies, while G'', the loss modulus, increases with frequency [119]. This result suggests that the measurement of the effective Young's modulus presented in this work remains valid when repetitive loading is applied, at least for normal RBCs. Finally, it should be noted that AFM has been used to measure the viscoelastic behavior of epithelial cells [102, 115]. In principle, the employed methods can be used to perform viscoelasticity measurements on normal and pathological RBCs.

Parabolic tip

When the shape of the AFM tip is approximated by a paraboloid with a radius of curvature R at the apex, the force $F_{parabolic}$ as a function of indentation u_z is described by the following equation [111-113]:

$$F_{parabolic} = \frac{4}{3}\sqrt{R}E^{'}u_z^{\frac{3}{2}} \quad (14)$$

where E' is the reduced Young's modulus of the tip-sample system defined as

$$\frac{1}{E'} = \frac{1-v_{sample}^2}{E_{tip}} + \frac{1-v_{sample}^2}{E_{sample}} \quad (15)$$

in which E_{tip}, v_{tip} and E_{sample}, v_{sample} are the Young's moduli and the Poisson ratios for the materials of the tip and the sample, respectively. If $E_{sample} \leq E_{tip}$ (in the case of Si_3N_4 tips, the Young's modulus is 150 GPa [103]), E' can be simplified as:

$$E^{'} = \frac{E_{sample}}{1-v_{sample}^2} \quad (16)$$

Poisson's ratio, v, is defined as the ratio of the transverse, or orthongonal, strain to the strain along the direction of elongation. It is useful for determining how much the material extends orthogonally to the direction in which the force is applied. The value of v is always between 0 and 0.5 [120-121].

Pyramidal tip

When the shape of the AFM tip is a four-sided pyramidal indenter, the force $F_{pyramid}$ as a function of indentation u_z is described by the following equation [102, 110, 114-115]:

$$F_{pyramid} = \frac{3E \tan\theta}{4(1-\nu^2)} u_z^2 \quad (17)$$

with an effective radius of contact $a = u_z \, tan\theta / 2^{1/2}$ with θ defined as nominal angle of the pyramidal geometry [102, 114-115].

Adhesion measurements

In the past, RBC adhesion was traditionally investigated via large-scale flow adhesion assays [122-125], which measure the average adherence of a large number of RBCs to a functionalized-substrate under flow-induced shear stress [126-127]. These measurements provide only estimates of the adhesion force to which cells are subjected because the shear force exerted on cells in these assays depends on parameters such as cell size, cell shape, how the cell attaches to the substrate, as well as the viscoelastic and elastic properties of the cells [128-130]. For example, it is known that RBCs from SCD patients show variability in their viscoelastic and elastic properties [100, 119], and these properties can change after biochemical or pharmacologic treatment [87]. Specifically, RBCs from patients taking the drug hydroxyurea are more compliant than RBCs from patients who are not taking the drug [77]. Further, given the nature of flow adhesion assays, they are unable to provide information regarding receptor activity, including detachment forces, receptor localization, and changes in the number of active receptors upon biochemical stimulation. To obtain more controlled and quantitative measurements of RBC adhesion, single-cell methods must be employed.

AFM studies of RBC adhesion have been employed to provide quantitative evidence of changes in surface receptor distribution, and unbinding forces with specific ligands [30]. A technique known as SMFS utilizes cantilever tips functionalized with specific ligands to probe the cell

surface. SMFS measures the unbinding, or detachment force, between a specific ligand on the AFM tip and its corresponding receptor on a single cell with piconewton sensitivity [30, 90-92, 131-132]. Because SMFS is broadly used in conjunction with optical microscopy, the user has the ability to choose a RBC of interest for measurements. SMFS operates by collecting a set of force-distance curves of the approach-retract cycle of the functionalized tip from the cell surface. Specifically, the retraction curve, obtained when the functionalized probe pulls away from the RBC surface gives the detachment force. Individual approach/retract curves can be obtained at many points on a sample to create a two-dimensional map of detected surface adhesion receptors [30]. Forces probed by SMFS reflect interactions within or between molecules [133]. Specifically, this technique allows for (i) quantifying the detachment force of specific receptor-ligand bonds, (ii) mapping the distribution of active receptors on cellular surfaces with high resolution, (iii) calculating the density of active receptors on the cell surface [90-91, 94-98]. While SMFS presents a very powerful tool to study RBC adhesion at the single-molecule level, it cannot measure the overall adhesion of a living cell to a substrate or another living cell. Further, it is currently unknown how SMFS measurements compare to whole cell measurements.

To overcome these limitations, SCFS assays, that are using a living cell as a probe, were developed [130, 134-138]. This AFM-based method is highly versatile because of its ability to measure a wide range of forces, from ~5 pN to ~100 nN [130]. In SCFS, a RBC attached to an AFM cantilever is positioned above a functionalized substrate or another living cell. Similar to SMFS measurements, SCFS also records force-distance curves of an approach/retract cycle between the RBC probe and the functionalized substrate or cell. The RBC is lowered onto the substrate until a preset contact force is reached, and then held stationary for a defined time. Subsequently, the cell is withdrawn from the substrate at a constant speed and bonds between the cell and substrate break sequentially until the two entities are completely separated. In this

case, the maximum detachment force is characterized as the force required to fully remove the RBC from the functionalized substrate.

Chapter 3. Microelasticity of Red Blood Cells in Sickle Cell Disease

3.1. Abstract

Translation of cellular mechanics findings is crucial in many diseases, including Alzheimer's disease, Parkinson's disease, type II diabetes, malaria, sickle cell disease, and cancer. Atomic force microscopy (AFM) is appropriate for measuring mechanical properties of living and fixed cells due to its high force sensitivity and its ability to measure local and overall properties of individual cells under physiological conditions. A systematic force-displacement curve analysis is reported on the quantification of material stiffness via AFM using two theoretical models derived from the Hertz model. This analysis was applied to red blood cells from patients with sickle cell disease to determine the Young's modulus of these cells in the oxygenated and deoxygenated state. Sickle cell disease pathophysiology is a consequence of the polymerization of sickle hemoglobin in red blood cells upon partial deoxygenation and the impaired flow of these cells in the microcirculation. We determined the model for a four-sided pyramidal indenter to be a better fit for our application as compared to the model for a parabolic indenter. Our findings conclude that deoxygenation and therapeutic treatment have a significant impact on the stiffness. This analysis presents a new approach to addressing medical disorders.

3.2. Introduction

A detailed knowledge of the mechanical properties of the cell is required in understanding how mechanical stresses and deformations regulate cellular functions including fundamental cell processes including mechanotransduction, growth, differentiation, protein and DNA synthesis, motility, and apoptosis [139-140]. The most common approach reported to study cell mechanics is to determine the stiffness or an apparent elastic modulus of the cell, assuming that it is an elastic body. Atomic force microscopy (AFM) [89] is appropriate for measuring the mechanical

properties of living and fixed cells due to its high force sensitivity and its ability to measure local and overall properties of individual cells under physiological conditions [101, 141-146]. AFM allows simultaneous evaluation of the local mechanical properties and the morphology of the living cells at a high spatial resolution and force sensitivity. The basic technique for quantitative study of mechanical characteristics of cells and tissues via AFM is the force-displacement curve analysis. By recording the force-displacement curves on the sample surface, vertical deflection of the cantilever represents a basis for estimation of sample Young's modulus. In the current study, we apply the force-displacement curve analysis to explore the pathophysiology of sickle cell disease. Understanding the relationship between proteins and cellular material properties will allow for detection of diseases and new approaches to addressing medical disorders [147].

3.3. Sickle Cell Disease

In the current study, we measure the Young's modulus of red blood cells (RBCs, erythrocytes) from patients with sickle cell disease (SCD), a severe disease caused by polymerization of abnormal hemoglobin [148], a globular protein which transports oxygen from the lungs to tissues [59] . Hemoglobin (Hb) is formed by four polypeptide chains, two of type α and two of type β. In sickle cell hemoglobin (HbS), the normal sequence of *Val-His-Leu-Thr-Pro-Glu-Glu-Lys* is changed to *Val-His-Leu-Thr-Pro-Val-Glu-Lys*, with the amino acid valine substituting for the glutamic acid in the β6 site. The replacement of two charged groups by two hydrophobic ones leads to polymerization of deoxygenated Hb and to formation of long stiff rodlike fibers [33, 35-36], which force RBCs to assume a wide variety of irregular shapes [37]. The fibers form noncovalent cross-links and create a gel that gives RBCs their irregular shapes and alters their viscoelastic behavior, increases their rigidity, fragility, and cytoadherence [36, 69-70]. Other factors such as lowered pH, RBC dehydration and hyperthermia are also known to prompt sickling [38]. Pathology in SCD begins with loss of deformability and increased cell adherence of

the sickle cells resulting in serious and often life threatening complications such as chronic hemolytic anemia and vaso-occlusion [31, 64, 67, 69]. Persons with sickle cell trait (SCT) have only one abnormal hemoglobin β gene producing thus both normal hemoglobin (HbA) and sickle hemoglobin HbS with a prevalence of HbA [44-45].

In the case of SCD, it has been hypothesized that increased association of HbS with the membrane proteins contributes to the change of the mechanical behavior of sickle erythrocytes [149]. HbS could alter the mechanical properties of RBCs not only by extending the spectrin filaments, and by the interaction between HbS filaments and the lipid bilayer but also by altering the functionality of the membrane proteins [150]. It is known that Hb interacts with the spectrin network via the protein band 3 [40, 151-152] and the introduction of HbS has recently been found to have an effect on the mechanical properties of SCT erythrocytes [93]. In the present study, we employ AFM techniques to measure the Young's modulus of RBCs from patients with SCD under both oxygenated and fully deoxygenated conditions.

3.4. Atomic Force Microscopy Probing of Cell Elasticity

In the current work, we perform nanoindentation of RBCs to measure the local cell stiffness. The measurements are performed via AFM by pushing a tip onto the surface of the sample at the position of interest. From the resulting force-displacement curves the local Young's modulus is determined.

Introduction to contact problems

The general theory of elasticity has been applied to AFM measurements based on the contact theory of Hertz and Sneddon [105-107]. AFM stiffness measurement is modeled as indentation of an elastic half-space, $z < 0$, by a frictionless rigid punch [108], as shown in Figure 3.4.1. The

profile of the punch is described by the function $f(x,y)$, and $u_z(x,y)$ is the normal deformation of the indented elastic half-space surface. In this case, the half-space represents the indented RBC. The gap $g(x,y)$ between the punch and the half-space is defined as

$$g(x,y) = u_z(x,y,0) - f(x,y) \geq 0. \quad (1)$$

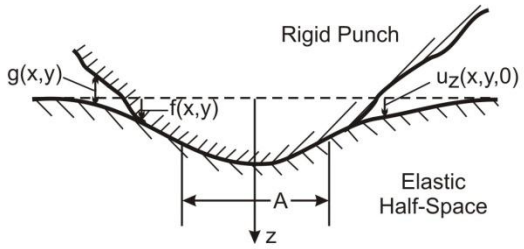

Figure 3.4.1. The general indentation problem for a smooth, rigid, frictionless punch.

When the shape of the employed indenter exhibits a two-fold symmetry (e.g. pyramidal or parabolic) then the contact area A preserves the same symmetry as the base of the indenter, with the center of A at the coordinate origin (x = 0, y = 0, z = 0). The contact tractions act normal to the surface and are compressive inside A and zero exactly at the contact perimeter, as well as outside A.

The gap is zero within the contact region A and positive in the separation region $\bar{A}$, since interpenetration of material is prohibited. Therefore, we have two conditions

$$u_z(x,y,0) = f(x,y); \text{ in } A \quad (2)$$

$$u_z(x,y,0) > f(x,y); \text{ in } \bar{A}. \quad (3)$$

The definition of the frictionless contact problem is completed by assuming that the tangential traction is zero throughout the surface of the half-space,

$$\sigma_{zx} = \sigma_{zy} = 0; \text{ all } x, y, z = 0 \tag{4}$$

and that the contact pressure $p(x,y) = -\sigma_{zz}(x,y,0)$ is zero in the separation region $\bar{A}$ and positive in the contact region A, that is

$$p(x,y) = 0 \text{ in } \bar{A} \tag{5}$$

$$p(x,y) > 0 \text{ in } A. \tag{6}$$

If the contact region A is specified, the equality conditions (2), (4), (5) define a well-posed boundary value problem for the half-plane which has a unique solution. Then the total contact force is obtained by

$$P_z = \iint_A p(x,y)dxdy \tag{7}$$

The inequalities (3) and (6) serve to determine the extent of the contact area for the contact problem, but it has been shown [109] that the value of A, which satisfies (3) and (6), maximizes the total force P_z given by equation (7).

In the case of a spherical indenter, by solving the boundary contact problem as performed by Hertz [106], the following result is obtained,

$$P_z(r_s) = p_0\sqrt{a^2 - r_s^2} \quad (8)$$

where $s = |r| = (r^2 + r_s^2 - 2rr_s cos\theta + {u_z}^2)^{1/2}$ is the distance between source $(r_s, 0,0)$ and observation point (r, θ, u_z); θ is the angular distance and $p_0 = 2E/\pi R(1 - v^2)$, where E is the Young's modulus. The contact radius, a, is given in terms of the applied force, F, and the Poisson's ration, v, of the sample

$$a = \left(\frac{3}{4}\frac{1-v^2}{E}FR\right)^{1/3} \quad (9)$$

Sneddon extended the Hertz model from a spherical indenter to an indenter of arbitrary profile deforming elastic half space [107, 110]. Solutions of the boundary contact problem for other tip geometries with two-fold symmetry generated models for parabolic [111-113] and pyramidal [102, 110, 114-115] indenters. The general solution for force as a function of indentation for a parabolic indenter can be approximated as

$$F_{parabolic} = \frac{4}{3}\sqrt{R}E'{u_z}^{\frac{3}{2}} \quad (10)$$

where E' is the reduced Young's modulus of the tip-sample system defined as

$$\frac{1}{E'} = \frac{1-v^2}{E} \quad (11)$$

The general solution for force as a function of indentation for a pyramidal indenter [102, 114-115] can be approximated as

$$F_{pyramid} = \frac{3E \tan\theta}{4(1-\nu^2)} {u_z}^2 \quad (12)$$

Atomic force microscopy contact problems

In a force curve on a sample indented via AFM, the indentation, u_z, is equal to

$$u_z = d - \delta \quad (13)$$

where δ is the deflection of the cantilever on the rigid substrate and d is the deflection of the cantilever on the indented half-space. In this particular study, δ is the deflection of the cantilever on the poly-l-lysine coated mica substrate and d is the deflection of the cantilever on the indented erythrocyte surface.

Three important assumptions of the Hertz-Sneddon model are the following: (i) the indenter must have a parabolic shape, (ii) the indented sample is assumed to be extremely thick in comparison to the indentation depth, and (iii) there is no adhesive interaction between the sample and the indenter. The first assumption remains a valid one for the case when a spherical tip radius is much larger than the indentation depth ($u_z < 0.3R$) [116]. The second assumption states that elastic models based on Hertz-Sneddon contact mechanics are accurate when the indentation depth is small compared to the thickness of the cell. This corresponds with the well known fact that the effect of the substrate over which the cells are placed is negligible if the indentation depth is less than 10% of the total thickness of the specimen [117]. In cases where the third assumption is not satisfied, the Johnson-Kendall-Roberts (JKR) model should be employed to incorporate the effect of adhesion [118]. The JKR model considers the effect of

contact pressure and adhesion within the area of contact. In the current study, we did not observe a pull-off force, or rupture force, in the experimental force-distance curves as shown in Figure 3.4.2. This can be attributed to the fact that our AFM indenter was not functionalized. Therefore, the Hertz-Sneddon model appropriately describes the measurements in the present study.

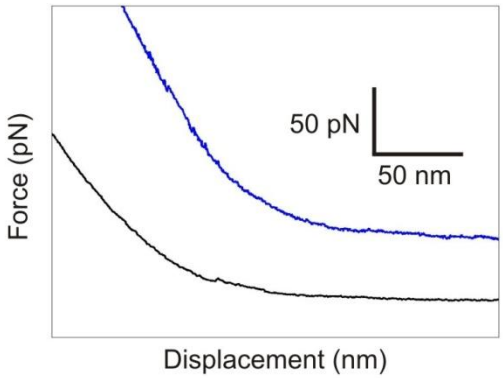

Figure 3.4.2. Force-distance curves obtained during the retraction cycle of the indention. The absence of a pull-off force, or rupture force, indicates that there is no adhesion present between the sample and the indenter during experimentation.

While in the current work only the elastic behavior of RBCs is studied, RBCs have been found to exhibit viscoelastic behavior under repetitive deformations [119]. The viscoelastic properties of normal RBCs have been studied via magnetic twisting cytometry. Results indicate that G', the storage modulus which represents the Young's modulus, is nearly constant for different frequencies, while G'', the loss modulus, increases with frequency [119]. This result suggests that the measurement of the effective Young's modulus presented in this work remains valid when repetitive loading is applied, at least for normal RBCs. Finally, it should be noted that AFM has been used to measure the viscoelastic behavior of epithelial cells [102, 115]. In principle, the employed methods can be used to perform viscoelasticity measurements on normal and pathological RBCs.

Parabolic tip

When the shape of the AFM tip is approximated by a paraboloid with a radius of curvature R at the apex, the force $F_{parabolic}$ as a function of indentation u_z is described by the following equation [111-113]:

$$F_{parabolic} = \frac{4}{3}\sqrt{R}E'u_z^{\frac{3}{2}} \quad (14)$$

where E' is the reduced Young's modulus of the tip-sample system defined as

$$\frac{1}{E'} = \frac{1-v_{sample}^2}{E_{tip}} + \frac{1-v_{sample}^2}{E_{sample}} \quad (15)$$

in which E_{tip}, v_{tip} and E_{sample}, v_{sample} are the Young's moduli and the Poisson ratios for the materials of the tip and the sample, respectively. If $E_{sample} \leq E_{tip}$ (in the case of Si_3N_4 tips, the Young's modulus is 150 GPa [103]), E' can be simplified as:

$$E' = \frac{E_{sample}}{1-v_{sample}^2} \quad (16)$$

Poisson's ratio, v, is defined as the ratio of the transverse, or orthongonal, strain to the strain along the direction of elongation. It is useful for determining how much the material extends orthogonally to the direction in which the force is applied. The value of v is always between 0 and 0.5 [120-121].

Pyramidal tip

When the shape of the AFM tip is a four-sided pyramidal indenter, the force $F_{pyramid}$ as a function of indentation u_z is described by the following equation [102, 110, 114-115]:

$$F_{pyramid} = \frac{3E \tan\theta}{4(1-\nu^2)} u_z^2 \quad (17)$$

with an effective radius of contact $a = u_z \, tan\theta / 2^{1/2}$ with θ defined as nominal angle of the pyramidal geometry [102, 114-115].

3.5. Methods

Experiments were carried out using an Asylum MFP 3D-BIO (Asylum Research, Santa Barbara, CA) AFM equipped with a “liquid cell” setup.

Red blood cell preparation

Whole blood was drawn from patients with sickle cell disease during clinical visits to the Lea Center for Hematologic Disorders at the University of Connecticut Health Center (UCHC) following the guidelines of the Human Subjects Protection Office at UCHC. Blood was drawn by venipuncture into 5 IU/ml heparin and centrifuged at 400 *g* for 15 min at 25°C to isolate the RBCs. The yellowish supernatant containing plasma and the white fluffy coat on the pellet was discarded. All buffers were pre-warmed to 37°C prior to use. RBCs were washed three times with phosphate-buffered saline (PBS) and finally re-suspended in PBS at a concentration 5%. Deoxygenated red blood cells were obtained by bubbling N_2 through a suspension of RBCs in a sealed flask for 1 hr. The state of deoxygenation of the erythrocytes was expected to be

maintained for 1-1.5h [153] and experiments were performed during this time.

Erythrocyte immobilization

Cells were immobilized on AFM grade mica (Novascan Technologies, Inc., Ames, IA) coated with poly-L-lysine (PLL) (Sigma-Aldrich, St. Louis, MO) to increase cell adherence. 150 µl of 1 mg/ml PLL solution was allowed to adsorb for 5 min to an unmodified mica surface, and excess solution was drained away. RBCs of 0.5% concentration in PBS were allowed to adhere to each PLL-coated mica surface for 10 min in the incubator. Unattached cells were removed by gentle rinsing of the slide with PBS solution at 25°C. For imaging, fixation was performed by a 1-min treatment of the cells with 0.5% glutaraldehyde (Sigma-Aldrich, St. Louis, MO) in PBS buffer. The sample was again rinsed several times with PBS and a volume of PBS was added for experiments. Glutaraldehyde was not employed for stiffness measurements.

Imaging

Erythrocytes were imaged in tapping mode with a scan rate of 0.2 Hz, and the minimal force necessary to obtain good image contrast was determined by gradually increasing the force applied to the sample from zero force (noncontact) to the necessary minimal force. Silicon nitride probes with a nominal spring constant of 0.01 N/m (Veeco Probes, Camarillo, CA) were employed for imaging.

Measurements

Erythrocyte's stiffness measurements were carried out in contact mode using silicon nitride cantilevers with a nominal spring constant of 0.03 N/m (Veeco Probes, Camarillo, CA). Exact values for the cantilever spring constants were obtained via a thermal noise based method

implemented by the manufacturer and were used in all calculations. Probes had nominal tip radii R of 20 nm and nominal angle θ of 20°, as provided by the manufacturer. Tip height was 2.5 μm, as provided by the manufacturer. All measurements were performed in PBS at 25°C. Local elastic properties of erythrocytes were quantitatively determined from the force-distance curves. The force curves were generated at a loading rate of 15,000 pN/s, and for both states, oxygenation and deoxygenation, more than 500 measurements were collected.

Data processing

Data was imported into MATLAB (The MathWorks, Natick, MA) and the value of E was obtained by fitting the theoretical curves generated by Eq. (2) and Eq. (5) to the experimental data up to a minimum depth of 250 nm, which is approximately 10% of the total thickness of the cell. The method is in agreement with the well known fact that the effect of the substrate over which the cells are placed is negligible if the indentation depth is less than 10% of the total thickness of the specimen [117].

3.6. Results

Morphology of SCD erythrocytes via AFM imaging

Under both oxygenated and deoxygenated states, highly irregular morphologies were observed in the RBC samples. Normal RBCs are characterized by a biconcave shape which not only increases the surface area and facilitates O_2 and CO_2 diffusion into and out of the cell [59-60] but also increases the compliance of the erythrocytes [61]. Polymerization of Hb fibers forces RBCs to assume a wide variety of irregular shapes [37]. Two representative examples are shown in Figure 3.6.1. Repeated cycles of oxygenation and deoxygenation lead to irreversible sickling, a phenomenon we suspect has occurred to the erythrocyte in Figure 2.6.1A, imaged

under oxygenated conditions. This cell is characterized by protrusions likely resulting from polymerized Hb fibers and also an enlarged morphology. Upon deoxygenation, as in Figure 2.6.1B, HbS fibers are expected to polymerize and aggregate, thus forming the highly elongated and irregular structure shown. In addition, this cell also contains bumps and surface irregularities which are possibly associated with protruding polymerized HbS fibers and changes in the RBC membrane cortex.

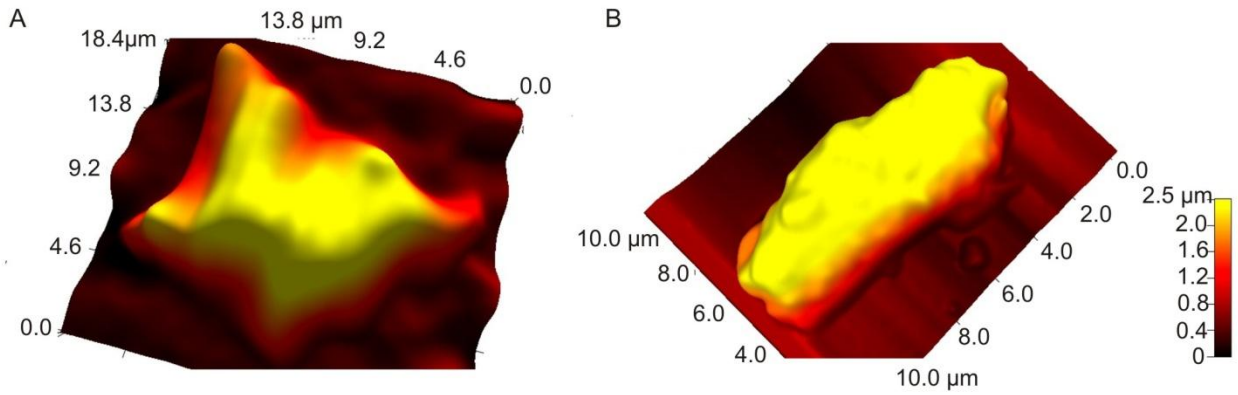

Figure 3.6.1. Three-dimensional topographical images of SCD erythrocytes obtained via AFM (A) in an oxygenated environment and (B) in a fully deoxygenated state. Both RBCs have a highly irregular morphology as compared to the characteristic biconcave shape of a normal erythrocytes. It is evident that polymerized Hb results in highly irregular RBC morphologies characterized by protrusions, elongation, bumps, and enlargement associated with aggregation of HbS fibers.

Determination of the indentation depth

The quantitative determination of the elastic properties of a particular material can be obtained from the relationship between the applied force F and the indentation depth δ using Eq. (14) and Eq. (17). When force is measured on a hard substrate, the cantilever deflection is proportional to the relative sample position resulting in a linear slope for the portion of the curve where the tip and the sample are in contact. When soft samples like erythrocytes are investigated, the recorded cantilever deflection as a function of the relative sample position is not linear due to the deformable structure of the RBC. Prior to taking force measurements on

the RBC surface, the force is measured on the PLL-coated mica substrate. This curve is used for calibration since no permanent sample deformation is observed. The indentation produced by the AFM tip was determined by subtracting the calibration curve from the curve recorded for the erythrocyte using the Igor Pro 6.04 (Wavemetrics, Portland, OR) software program.

Force-displacement curve analysis

The MATLAB output of both the pyramidal indenter model obtained from Eq. (17) and the parabolic indenter model obtained from Eq. (14) fit to the force v. indentation curve obtained via experimentation is shown in Figure 3.6.2. The model of the pyramid indenter appears to provide a better fit, as shown by the representative curves shown in Figure 3.6.2. At small Young's modulus values (E < 3 kPa), as in Figure 3.6.2A and Figure 3.6.2B, we observed that both the pyramid model and the parabolic model appeared to fit the experimental force-displacement curves to a minimum depth of 250 nm, which is approximately 10% of the thickness of the cell [112].

However, as indentation continues, the pyramid model continues to follow the trend of the experimental force-displacement curves while the paraboloid model greatly diverges. As the stiffness of the erythrocyte's increased, the pyramid model continued to provide a more accurate fit to the experimental data as shown in Figure 3.6.2C and Figure 3.6.2D. Although the paraboloid model appears to fit the data up to 50 nm indentations, the pyramid model continues to fit the data up to approximately 250 nm, representative of 10% of the total thickness of the cell. Based on our theoretical model analysis, we opted to continue our cell stiffness analysis via the model for the four-sided pyramidal indenter.

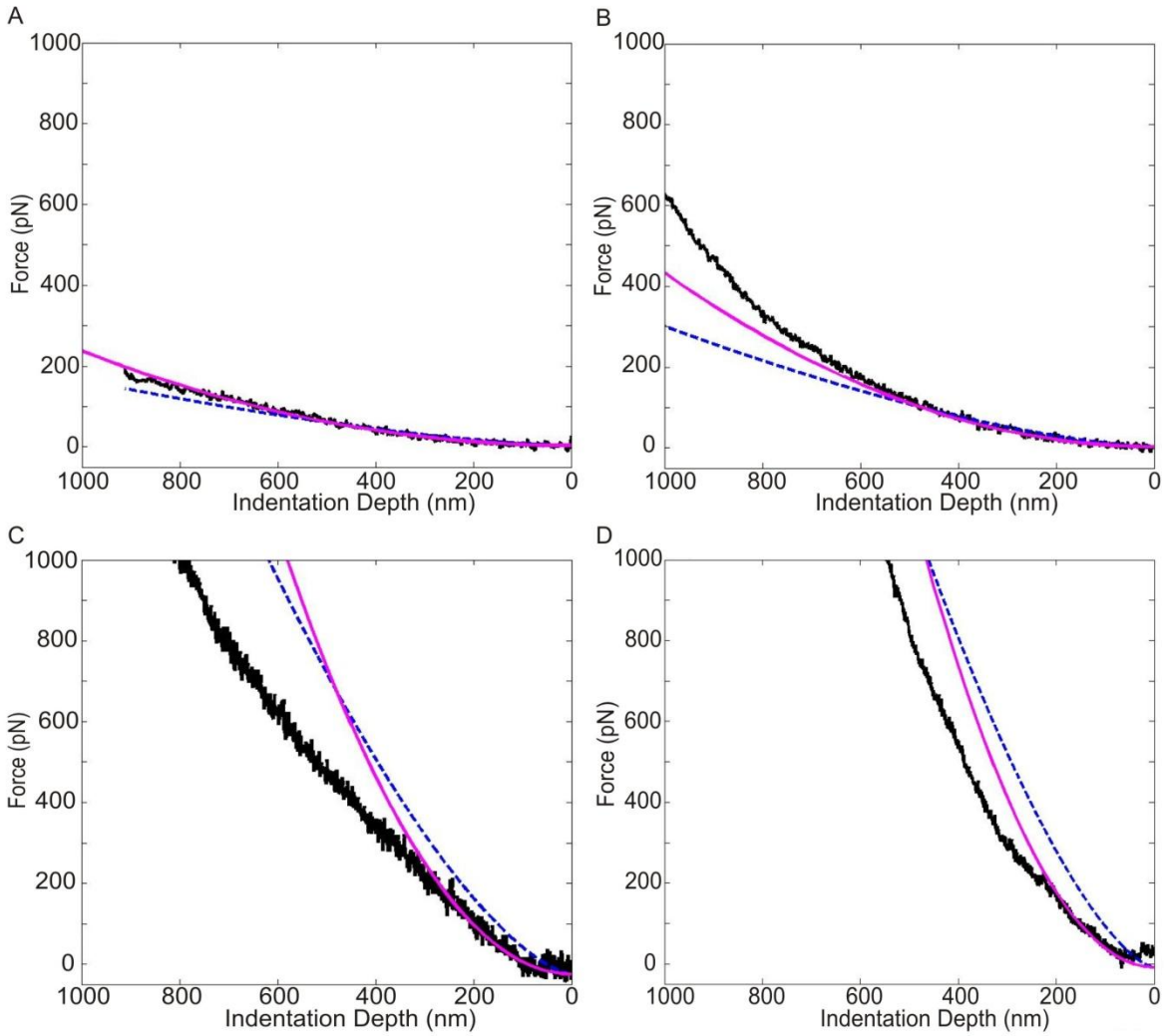

Figure 3.6.2. Theoretical models for a pyramid indenter and a parabolic indenter fitted to the experimental data for clinical SCD erythrocytes obtained via AFM. In these curves, the Young's modulus values are (A) 0.65 kPa, (B) 1.20 kPa, (C) 8.50 kPa, and (D) 13.0 kPa. The curves shown above are representative of force curves obtained for all SCD clinical samples of varying stiffness values. From the given data at a broad range of Young's modulus values, it appears that the pyramid indenter model provides a better fit. Legend in (A) applies for all.

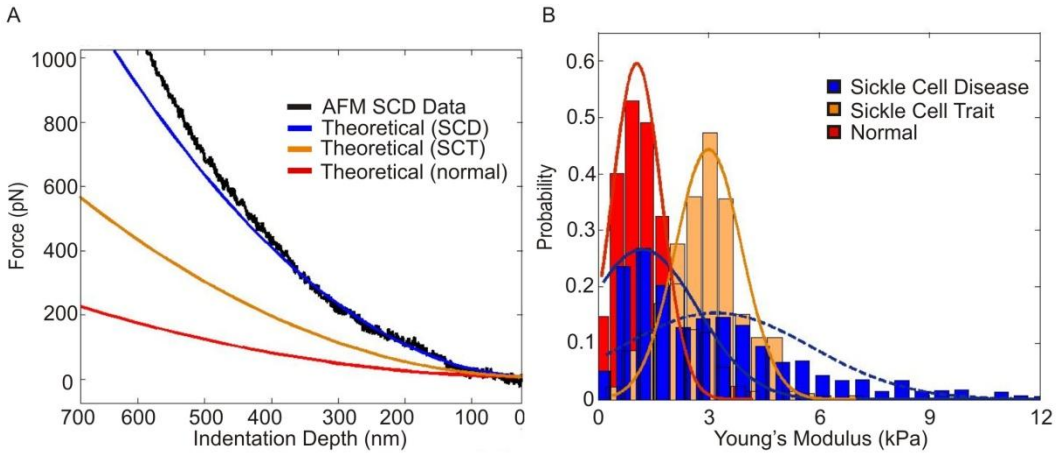

Figure 3.6.3. Experimental data for Young's modulus. (A) The data above show the theoretical pyramid model (Eq. 4) fitted to the experimental data for normal, SCT, and SCD erythrocytes. In these curves, the Young's modulus values for the normal, SCT, and both oxygenated and deoxygenated SCD RBCs are 1.30, 3.30 kPa, and 7.0 kPa, respectively. Curves shown are representative of the 500-600 force curves obtained for each normal and SCT RBCs, and 1000+ curves for SCD clinical samples. (B) Histograms of the Young's modulus values determined for RBCs from normal, SCT, and both oxygenated and deoxygenated SCD erythrocytes. Values for normal RBCs are E_{normal} = 1.10 kPa ± 0.40 kPa and SCT RBCs are E_{SCT} = 3.05 kPa ± 1.09 kPa. SCD clinical samples reveal a bimodal distribution with E_1 = 1.0 kPa ± 1.1 kPa, and E_2 = 3.0 ± 2.7 kPa, as well as higher (E > 7.0 kPa) values.

Cell stiffness determination

A representative curve showing experimental data for erythrocytes from patients with SCD is shown in Figure 3.6.3A. This data was fitted to the theoretical pyramid model and theoretical pyramid model curves representative of normal and SCT erythrocytes also shown for comparison. The average values of Young's modulus for oxygenated and deoxygenated SCD erythrocytes were obtained by fitting the Gaussian distribution to the generated histograms of the measured Young's modulus values (Figure 3.6.3B). It appears that both oxygenated and deoxygenated sickle cell disease RBCs maintain a bimodal distribution with peaks at E_1 = 1.0 kPa ± 1.1 kPa, and E_2 = 3.0 ± 2.7 kPa. A similar value has been found via optical tweezers [154]. By overlaying the histogram of the distribution of oxygenated SCD erythrocyte elasticity values atop the normal and SCT distribution, it is evident that each peak in the focused sickle cell disease erythrocyte distribution corresponds to the same Young's modulus value as the

SCT and normal RBCs, 3.0 kPa and 1.0 kPa, respectively [93]. As seen in Figure 3.6.4, oxygenated RBCs have an additional peak at approximately 15 kPa, while deoxygenated RBCs have an additional peak at approximately 40 kPa.

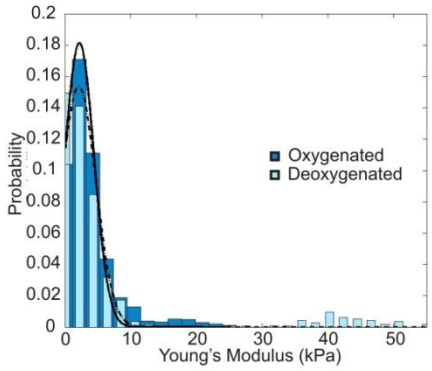

Figure 3.6.4. Histograms of the Young's modulus determined for sickle cell disease RBCs maintained in oxygenated and deoxygenated environments. The Young's modulus values obtained from fitting the theoretical pyramid indenter model to the experimental data were fitted with the Gaussian distribution. The full distribution shows evidence of an additional peak appearing around 15 kPa for the oxygenated RBCs and 40 kPa for the deoxygenated RBCs.

3.7. Discussion

The Young's modulus is the basic material coefficient of elasticity. It can range from ~100 GPa for high-strength materials (steel, titanium) [155-156] to 100s MPa for typical polymers (polystyrene), and 1 MPa for soft gel-like materials (gelatin in its gel-phase) [156]. Typical values for cells range from 1 kPa to 100 kPa [143-144, 157-163]. In the present study, we determined that sickle erythrocytes possess Young's modulus values between 1-60 kPa depending on their degree of oxygenation and the percentage of HbS present in the erythrocytes. Both oxygenated and deoxygenated samples of RBCs from patients with SCD maintain a bimodal distribution with peaks representative of normal RBCs (E_1 = 1.0 kPa ± 1.1 kPa) and SCT RBCs (E_2 = 3.0 ± 2.7 kPa) [93]. Evidence of an additional peak is also present for both oxygenated and deoxygenated samples at E = 15 kPa and E = 40 kPa, respectively. The

large variation and presence of multiple peaks within the distribution can likely be attributed to patient treatment with hydroxyurea.

Significantly higher Young's modulus values resulting in peaks at E = 15 kPa for oxygenated cells and E = 40 kPa for deoxygenated cells are a result of the presence of polymerized HbS in the RBC samples from SCD patients. At high concentrations, deoxy sickle hemoglobin results in the formation of a seven stranded polymer structure which increases RBC rigidity [164]. Polymerization of deoxygenated HbS is dependent on intraerythrocytic HbS concentration, degree of cell oxygenation, pH, and the intracellular concentration of HbF. Polymerized HbS fibers form noncovalent cross-links and create a gel that results in increased rigidity of RBCs [36, 69-70]. In addition, spectrin, which is the main protein responsible for the mechanical strength of the erythrocyte, has been found to bind to hemoglobin via the Band 3 protein that binds almost exclusively to hemoglobin fibers [152, 165]. Thus, in the deoxygenated state, interaction between the HbS fibers that are connected to the membrane and the HbS fibers in the cytoplasm could also contribute to the measured increase in stiffness [166]. Our data present evidence of a minimal doubling of the Young's modulus upon full deoxygenation of SCD erythrocytes. This can present major problems in SCD patients because rigid sickle RBC can cause microcirculatory obstruction, resulting in vaso-occlusive crisis.

Small Young's modulus values found in the present study for both oxygenated and deoxygenated SCD erythrocytes are likely due to hydroxyurea treatment, a variable in the obtained clinical samples. Hydroxyurea is the only approved medication for the treatment of sickle cell disease in adults; there are no approved drugs for children [7, 77]. Hydroxyurea stimulates the production of fetal hemoglobin (HbF) in patients with SCD, which inhibits sickling [167] by preventing effective contact between adjacent HbS molecules and also by forming

mixed hybrids with HbS that have greater solubility than HbS polymers [77]. Increases in HbF contribute to an increase in total Hb and a decrease in hemolysis with the release of free hemoglobin [7]. It has been proposed that hydroxyurea increases HbF indirectly by killing rapidly dividing late erythroid cells, causing recruitment of more primitive erythroid precursors which in turn produce high levels of HbF, or by acting directly on the primitive precursors thereby stimulating HbF production, the exact mechanism by which hydroxyurea induces HbF is unclear [77].

In summary, the present study suggests a significant impact of deoxy sickle hemoglobin in significantly increasing the rigidity of SCD erythrocytes, thus resulting in vaso-occlusive crisis. Our data conclude that Young's moduli and standard deviations were E_1 = 1.0 kPa ± 1.1 kPa and E_2 = 3.0 ± 2.7 kPa for both oxygenated and deoxygenated SCD erythrocytes. Deoxygenated SCD erythrocytes also possessed an additional peak at E = 40 kPa, while oxygenated SCD erythrocytes possessed an additional peak at the significantly lower value of E = 15 kPa. However, in contrast to normal RBCs and sickle trait RBCs, SCD erythrocytes substantially deviate from the characteristic biconcave shape and possess highly irregular morphologies characterized by protrusions, elongation, bumps, and enlargement associated with aggregation of HbS fibers.

Chapter 4. Sickle Cell Trait Human Erythrocytes Show a Significant Increase in their Stiffness Compared to Erythrocytes from Healthy Individuals

4.1. Abstract

Atomic force microscopy (AFM) allows for high-resolution topography studies of biological cells and measurement of their mechanical properties in physiological conditions. In this work, AFM was employed to measure the stiffness of abnormal human red blood cells (RBCs) from patients with the genotype for sickle cell trait. The determined Young's modulus was compared with that obtained from measurements of erythrocytes from healthy subjects. The results showed that the Young's modulus of pathological erythrocytes was approximately three times higher than in normal cells. Observed differences indicate the effect of the polymerization of hemoglobin S as well as possible changes in the organization of the cell cytoskeleton associated with the sickle cell trait.

4.2. Introduction

Sickle cell disease (SCD) is an inherited blood disorder caused by a single point mutation in one of the genes encoding hemoglobin. Four polypeptide chains, two of type α and two of type β, form the globular protein Hb. In sickle cell hemoglobin (HbS), the normal sequence of *Val-His-Leu-Thr-Pro-Glu-Glu-Lys* is changed to *Val-His-Leu-Thr-Pro-Val-Glu-Lys*, with the amino acid valine substituting for the glutamic acid in the β6 site. The replacement of two charged groups by two hydrophobic ones leads to polymerization of deoxygenated Hb and to formation of long stiff rodlike fibers [33, 35-36] which force RBCs to assume a sickle shape. Other factors such as lowered pH, RBC dehydration and hyperthermia are also known to prompt sickling [52]. Healthy RBCs are very deformable and easily pass through narrow capillaries during their approximately three-month life span. The characteristic biconcave shape of RBCs does not only increase the

surface area and facilitate O_2 and CO_2 diffusion into and out of the cell [59-60] but it has been shown that it is compatible with the increased compliance of the erythrocytes [61]. The abnormal morphology and rheology of the sickle cells triggers the obstruction of the microvasculature which results to the development of hypoxia, vaso-occlusive crisis and organ damage.

SCT has a very significant social impact because approximately three million people in the United States have this genotype, making it 40 to 50 times more prevalent than SCD [46]. People with sickle cell trait do not have the symptoms of SCD [168] and thus SCT is not usually regarded as a disease state because it has complications that are either uncommon or mild [46]. Although SCT is considered to be benign, in extreme conditions including hypoxia, acidosis, dehydration, hyperosmolarity, or elevated erythrocyte 2,3-diphosphoglycerate (DPG), individuals with SCT can develop a syndrome resembling SCD with vaso-occlusive sequelae resulting from rigid erythrocytes [46, 49-50, 56]. Other complications associated with SCT include increased urinary tract infection in women, gross hematuria, complications of hyphema, splenic infarction with altitude hypoxia or exercise, and life-threatening complications of exercise, exertional heat illness (exertional rhabdomyolysis, heat stroke, or renal failure) or idiopathic sudden death [46, 53, 57].

The red cell membrane derives its resilience and resistance to mechanical stresses from the membrane skeleton, a hexagonal lattice network composed of spectrin tetramers. These are formed by the side-by-side alignment of pairs of heterodimers attached at their ends to complexes consisted mainly of actin and of several other proteins [59-60, 169]. Horizontal connections between the spectrin filaments are formed at the actin junctions with proteins such as protein 4.1R, tropomyosin, tropomodulin, and adducing. Vertical connections between the

spectrin network and the lipid bilayer are formed at the ankyrin linkers which connect the β-spectrin filaments to the band 3 protein along with protein 4.2 (pallidin). A second type of vertical connection is formed at the actin junctions where, protein 4.1 binds the spectrin network to the lipid bilayer via the integral protein, glycophorin C [60, 170-171]. Mutations in membrane proteins related to vertical connections cause hereditary spherocytosis related to membrane loss because of reduced support to lipid bilayer. Mutations in proteins associated to horizontal connections cause hereditary elliptocytosis [172].

Normal erythrocytes in adults contain approximately 250 million adult hemoglobin (HbA) molecules, totaling 25-30% of the cell [33]. Sickle cell trait (SCT, sicklemia), in contrast, is marked by the presence of both HbS and HbA. Sickle hemoglobin comprises approximately 20-46% of the total hemoglobin content in persons with sickle cell trait [44], with most individuals having 40-42% HbS [45]. In the case of SCD, it has been hypothesized that increased association of HbS with the membrane proteins contributes in the change of the mechanical behavior of Sickle cells [149]. HbS could alter the mechanical properties of RBCs not only by extending the spectrin filaments, and by the interaction between HbS filaments and the lipid bilayer but also by altering the functionality of the membrane proteins [150]. There is considerable evidence that HbS is associated with the inner membrane of RBCs and in particular with the cytoplasmic tail of the band 3 protein [33].

Many case studies have shown that translation of cellular mechanics findings is crucial in many diseases, including Alzheimer's disease, Parkinson's disease, type II diabetes, malaria, sickle cell disease, and most recently cancer [144, 147]. Understanding the relationship between proteins and cellular material properties will allow for detection of diseases and new approaches to addressing medical disorders [147]. Recently, atomic force microscopy methods have shown

that the stiffness of metastatic cancer cells is more than 70% softer than their benign counterparts [144]. Because these findings correlate well with the commonly employed immunohistochemical testing, it is reasonable to argue that AFM methods can enhance cancer detection methods. SCD is a characteristic case where molecular changes in a protein alter their structural properties causing the initiation of a disease state. Additional reason for the SCD is the increased adherence of sickle cells on the endothelial cells and on leucocytes which can generate an inflammation and chronic vasculopathy [34]. AFM can return information not only on the stiffness of the cells but also on the specific interaction between proteins expressed on the cellular erythrocyte membrane and proteins expressed on leucocytes, on endothelial cells and/or the extracellular matrix [34]. Because of this characteristic, AFM could decisively enhance our knowledge on the biology and consequently on the therapy of SCD.

Characterization of erythrocyte mechanical properties has been conducted via micropipette aspiration [173-174], cell poking [175], atomic force microscopy [111-112, 117], optical tweezers [176-177], optical stretching [177-178], and magnetic tweezers [119], and magnetic twisting cytometry [179]. However, values of mechanical moduli derived from experimental data tend to vary largely based on which of the aforementioned techniques is used [180]. In the present student, we quantified the stiffness of erythrocytes from patients with the genotype for sickle cell trait using atomic force microscopy, a tool for imaging and characterization of materials at the nanometer scale [89]. The high force sensitivity of AFM and its ability to measure local and overall properties of individual cells under physiological conditions make this technique particularly appropriate for measuring the mechanical properties of living and fixed cells [101, 112, 117, 181-182]. We established that the stiffness of cells from patients with the genotype for SCT was approximately three times greater than normal RBCs.

4.3. Methods

AFM allows for high-resolution topography studies of biological cells and measurement of their mechanical properties in physiological conditions [183]. Experiments were carried out using an Asylum MFP 3D-BIO (Asylum Research, Santa Barbara, CA) AFM equipped with a “liquid cell” setup. Normal RBCs and RBCs from patients with the sickle cell trait were purchased from Research Blood Components, LLC (Brighton, MA). RBCs were maintained in PBS at room temperature during experiments.

Erythrocyte immobilization

Cells were immobilized on AFM grade mica (Novascan Technologies, Inc., Ames, IA) coated with poly-L-lysine (PLL) (Sigma-Aldrich, St. Louis, MO) to increase cell adherence. 150 µl of 1 mg/ml PLL solution was allowed to adsorb for 5 min to an unmodified mica surface, and excess solution was drained away. RBCs of 0.5% concentration in PBS were allowed to adhere to each PLL-coated mica surface for 10 min in the incubator. Unattached cells were removed by gentle rinsing of the slide with PBS solution at 25°C. For imaging, fixation was performed by a 1-min treatment of the cells with 0.5% glutaraldehyde (Sigma-Aldrich, St. Louis, MO) in PBS buffer. The sample was again rinsed several times with PBS and a volume of PBS was added for experiments. Glutaraldehyde was not employed for stiffness measurements.

Erythrocyte imaging

Erythrocytes were imaged in tapping mode with a scan rate of 0.2 Hz, and the minimal force necessary to obtain good image contrast was determined by gradually increasing the force applied to the sample from zero force (noncontact) to the necessary minimal force. Silicon nitride probes with a nominal spring constant of 0.01 N/m (Veeco Probes, Camarillo, CA) were employed for imaging. While the characteristic biconcave shape was observed for the fixed

normal erythrocyte (Figure 4.3.1A) the SCT erythrocyte appeared to have an irregular biconcave shape accompanied by a decrease in size which is most likely due to dehydration associated with the polymerization of HbS (Figure 4.3.1B).

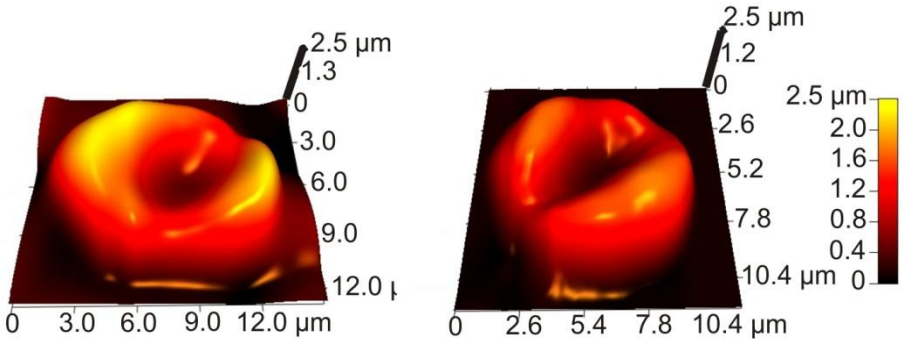

Figure 4.3.1. Three-dimensional topographical images of RBCs from a (A) normal subject and (B) a patient with the SCT genotype measured by AFM. While the normal RBC has the characteristic biconcave shape, the SCT erythrocyte has an irregular biconcave morphology. In addition, the SCT erythrocyte is smaller than the normal erythrocyte, most likely due to dehydration associated with HbS polymerization.

Cell stiffness determination

Stiffness measurements were carried out in contact mode using silicon nitride cantilevers with a nominal spring constant of 0.03 N/m (Veeco Probes, Camarillo, CA). Exact values for the cantilever spring constants were obtained via a thermal noise based method implemented by the manufacturer and were used in all calculations. Probes had nominal tip radii of 20 nm and nominal angle of 20°, as provided by the manufacturer. The force curves were generated at a loading rate of 10,000 pN/s, and for each cell type between 500-600 measurements were collected.

The Young's modulus was calculated using the Hertz model describing the elastic deformation of the two bodies in contact under load. This theory was extended by Sneddon assuming an

appropriate shape of indenter deforming elastic half space [107, 110]. It characterizes the relationship between the applied force and the indentation depth [142, 184]. When the shape of the AFM tip is a four-sided pyramidal indenter, the force as a function of indentation is described by the following equation:

$$F = \frac{3E \tan\theta}{4(1-\nu^2)}\delta^2 \qquad (1)$$

where E and ν are the Young's modulus and the Poisson's ratio of the cell, respectively [102, 114-115]. The Poisson ratio used in the present study was assumed to be 0.5 [111].

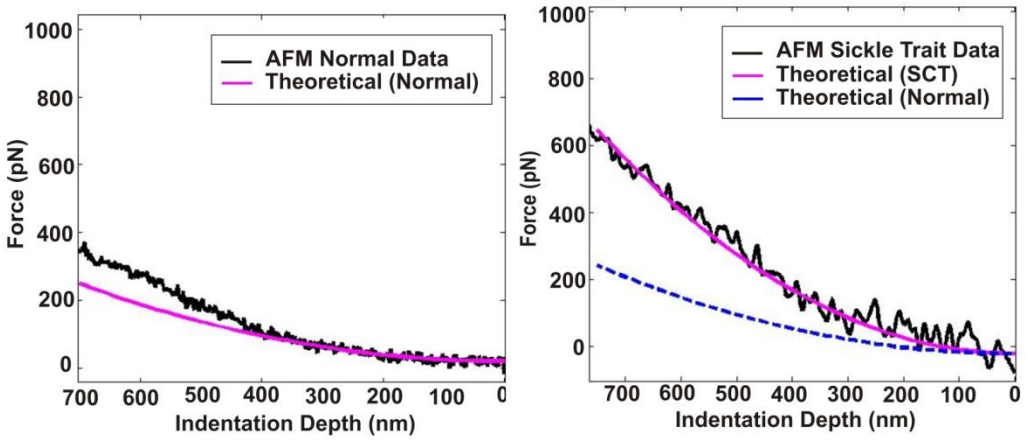

Figure 4.4.1. Theoretical model for a pyramidal shaped indenter fitted to the experimental data for normal and SCT erythrocytes obtained via AFM. In these curves, the Young's modulus values for the normal and SCT cell are 1.30 and 3.30 kPa, respectively. The curves shown above are representative of the 500-600 force curves obtained for each normal and SCT erythrocytes. Minor variations can be seen in other curves obtained during experimentation, representative of the standard deviation we observe in the calculation of the Young's modulus.

4.4. Results

Determination of the indentation depth

The quantitative determination of the elastic properties of a particular material can be obtained from the relationship between the applied force F and the indentation depth δ using Eq. (1). When force is measured on a hard substrate, the cantilever deflection is proportional to the relative sample position resulting in a linear slope for the portion of the curve where the tip and the sample are in contact. When soft samples like erythrocytes are investigated, the recorded cantilever deflection as a function of the relative sample position is not linear due to the deformable structure of the RBC. Prior to taking force measurements on the RBC surface, the force is measured on the PLL-coated mica substrate. This curve is used as calibration curve since no permanent sample deformation is observed.

The indentation produced by the AFM tip was determined by subtracting the calibration curve from the curve recorded for the erythrocyte using the Igor Pro 6.04 (Wavemetrics, Portland, OR) software program. The force vs. indentation curves obtained for normal erythrocytes indicate a greater compliance than that of the sickle trait RBCs.

Data processing

Data was imported into MATLAB (The MathWorks, Natick, MA) and the value of E was obtained by fitting the theoretical curve generated by Eq. (1) to the experimental data up to a minimum depth of 250 nm, which is approximately 10% of the total thickness of the cell. The method is in agreement with the well known fact that the effect of the substrate over which the cells are placed is negligible if the indentation depth is less than 10% of the total thickness of the specimen [117]. Figure 4.4.1 shows the MATLAB output of the pyramidal indenter model fit

to the force v. indentation curve obtained via experimentation. It appears that the theoretical model for a pyramidal indenter fits the SCT data up to a greater indentation depth (700 nm) than that of the normal RBC (400 nm), indicating that SCT follow the elastic model for larger indentation depth.

The average values of Young's modulus for normal erythrocytes and SCT erythrocytes were obtained by fitting the Gaussian distribution to the generated histograms of the measured Young's modulus values (Figure 4.4.2A-B, respectively). The measured Young's moduli and standard deviations were: E_1 = 1.10 kPa, σ_1 = 0.40 kPa, and E_2 = 3.05 kPa, σ_2 = 1.09 kPa, for normal and sickle cell trait, respectively.

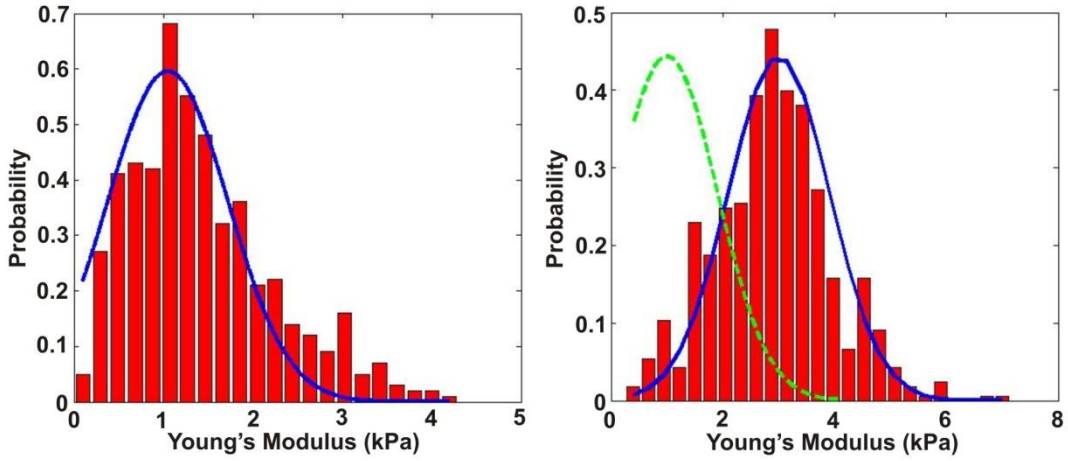

Figure 4.4.2. Histograms of the Young's modulus determined for RBCs from (A) normal and (B) sickle cell trait blood samples. The Young's modulus values obtained from fitting the theoretical model to the experimental data were fitted with the Gaussian distribution. Normal RBCs are more elastic and their Young's modulus values have a lesser standard deviation (E_1 = 1.10 kPa, σ_1 = 0.40 kPa) while SCT erythrocytes have a stiffness approximately three times greater as well as a larger standard deviation (E_2 = 3.05 kPa, σ_2 = 1.09 kPa). The observed increase in stiffness for the pathological erythrocytes is likely due to changes in the affinity of spectrin and actin filaments resulting from the presence of abnormal hemoglobin, HbS.

4.5. Discussion

The main goal of this work was the determination of the erythrocyte's stiffness in blood samples taken from patients with the sickle cell trait genotype. The obtained Young's modulus of erythrocytes from patients with SCT was approximately three times larger than that of normal erythrocytes.

Hemoglobin S is responsible for converting normal RBCs into "sickled" cells in patients with SS-SCD. At high concentrations, deoxy sickle hemoglobin results in the formation of a seven stranded polymer structure which increases RBC rigidity [164]. As expected, we observe the characteristic biconcave shape for normal erythrocytes (Figure 4.3.1a) when imaging on a PLL-coated mica substrate. In contrast, due to an increased membrane stiffness and dehydration, the sickle trait RBC digresses from its characteristic biconcave shape (as shown in Figure 4.3.1b) and also experiences a decrease in size.

Our findings show that the Young's modulus of normal erythrocytes is 1.10 kPa with a standard deviation of 0.40 kPa, while erythrocytes from patients with the genotype for sickle cell trait have a Young's modulus of 3.05 kPa with a standard deviation of 1.09 kPa. Other techniques, such as micropipette aspiration and optical tweezers, result to RBC moduli values in similar range [154, 174, 185]. AFM has previously been used in the measurement of the Young's modulus of various types of cells e.g., platelets (1-50 kPa), lymphocytes (1.24 kPa), fibroblasts (1-5 kPa), mesenchymal stem cells (1-2.5 kPa) and osteoblasts (1-200 kPa) [143, 157-163].

The threefold increase in the stiffness of SCT erythrocytes is probably due to changes in the affinity of the spectrin and actin filaments that comprise the membrane skeleton. It has been

proposed that SCT erythrocytes show an increased concentration in Ca^{+2} which results in a higher cytoskeleton rigidity via an increased binding of Band 3 to the spectrin bound ankyrin [186-187]. Another possible source of the measured increased stiffness is the dehydration of the SCT erythrocytes that promotes polymerization of deoxygenated HbS [188-189]. It has been shown that activation of the Gardos channel by an increase of the intracellular free Ca^{+2} concentrations results to expulsion of potassium and H_2O. In addition, spectrin which is the main protein responsible for the mechanical strength of the erythrocyte has been found to bind to hemoglobin via the Band 3 protein that binds almost exclusively to hemoglobin fibers [152, 165]. Thus, interaction between the HbS fibers that are connected to the membrane and the HbS fibers in the cytoplasm could also contribute to the measured increase in stiffness [166].

In summary, the present study suggests that sickle hemoglobin promotes a threefold increase in the stiffness of sickle trait erythrocytes. Our data conclude that Young's moduli and standard deviations were E_1 = 1.10 kPa, σ_1 = 0.40 kPa, and E_2 = 3.05 kPa, σ_2 = 1.09 kPa, for normal and sickle trait erythrocytes, respectively. In contrast to normal RBCs with a characteristic biconcave shape, SCT erythrocytes deviate from this configuration with irregularities in the expected morphology and a decrease in both diameter and height.

Chapter 5. Dietary Supplementation with Docosohexanoic Acid (DHA) Increases Red Blood Cell Membrane Flexibility in Mice with Sickle Cell Disease

5.1. Abstract

Humans and mice with sickle cell disease (SCD) have stiff red blood cells (RBCs). Omega-3 fatty acids, such as docosahexanoic acid (DHA), may influence RBC deformability via incorporation into the RBC membrane during dietary supplementation. In this study, sickle cell (SS) mice were fed natural ingredient rodent diets supplemented with 3% DHA (DHA diet) or a control diet matched in total fat (CTRL diet). After 8 weeks of feeding, we examined the RBCs for: 1) stiffness, as measured by atomic force microscopy; 2) deformability, as measured by ektacytometry; and 3) percent irreversibly sickled RBCs on peripheral blood smears. Using atomic force microscopy, stiffness is increased and deformability decreased in RBCs from SS mice fed CTRL diet compared to wild-type mice. In contrast, RBCs from SS mice fed DHA diet had markedly decreased stiffness and increased deformability compared to RBCs from SS mice fed CTRL diet. Furthermore, examination of peripheral blood smears revealed less irreversibly sickled RBCs in SS mice fed DHA diet as compared to CTRL diet. In summary, our findings indicate that DHA supplementation improves RBC flexibility and reduces irreversibly sickled cells in SS mice. These results point to potential therapeutic benefits of dietary omega-3 fatty acids in SCD.

5.2. Introduction

Individuals with sickle cell disease (SCD) exhibit increased red blood cell (RBC) stiffness and adhesion, multiorgan and vascular pathology, and complex pain syndromes [12, 122, 190-198]. In addition, there is evidence of activation of the inflammatory and coagulation pathways [80,

199-204]. Berkeley sickle cell (SS) mice exclusively express human sickle hemoglobin and have a phenotype that mimics many features of severe SCD in humans [205-207].

Omega-3 fatty acids, such as docosahexanoic acid (DHA), are essential fatty acids that have anti-inflammatory and anti-thrombotic activities [208-210]. As dietary supplements, omega-3 fatty acids are beneficial in many cardiovascular diseases [208-209, 211-213]. In addition, Ren et al [214-216] demonstrated that humans with SCD have decreased omega-3 fatty acids and increased arachidonic acid (AA, an omega-6 fatty acid) in the RBC membrane. To date, trials in humans with SCD have indicated that dietary supplementation with omega-3 fatty acids may reduce severe anemia, vaso-occlusive pain episodes, white blood cell count, and prothrombotic activity [217-219].

Several studies have demonstrated that dietary supplementation with omega-3 fatty acids results in increased incorporation of these fatty acids into the RBC membrane, which can influence RBC deformability [220-221]. In the present study, we sought to determine whether dietary supplementation with the omega-3 fatty acid DHA would improve RBC stiffness and other hematologic and disease parameters in SS mice. Our results indicate that 8-week dietary supplementation with DHA increases RBC flexibility and decreases irreversibly sickled RBCs in SS mice.

5.3. Methods

Mice

C57BL/6J mice (hereafter, WT mice) were purchased from The Jackson Laboratory (Bar Harbor, ME; stock number 000664). Berkeley SCD mice (Tg(Hu-miniLCR$\alpha 1^{G}\gamma$ $^{A}\gamma\delta\beta^{S}$) *Hba*^{0}*//Hba*^{0} *Hbb*^{0}*//Hbb*^{0}; hereafter, SS mice) on the Berkeley mixed genetic background have

been previously described [205-206]. Mice were cared for according to AAALAC specifications. Animal experiments were approved by the Institutional Animal Care and Use Committee of the Medical College of Wisconsin. Experimental groups contained comparable numbers of male and female mice; the average age of mice when placed on diets was 27 wks (range 14 - 36 wks).

Table 5.3.1. Fatty Acid Composition

Fatty Acid	CTRL Diet	DHA Diet
Saturated, % of total fatty acids	32	29
Monounsaturated, % of total fatty acids	19	22
Polyunsaturated, % of total fatty acids	48	49
Fatty acid profile, % of total fatty acids		
C8:0 Caprylic	1.0	0.0
C10:0 Capric	1.1	0.9
C12:0 Lauric	5.4	3.6
C14:0 Myristic	4.4	9.9
C16:0 Palmitic	13.8	12.8
C16:1 Palmitoleic	0.4	1.1
C18:0 Stearic	4.7	1.2
C18:1 Oleic	18.1	20.1
C18:2 Linoleic	47.0	18.0
C18:3 Linolenic	1.3	1.2
C22:6 DHA	0.0	30.1
Predominant fatty acid	18:2 linoleic acid	22:6 DHA
Energy Density, kcal/g	3.5	3.5

Dietary Feeding

Mice were fed natural ingredient 2016 Teklad Global 16% Protein Rodent Diet supplemented with 3% DHA, an omega-3 fatty acid (DHA diet), or a control diet supplemented with safflower oil, which predominantly contains the omega-6 fatty acid linoleic acid (CTRL diet) (Table 5.3.1). The macronutrient composition of the CTRL and DHA diets is shown in Table 5.3.1. Diets were

matched in total fat and had a similar distribution of saturated/monounsaturated versus polyunsaturated fatty acids (Table 5.3.1). Detailed information on the base 2016 Teklad Global 16% Protein Rodent Diet can be found at http://www.harlan.com/products_and_services/research_models_and_services/laboratory_animal_diets/teklad_natural_ingredient_diets/teklad_global_diets/global_rodent_diets/teklad_global_rodent_diet_16_protein_2016.hl#Macronutrient_Information. DHA oil was a kind gift from Martek Biosciences (a division of DSM Nutritional Products, Columbia, MD). DHA and CTRL diets were designed in consultation with nutritionists at Harlan-Teklad Laboratories and diets were compounded at Harlan-Teklad Laboratories (Madison, WI). Mice were weighed prior to being placed on CTRL or DHA diet, fed their respective diets for 8 weeks, and then weighed again prior to harvest. No significant differences in weight gain were observed between CTRL and DHA diet groups (data not shown).

CBC and reticulocyte measurements

Blood was obtained from deeply anesthetized mice by cardiac puncture and drawn into heparin anticoagulant. Complete blood count (CBC) and reticulocyte analyses were performed as previously described [222].

Flow adhesion assay

RBCs were separated from whole blood and washed twice in citrate/glucose/saline buffer as previously described [122, 223]. Washed RBCs were resuspended at a 2% hematocrit in M199 serum free medium (Sigma, St. Louis, MO) containing 0.2% bovine serum albumin (Sigma, St. Louis, MO). RBC adhesion to immobilized thrombospondin (TSP, 1 μg/75 μl) was carried out using Vena8 Fluoro Biochips on the VenaFlux Platform (Cellix, Dublin, Ireland). RBCs were perfused through the channel at a wall shear stress of 0.4 dyne/cm^2, and adherent RBCs manually quantified by analyzing five different images captured from the middle of the channel.

Atomic Force Microscopy

Whole blood was collected as described above and stored overnight at 4^{o}C. RBCs were sedimented by centrifugation at 500 x *g* at 4°C for 10 minutes and the plasma, buffy coat, and uppermost erythrocytes removed by aspiration and discarded. The remaining erythrocytes were washed three times in Cell Wash Buffer (21.0 mM tris (hydroxymethyl)aminomethane, 4.7 mM KCl, 2.0 mM $CaCl_2$, 140.5 mM NaCl, 1.2 mM $MgSO_4$, 5.5 mM glucose, 0.5% bovine serum albumin (BSA) fraction V; pH 7.4) [224]. Cells were immobilized on a glass surface coated with 1 mg/ml poly-L-lysine solution for 10 min in the incubator (37°C, 5% CO_2). Unattached cells were removed by gentle rinsing of the surface with Cell Wash Buffer. Cells were prepared on the day of use and experiments were performed in Cell Wash Buffer maintained at 37°C.

Stiffness measurements were carried out as previously described [93] on non-fixed adhered erythrocytes. All force measurements were recorded with a loading rate of 24000 pN/s for small indentation depths up to 150 nm and small indentation forces up to 300 pN [101, 112, 117]. The Young's modulus was calculated using the Hertz model which describes the elastic deformation of two bodies in contact under load, in this case the contact between the erythrocyte and the AFM probe. Further detail regarding AFM measurements and calculations is found in Supplemental Methods. Five mature RBCs were evaluated for stiffness measurements from each mouse; reticulocytes were excluded based on their larger size [225].

Ektacytometry

Red cell membrane deformability was assessed by ektacytometry as described previously [226], using a Technicon model 152 Ektacytometer (Spectra Physics, France) at Purdue University. Whole blood was collected as described above and stored overnight at 4^{o}C, followed by centrifugation at 1000 x g for 3 min to pellet RBCs. Packed RBCs were washed twice with Cell

Wash Buffer lacking BSA, then resuspended at 0.3% hematocrit in isoosmotic sample buffer (136mM NaCl, 6.3mM Na_2HPO_4, 1.2mM NaH_2PO_4) containing ~4% polyvinylpyrrolidone (PVP). Samples were loaded into the ektacytometer and subjected to increasing shear stresses (0-250 dynes/cm^2, increased linearly over 125s) at constant osmolarity. The deformation of the cells was quantified by laser diffraction as elongation index (EI) which was recorded as a function of time. RBCs from each mouse were analyzed in duplicate ektacytometer runs, and the overall RBC deformability for each mouse was determined from the average maximum EI of the duplicate trials.

Quantification of Irreversibly Sickled RBCs

Blood smears were prepared on glass slides using anticoagulated whole blood. Unstained smears were examined using a Nikon Eclipse 80i microscope and fields of well-separated RBCs selected for photography using a Nikon Digital DS-Fi1 camera. The total number of RBCs in each field and the number of irreversibly sickled RBCs, defined as having a length greater than 2-fold its width [227], were enumerated by manual counting. Five representative fields were examined and the average percent of irreversibly sickled RBCs was determined for each mouse.

Statistics

GraphPad Instat or GraphPad Prism were used for all statistical analyses. For data that passed tests for normality, unpaired t-tests were used, with Welch's correction applied when comparing populations with unequal SDs. For data that were not normally distributed, nonparametric Mann-Whitney U-tests were used for comparisons of two groups. Kruskal-Wallis nonparametric ANOVA with Dunn's Multiple Comparisons Post-Hoc Test was used for comparisons of more than two groups. $P<0.05$, with corrections for multiple comparisons when appropriate, was considered significant.

5.4. Results

DHA supplementation decreases RBC stiffness in SCD mice

Atomic force microscopy (AFM) was used to assess RBC stiffness of mature RBCs in wild-type (WT) and SS mice after 8-week dietary feeding on CTRL or DHA diets. RBC stiffness is comparable in WT mice fed either CTRL or DHA diets (Figure 5.4.1A, left panel, representative WT-CTRL and WT-DHA mice; Figure 5.4.1C, group data). RBC stiffness in WT-CTRL and WT-DHA mice is similar to that seen in WT mice fed a standard fat diet (Figure 5.4.1A, right panel, representative WT mouse on standard Teklad Global 2016 diet; Figure 5.4.1C, group data), indicating that the increased fat composition of the diets used in this study does not alter normal RBC stiffness.

In comparison to WT RBCs, RBC stiffness is increased in SS mice fed CTRL diet (Figure 5.4.1B, left panel, filled bars, representative SS-CTRL mouse; Figure 5.4.1C, group data, $P<0.001$ vs. WT-2016, WT-CTRL, or WT-DHA). RBC stiffness in SS-CTRL mice is comparable to that obtained from SS mice fed a standard fat diet (Figure 5.4.1A, right panel, representative SS mouse on standard Teklad Global 2016 diet; Figure 5.4.1C, group data), indicating that the increased fat composition of the CTRL diet is not the cause of increased RBC stiffness in CTRL diet-fed SS mice. In addition, since only mature RBCs were assessed for RBC stiffness measurements, the observed difference in RBC stiffness between SS and WT mice is not influenced by the higher presence of reticulocytes in SS as compared to WT blood samples. In marked contrast, RBCs from DHA diet-fed SS mice had decreased stiffness compared to RBCs from CTRL diet-fed SS mice (Figure 5.4.1B, open bars, representative SS-DHA mouse; Figure 5.4.1C, group data, $P<0.001$ vs. SS-CTRL or SS-2016). In fact, RBC stiffness in SS-DHA mice was decreased to nearly WT levels (Figure 5.4.1C, P value is not significant for SS-DHA vs.

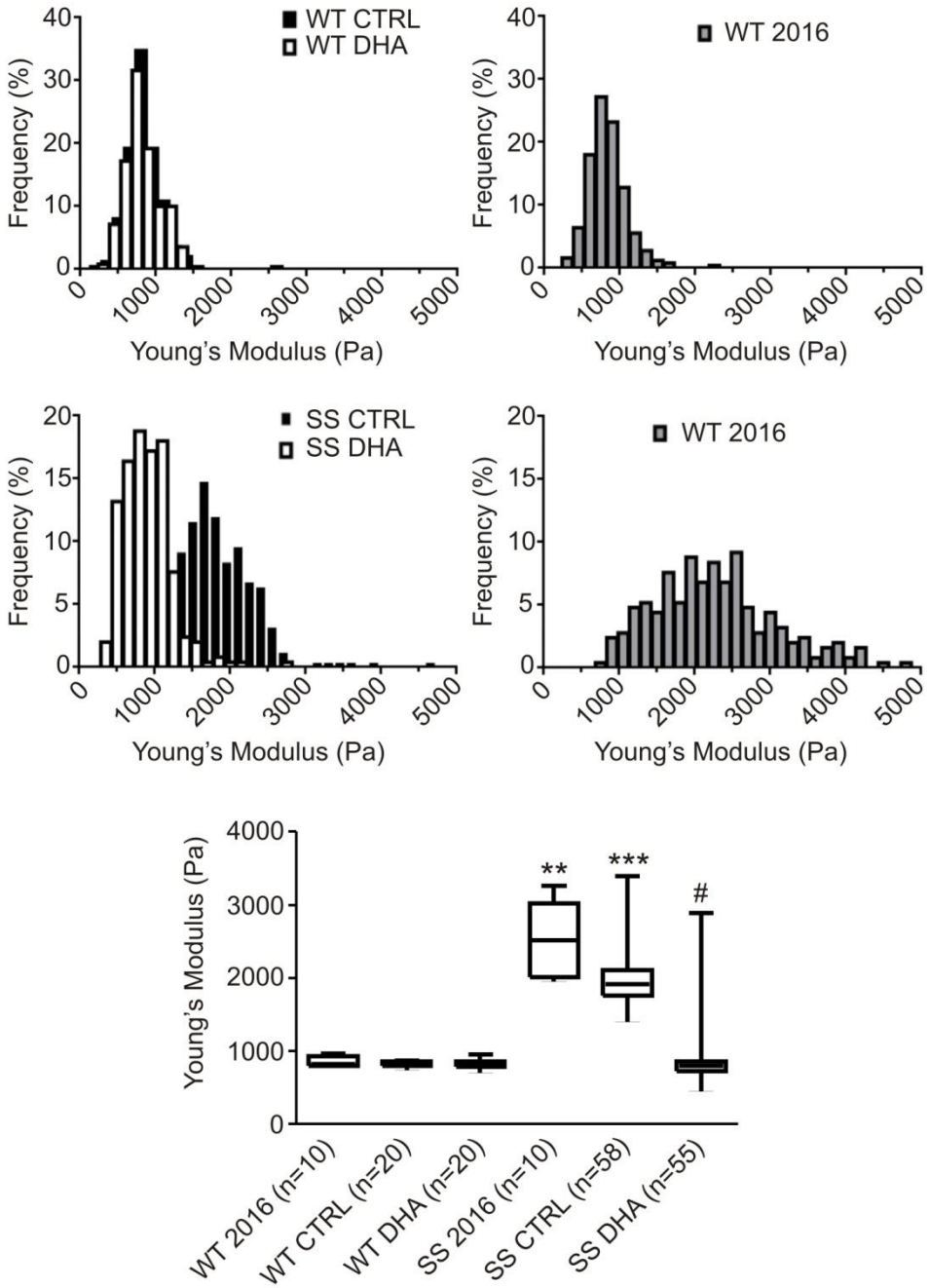

Figure 5.4.1. Dietary supplementation with DHA decreases RBC stiffness in SS mice. (A, B): Representative results from individual wild-type (WT) (A) and sickle (SS) (B) mice fed either: left panels: CTRL (filled bars) or DHA (open bars) diet; right panel: Teklad Global Diet 2016 standard fat diet (grey bars; "2016"). Data are presented as Gaussian histograms of the frequency of measurements versus the Young's modulus in Pascals (Pa). (C): Box-Whisker plot of Young's modulus from the groups indicated on the X axis. Data are presented as median with max and min whiskers. The 'n' indicated on X-axis indicates the total number of mature RBCs analyzed in each group, obtained from the following numbers of mice: WT-2016: 2 mice; WT-

CTRL and WT-DHA: 4 mice; SS-2016: 2 mice; SS-CTRL: 12 mice; SS-DHA: 11 mice. Statistical comparisons by Kruskal-Wallis nonparametric ANOVA with Dunn's Multiple Comparisons Post-Hoc Test: **, P<0.001 SS-2016 vs. WT-2016, WT-CTRL, or WT-DHA; ***, P<0.01 SS-CTRL vs. WT-2016, and P<0.001 SS-CTRL vs WT-CTRL or WT-DHA; #, P<0.001 SS-DHA vs. SS-2016 or SS-DHA. All other differences (including SS-DHA vs. WT-2016, WT-CTRL, or WT-DHA) are not significant.

Table 5.4.1. Red blood cell and reticulocyte measures

Group	Diet	Hgb, g/dL	Hct, %	MCV, fl	MCHC, g/dL	Retic, %
WT	CTRL	13.3±0.6	41.2±2.5	45±1	32.2±1.6	ND
	DHA	12.6±0.6	40.5±2.5	45±1	31.1±1.0	ND
SS	CTRL	5.0±1.1	15.0±3.3	45±4	33.8±4.4	60±16
	DHA	5.0±1.1	16.1±3.7	48±6	31.4±2.9	41±18[†]

All values mean±SD. ND, not determined; retic (reticulocytes) is given as % of total RBCs. WT-CTRL, n=10; WT-DHA, n=11. SS-CTRL, n=18 for Hgb/Hct/MCV/MCHC and n=7 for Retic; SS-DHA, n=22 for Hgb/Hct/MCV/MCHC and n=9 for Retic. No significant differences between WT-CTRL and WT-DHA or between SS-CTRL and SS-DHA groups for Hgb, Hct, MCV or MCHC after correcting for multiple comparisons. [†]Difference in retic % between SS-CTRL and SS-DHA groups is not significant but trending towards a decrease in SS-DHA mice (P=0.051).

WT-2016, WT-CTRL, or WT-DHA). Analysis of hematologic parameters revealed no statistically significant differences in red blood cell or reticulocyte parameters in CTRL versus DHA diet groups, although there was a trend (P=0.051) towards decreased reticulocytes in SS-DHA as compared to SS-CTRL mice in the small sample subset analyzed (Table 5.4.1).

DHA supplementation improves RBC deformability in SCD mice

To verify the decrease in RBC stiffness seen by AFM, deformability of RBCs from a subset of SS mice fed CTRL or DHA diets was examined using ektacytometry. Consistent with other studies [228-233], RBCs from SS mice fed CTRL diet exhibit low deformability by ektacytometry as compared to RBCs from WT mice (Figure 5.4.2; WT data for comparison only). Similar to the AFM results, RBCs from SS mice fed DHA diet had improved deformability compared to RBCs

from SS mice fed CTRL diet (Figure 5.4.2, P<0.02).

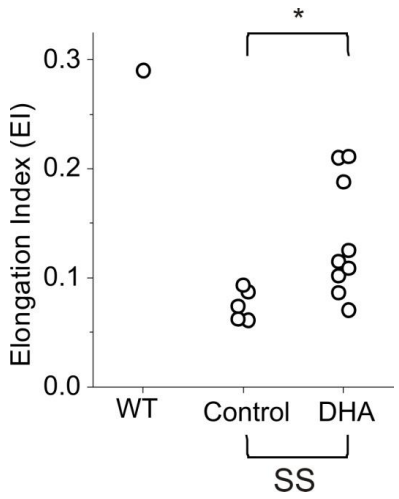

Figure 5.4.2. Dietary supplementation with DHA increases RBC deformability in SS mice. Scatter plot of average maximum Elongation Index (EI) for SS mice fed CTRL (SS-CTRL, n=5) or DHA (SS-DHA, n=9) diets. Each symbol represents the maximum EI (average of two replicates) for an individual mouse; horizontal line represents mean for each SS diet group. WT data average of two samples from normal mice fed standard diet, and is shown for comparison only. *, P<0.05, SS-CTRL vs. SS-DHA, unpaired t-test with Welch correction.

DHA supplementation decreases irreversibly sickled RBCs in SCD mice

Both AFM and ektacytometry indicated increased RBC flexibility in SS mice fed DHA diet, suggesting a change in RBC membrane properties. RBC adhesion is known to be elevated in human and murine SCD, and has been attributed to multiple factors including altered membrane properties [122, 124, 197, 234-235]. In addition, repeated cycles of sickling of RBCs results in cytoskeletal damage and membrane changes that eventually become permanent, leading to the appearance of “irreversibly sickled RBCs” with altered shape even in the presence of oxygenated sickle hemoglobin [227, 236].

Therefore, we next examined whether there was a decrease in: 1) *in vitro* RBC adhesion; or 2)

numbers of irreversibly sickled RBCs in SS-DHA as compared to SS-CTRL mice. While the mean RBC adhesion to thrombospondin *in vitro* was reduced in DHA as compared to CTRL diet fed SS mice, this difference was not significant in the small number of samples examined (Figure 5.4.3A). In contrast, enumeration of irreversibly sickled RBCs from blood smears revealed a notable decrease in irreversibly sickled RBCs in SS-DHA as compared to SS-CTRL mice (Figure 5.4.3B, $P<0.04$). These data suggest that the improvement in RBC membrane flexibility after 8 weeks of dietary DHA supplementation decreases the cytoskeletal and membrane damage that leads to irreversibly sickled RBCs.

5.5. Discussion

The results of our studies indicate that 8-week dietary supplementation with DHA improves RBC flexibility and decreases irreversibly sickled RBCs in sickle cell mice. The complete normalization of RBC stiffness (Figure 5.4.1) as compared to only partial improvement in RBC deformability (Figure 5.4.2) is not completely surprising. Since deformability reflects not only cell stiffness but also hydration status [226, 237], the lack of complete normalization of RBC deformability in SS-DHA mice may reflect the improvement in RBC stiffness without a concomitant improvement in RBC hydration. In addition, only individual mature RBCs were evaluated for stiffness by AFM, while deformability measurements involve the assessment of a population of erythroid cells, which in SS mice includes ~40% reticulocytes. Therefore, it is also possible that the difference in the AFM versus ektacytometry results reflects incorporation of DHA into erythroid membranes with effects that are more pronounced in mature RBCs than in reticulocytes.

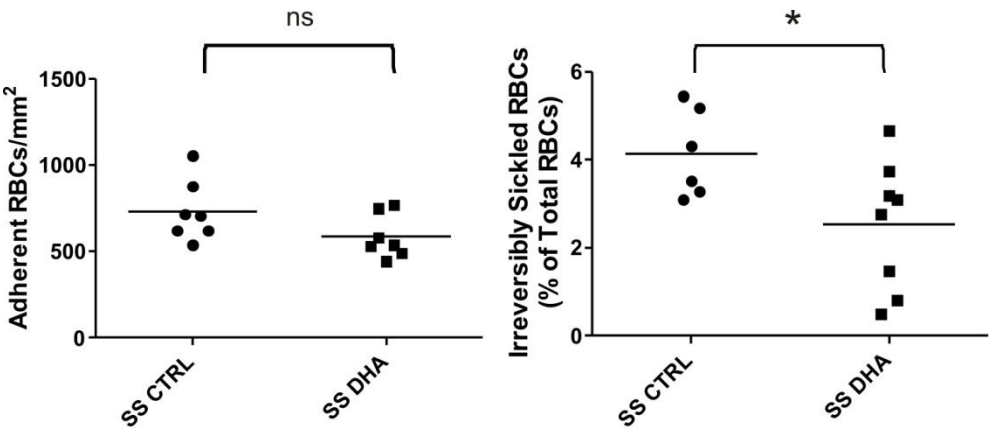

Figure 5.4.3. Dietary supplementation with DHA does not affect *in vitro* adhesion to TSP but decreases irreversibly sickled RBCs in SS mice. (A) Scatter plot of adhesion of washed RBCs from SS-CTRL (n=7) or SS-DHA (n=7) mice to human thrombospondin (TSP, 1 μg/75 μl) at a wall shear stress of 0.4 dyne/cm^2. Adherent RBCs per unit area were quantified as described in Methods. Each symbol represents an individual mouse; horizontal line represents mean for each group. (B) Scatter plot of percent irreversibly sickle RBCs in SS-CTRL (n=6) and SS-DHA (n=8) mouse groups. Each symbol represents an individual mouse; horizontal line represents mean for each group. ns, not significant SS-CTRL vs. SS-DHA, unpaired t-test; *, P<0.05, SS-CTRL vs. SS-DHA, unpaired t-test.

There are several potential avenues through which DHA supplementation could improve RBC flexibility in SS-DHA mice. Ren et al have demonstrated that humans with SCD have decreased omega-3 fatty acids and increased arachidonic acid (AA, an omega-6 fatty acid) in the RBC membrane [214-215]. It is known that omega-3 and omega-6 fatty acids compete for incorporation into the phospholipids of the erythrocyte membrane [238], suggesting that DHA is replacing AA in the RBC membrane in SS mice. Increasing the degree of unsaturation for a given phospholipid influences membrane fluidity less than increasing phospholipid content itself [239], indicating that the improvement in RBC membrane flexibility in SS-DHA mice is not primarily the result of the increased degree of unsaturation of DHA (22:6, n-3) compared to AA (20:4, n-6) or linoleic acid (18:2, n-6; the major fatty acid in the CTRL diet). However, DHA in phospholipid bilayers possesses higher stability toward non-enzymatic lipid peroxidation than AA or linoleic acid, which may also contribute to membrane stability [240].

In addition, omega-3 and omega-6 fatty acids can interact and react with the same receptors

and enzymes with divergent physiologic effects [239]. For instance, 15-lipoxygenase-1 (15-LOX-1) is activated after erythroblast enucleation and is instrumental in initiating the degradation of mitochondria in maturing reticulocytes [241]. Using AA as substrate, 15-LOX-1 produces the pro-inflammatory, pro-oxidant molecules 15-hydroxyeicosatetranoic acid (15-HETE) and lipoxins A4 and B4 [239]. In contrast, if DHA is the substrate, 15-LOX produces docosatrienes and protectins, which are anti-inflammatory and protect from oxidative stress [239]. Furthermore, dietary supplementation with omega-3 versus omega-6 fatty acids leads to enhanced transcription of antioxidant enzymes and suppressed transcription of enzymes that produce reactive oxygen species [239]. There is also increased activity of RBC catalase and lowered malondialdehyde levels in rat RBCs after dietary supplementation with omega-3 fatty acids [242]. Taken together, this suggests greater protection from RBC lipid peroxidation and oxidative injury. Finally, supplementation with omega-3 fatty acids influences the acylation of proteins and functions of ion channels, which can alter intracellular calcium, membrane flexibility, protein-protein interactions, and catalytic activity of enzymes [239].

To date, studies of omega-3 fatty acids in human SCD showed a decrease in acute painful/vaso-occlusive episodes [217-219], but have not carefully assessed the effect of DHA on sickle RBC structural and functional characteristics. Although individuals with SCD are known to have increased daily pain and allodynia [194], effects of omega-3 fatty acid supplementation on chronic or neuropathic pain in SCD have not been reported. SS mice are also known to exhibit nociceptive sensitivities at steady state that are exacerbated by acute sickling [207].

In summary, our findings indicate that DHA supplementation improves RBC membrane flexibility and reduces irreversibly sickled cells in SS mice. The current studies evaluated RBCs in SS mice at steady-state. The increased RBC flexibility and decrease in irreversibly sickled RBCs found in our studies at steady state suggest that the RBCs in SS-DHA mice may be more

resistant to an acute sickling event and resultant tissue injury, such as can be induced using hypoxia-reoxygenation in SS mice [243-244]. A recent study has shown that dietary supplementation with omega-3 fatty acids does not exacerbate oxidative stress in human SCD, a complication that has been suggested in studies of omega-3 supplementation in non-SCD individuals [245]. Therefore, dietary supplementation with omega-3 fatty acids may provide a safe and effective way to ameliorate pathologies associated with vaso-occlusive crises in human and murine SCD.

Chapter 6. Epinephrine Modulates BCAM/Lu and ICAM-4 Expression on the Sickle Cell Trait Red Blood Cell Membrane

6.1. Abstract

Collapse and sudden death in physical training are the most serious complications of sickle cell trait (SCT). During strenuous exercise, there is evidence that erythrocytes from SCT patients aggregate likely because of adhesive interactions with the extracellular matrix (ECM) and endothelial cells, and because of their irregular viscoelastic properties. This results in inflammation, blood flow impairment, and vaso-occlusive events. However, the exact role of stress conditions and how they lead to these complications is virtually unknown. Using single-molecule atomic force microscopy experiments, we report that epinephrine, a hormone secreted under stressful conditions, increases both the frequency and strength of adhesion events between BCAM/Lu (basal cell adhesion molecule) and ECM laminin, and between intercellular adhesion molecule-4 (ICAM-4) and endothelial $\alpha_v\beta_3$, compared to non-stimulated SCT erythrocytes. Increases in adhesion frequency present significant evidence of the role of epinephrine in BCAM/Lu-laminin and ICAM-4-$\alpha_v\beta_3$ bonding, and suggest mechanisms of vaso-occlusion during physical exertion in SCT.

6.2. Introduction

Sickle cell trait (SCT) is a risk factor for collapse and sudden death in physical training [9, 49-50, 53, 57, 246-247]. SCT is characterized by the presence of both normal adult hemoglobin (HbA) and abnormal sickle hemoglobin (HbS) in the red blood cell (RBC, erythrocyte). SCT affects over three million people in the United States, about 40 to 50 times more than sickle cell disease (SCD) [46]. In HbS, the normal sequence *Val-His-Leu-Thr-Pro-**Glu**-Glu-Lys* is changed to *Val-His-Leu-Thr-Pro-**Val**-Glu-Lys*, with the amino acid valine substituted for glutamic acid in

the β6 site. The replacement of two charged groups by two hydrophobic ones leads to polymerization of deoxygenated Hb and to the formation of stiff HbS fibers comprising a fibrous gel [33, 35, 42]. Between 40-42% of the hemoglobin content of most individuals with SCT is HbS [45]. In comparison to the homozygous SCD, the heterozygous SCT is traditionally regarded as a benign condition [28, 47-48]. However, during strenuous exercise, individuals can develop a syndrome resembling SCD with vaso-occlusive events resulting from changes in the RBC morphology, viscoelasticity, and adhesion [38, 49-54]. Vaso-occlusion occurs in crises in which the arterial circulation is blocked at one or many sites, leading to organ damage and ischemic pain [55]. Endothelial cell activation, cytoadherence, inflammation, and coagulation activation contribute to blood flow obstruction and play a critical role in the pathophysiology of vaso-occlusion [64, 66, 68].

It is known that SCD RBCs adhere abnormally to extracellular matrix (ECM) components as well as to endothelial cells (ECs) via changes in their adhesive interactions. Immature (reticulocytes) and mature erythrocytes express several adhesion receptors. One of them is the Lutheran (Lu) blood group RBC antigen and basal cell adhesion molecule (BCAM), known as BCAM/Lu which is a high-affinity laminin receptor. Another one is the intercellular adhesion molecule-4 (ICAM-4, LW glycoprotein), a receptor for a number of integrins [248].

While it is known that epinephrine enhances SCD erythrocyte adhesion, the mechanism has not yet been quantitatively explored in SCT or in SCD [72, 249]. Epinephrine is a hormone secreted from the adrenal medulla during periods of stress and strenuous exercise [250]. Increased circulating levels of epinephrine act on the RBC β2-adrenergic receptor, thereby activating $G\alpha_s$ proteins which stimulate adenylyl cyclase (AC). This enzyme catalyzes the conversion of adenosine triphosphate (ATP) to cyclic adenosine monophosphate (cAMP), leading to protein kinase A (PKA) activation, an intermediate step in the up-regulation of BCAM/Lu- and ICAM-4-

mediated adhesion [72, 249, 251]. The interaction of BCAM/Lu with the α5 chain of laminin (LAMA5) on the ECM, as well as the interaction of ICAM-4 with the $\alpha_v\beta_3$ integrin on ECs, may contribute to vaso-occlusive events in SCD due to over-expression of BCAM/Lu and ICAM-4 on SCD RBCs in the presence and absence of epinephrine [72, 248-249].

6.3. Design and Methods

Preparation of BCAM/Lu and ICAM-4 substrate

To attach purified CD239 (Sigma Aldrich, St. Louis, MO), commonly known as BCAM/Lu, onto a gold-coated mica substrate (Novascan Technologies, Inc., Ames, IA), the substrate was first incubated for 2 hours in 50 mM mercaptoethanesulfonate. Mercaptoethanesulfonate was prepared by adding sodium 2-mercaptoethanesulfonate to equal parts ethanol and 18 MΩ water. The gold surface was allowed to dry, then a drop of 1 µg/mL protein in PBS was added to the surface. After 20 min, the prepared gold surface was rinsed with PBS and a volume of PBS is added for experiments. The same method was employed in the attachment of ICAM-4-1 (Sigma Aldrich, St. Louis, MO) onto a gold-coated mica substrate.

Preparation of laminin and $\alpha_v\beta_3$ probes

Silicon nitride cantilevers were gently rinsed with ethanol and 18 MΩ water before being placed in a clean, dry petri dish with 30 µL APTES (3-aminopropy-triethoxysilane) and 10 µL triethylamine for 1h. N_3-dPEG-NH_2 linker was prepared by adding dry methylene chloride (0.5 mL), triethylamine (7 µL), and 7.5 mg (7.5 µL) of N_3-dPEG-NH_2 linker (Quanta Biodesign, Powell, OH) to a small, dry glass vial. The vial was sealed and inverted several times until all of the solid substances dissolved. After the atomic force microscopy (AFM) probes were tightly sealed with APTES for 1h, they were removed and immediately added to the N_3-dPEG-NH_2 linker at 4°C. After 1 h, the probes were rinsed with methylene chloride, ethanol, and then 18

MΩ water. The probes were placed in a parafilm-coated dish with their tips pointed upwards and inwards in a circular manner. 50 µL of 250 µg/mL purified Laminin α_5, clone 4C7 (Millipore, Temecula, CA) or 50 µL of 210 µg/mL purified human integrin $\alpha_v\beta_3$ (Millipore, Temecula, CA) is added to the center of the cantilevers, in contact with the probes. After 2 hours, AFM probes were rinsed with PBS buffer.

Erythrocyte preparation

The study included RBCs from a SCT adult subject (n = 1) and RBCs from a healthy adult subject (n = 1) purchased from Research Blood Components, LLC (Brighton, MA). An IRB approved consent form was obtained by the company for each donor giving permission to use the acquired sample for research purposes. Sodium citrate anticoagulant is used, RBCs were utilized for experiments within 14 days of blood draw, and maintained at 4ºC prior to use. Cell age did not appear to have an effect on the data. Erythrocytes were diluted to a concentration of 50% in Alsever's solution (Sigma Aldrich, St. Louis, MO) and maintained in 5% CO_2 at 37ºC prior to immobilization and experiments.

Erythrocyte immobilization

Cells were immobilized on glass-bottom petri dishes (MatTek Corporation, Ashland, MA) coated with poly-L-lysine (PLL) to increase cell adherence. 150 µl of 1 mg/ml PLL solution (Sigma Aldrich, St. Louis, MO) was allowed to adsorb for 5 min to a sterile glass surface, and excess solution was drained away. RBCs of 50% concentration in Alsever's solution were allowed to adhere to each PLL-coated glass surface for 10 min in the incubator (37ºC and 5% CO_2). Unattached cells were removed by gentle rinsing of the surface with Alsever's solution at 25°C and a volume of 3.0 mL Alsever's solution was added for experiments. In epinephrine-mediated adhesion experiments, a volume of 3.0 mL of 10 nM epinephrine (Sigma Aldrich, St. Louis, MO) was added for experiments.

Atomic force microscopy measurements

Adhesion maps and force-distance curves were obtained using an Asylum MFP 3D-BIO (Asylum Research, Santa Barbara, CA) AFM equipped with a "liquid cell" setup. A petri dish heater was employed to maintain the RBCs at physiological body temperature (37ºC) during experiments. The temperature inside the sample was controlled (±0.1ºC) via closed loop temperature control using an environmental controller (Asylum Research, Santa Barbara, CA). Baseline measurements were performed in Alsever's solution at 37ºC. Epinephrine-mediated experiments were performed in a 10 nM epinephrine solution, using Alsever's as the base, at 37ºC. Unless otherwise specified, all force measurements were recorded with a loading rate of 24000 pN/s, calculated by multiplying the tip retraction velocity (nm/s) by the spring constant of the cantilever (pN/nm).

The nominal spring constant k_c of the employed cantilever was 30 pN/nm, as provided by the manufacturer (Bruker Probes, Camarillo, CA). Exact values for the cantilever spring constants were obtained via a thermal noise based method implemented by the manufacturer and were used in all calculations. We chose this cantilever stiffness because it is known that when $k_c > 10$ pN/nm, the soft linkage of the protein-protein interaction dominates the behavior of the cantilever-protein effective spring system [104]. The approach and retraction velocities were held constant at 800 nm/s. Probes had nominal tip radii of 20 nm and nominal angle of 20°, as provided by the manufacturer.

Statistical analysis

Reported adhesion interaction forces for the BCAM/Lu-laminin complex and ICAM-4-$\alpha_v\beta_3$ complex in the text are average values obtained via the Gaussian distribution. The differences among the groups are assessed using the two-tailed t-test for independent samples to evaluate respectively the effect of the SCT genotype and that of the epinephrine stimulation. The

significance level is defined as $p < 0.05$. The statistical analyses are conducted with the Data Analysis Toolpack in Microsoft Excel (Microsoft, Redmond, WA).

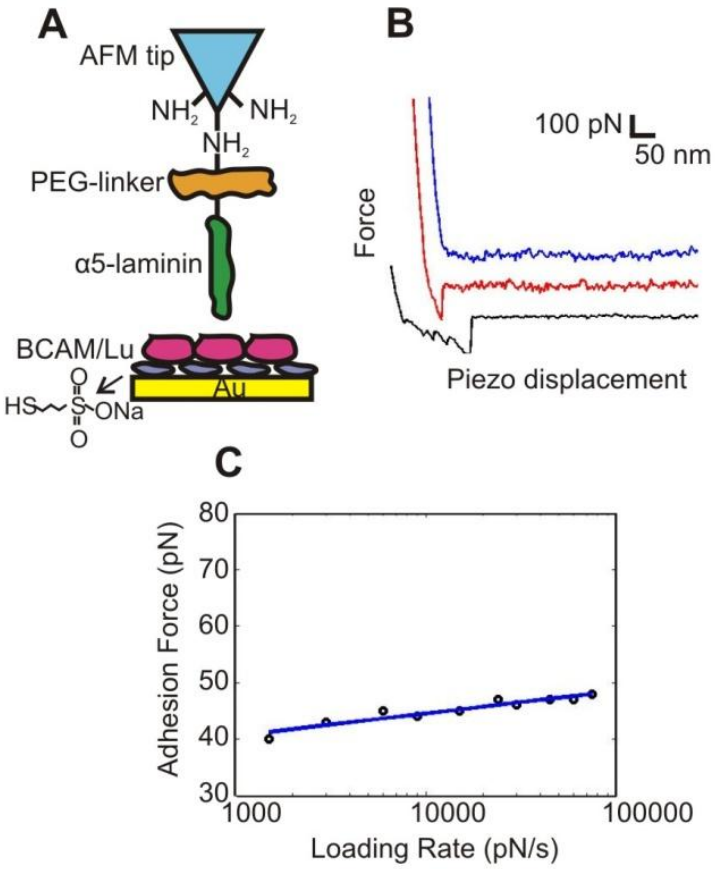

Figure 6.4.1. Strategy for measuring the BCAM/Lu-laminin binding force at the single-molecule level using AFM. (A) Schematic of the surface chemistry used to functionalize the AFM tip and substrate with LAMA5 and BCAM/Lu. A PEG-linker was attached to an AFM tip terminated with NH_2 groups, and BCAM/Lu was bound to a gold substrate via mercaptoethanesulfonate. (B) Force-distance curves are three representative examples obtained using independent tips and substrates. The blue curve demonstrates zero adhesive interaction, while the red and black curves show rupture forces associated with adhesion events. (C) Dynamics of the BCAM/Lu-laminin interaction. Dependence of the adhesion force on the loading rate applied during retraction, measured between a LAMA5 tip and a BCAM/Lu substrate, while keeping the interaction time (0 s) and loading rate during approach (24000 pN/s) constant. The mean adhesion force does not notably change with the loading rate, indicating the measurements were performed close to thermodynamic equilibrium

6.4. Results

Dynamics of the BCAM/Lu-laminin and ICAM-4-$\alpha_v\beta_3$ interaction

Direct measurements of the BCAM/Lu-laminin and ICAM-4-$\alpha_v\beta_3$ adhesive interactions are obtained via single molecule force spectroscopy [90, 94, 96]. Adhesive forces, defined as the maximum rupture force (Figure 6.4.1B) associated with the force-distance curves, are extracted from each of the 1024 force curves acquired to determine the rupture force. Upon investigation of the dynamics of the BCAM/Lu-laminin interaction, force curves between the LAMA5 tip and the BCAM/Lu-coated substrate are recorded at various retraction rates. The mean adhesion force does not substantially depend on the loading rate applied during retraction, over the experimentally tested range (Figure 6.4.1C). Dynamics of the ICAM-4-$\alpha_v\beta_3$ interaction shows a similar trend. This observation, in contrast to the behavior of several other receptor-ligand complexes that usually have an increase in adhesion force with the logarithm of loading rate, indicates that the force measurements are performed close to thermodynamic equilibrium [252].

Interaction force of the BCAM/Lu-laminin and ICAM-4-$\alpha_v\beta_3$ pairs

For the BCAM/Lu-laminin pair, force-distance curves are recorded between the LAMA5 probe and the BCAM/Lu-coated substrate. Adhesive forces are extracted from each of the 1024 force curves acquired and an average rupture force of 50 ± 11 pN (Figure 6.4.2A). In atomic force microscopy, the specificity of ligand-receptor binding is demonstrated by performing blocking experiments with free ligands, which are injected into the solution to block the receptor sites on the cell surface. Consequently, almost all specific recognition signals completely disappear and only occasional adhesion events are observed [56, 90]. The specificity of the interaction is demonstrated by performing experiments in 250 µg/mL laminin solution, thus blocking the BCAM/Lu receptors. By recording force-distance curves between the LAMA5 tip and the BCAM/Lu-coated substrate in the laminin solution, the number of curves showing adhesion events dramatically reduces from 26% to 6% ($p < 10^{-6}$, Figure 6.4.2A). For the ICAM-4-$\alpha_v\beta_3$ pair,

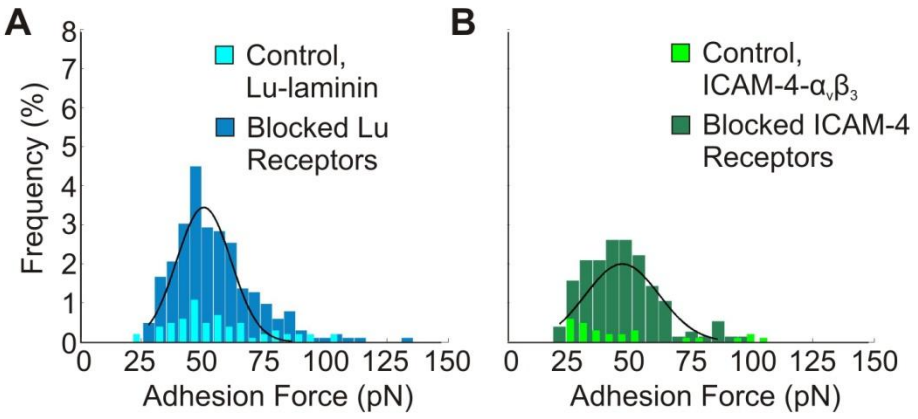

Figure 6.4.2. Measurement of the binding force of the BCAM/Lu-laminin and ICAM-4-$\alpha_v\beta_3$ complexes. (A) Adhesion force histogram obtained from 1024 force curves (*n* = 1024) measured in PBS between a LAMA5 tip and a BCAM/Lu substrate. The distribution of adhesion forces reveals a maximum value at 50 ± 11 pN as determined by a Gaussian fit. The frequency of adhesion events was 26%, as determined by the percentage of curves showing rupture forces. Overlay shows the adhesion force histogram (*n* = 1024) obtained after injection of free laminin (250 µg/mL) into the solution. The dramatic reduction of adhesion frequency and broadening of the distribution reflect the blocking of the BCAM/Lu receptors. (B) Adhesion force histogram obtained from 1024 force curves (*n* = 1024) measured in PBS between an integrin $\alpha_v\beta_3$ tip and a ICAM-4 substrate. The distribution of adhesion forces reveals a maximum value at 47 ± 15 pN as determined by a Gaussian fit. The frequency of adhesion events was 18%. Overlay shows the adhesion force histogram (*n* = 1024) obtained after injection of free integrin $\alpha_v\beta_3$ (210 µg/mL) into the solution. The dramatic reduction of adhesion frequency reflects the blocking of the ICAM-4 receptors.

force-distance curves are recorded between the $\alpha_v\beta_3$ probe and the ICAM-4-coated substrate, resulting in an average rupture force of 47 ± 15 pN (Figure 6.4.2B). The specificity of the interaction is demonstrated by performing experiments in 210 µg/mL integrin $\alpha_v\beta_3$ solution, thus blocking the ICAM-4 receptors. The number of curves showing adhesion events dramatically reduces from 18% to 3% ($p < 10^{-6}$, Figure 6.4.2B).

Non-stimulated SCT RBC adhesion to laminin and integrin $\alpha_v\beta_3$

In this paper, we measure, on single erythrocytes, the effects of epinephrine on the bond strength and on the frequency of binding events between (1) the BCAM/Lu antigen, expressed on the surface of SCT RBCs, and the laminin complex, expressed on the ECM, and (2) the ICAM-4 antigen expressed on the surface of SCT RBCs, and the $\alpha_v\beta_3$ integrin, expressed on

ECs. We also measure the adhesion of non-stimulated SCT RBCs compared to non-stimulated wild-type RBCs. The methodology followed requires functionalization of the AFM probe [90, 94-96] with LAMA5 or integrin $\alpha_v\beta_3$ to measure the interaction between the α5 chain of laminin and BCAM/Lu receptor expressed on the tested RBC (Figure 6.4.3), or the interaction between integrin $\alpha_v\beta_3$ and ICAM-4 receptor expressed on the tested RBC. From these measurements, the distribution of the BCAM/Lu and ICAM-4 receptor on the RBC surface is also obtained. The RBCs are placed in an environment with a physiologically relevant level of epinephrine to explore the effect of the stress-induced epinephrine environment on the frequency and distribution of adhesive interactions.

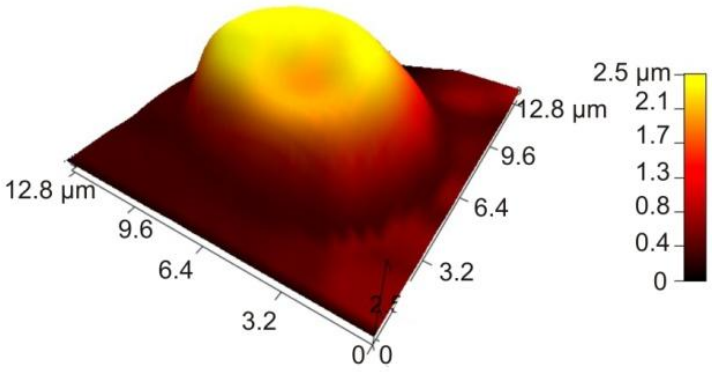

Figure 6.4.3. AFM topographic image of a SCT erythrocyte displaying the characteristic biconcave shape associated with healthy, wild-type RBCs. This erythrocyte is a representative example of those scanned during experiments to map the distribution of BCAM/Lu and ICAM-4 receptors on human erythrocytes.

To detect the distribution of the receptors on the cell surface, as well as to measure the physiologic BCAM/Lu-laminin bond strength, spatially-resolved adhesion maps are recorded using a LAMA5 tip over 1 µm x 1 µm areas. Adhesive forces are extracted from each of the 1024 force curves acquired from tests on n=6 wild-type and n=6 SCT erythrocytes. The average magnitude of the BCAM/Lu-laminin bond is the same for wild-type and SCT (Figure 6.4.4A) erythrocytes, 46 ± 6 pN and 46 ± 10 pN, respectively. This bond strength is also the same as

the average rupture force of 50 ± 11 pN (Figure 6.4.2A) measured between a BCAM/Lu-coated gold substrate and a functionalized LAMA5 probe. The number of observed binding events, however, shows an increase from 10.42% to 16.89% ($p < 0.05$).

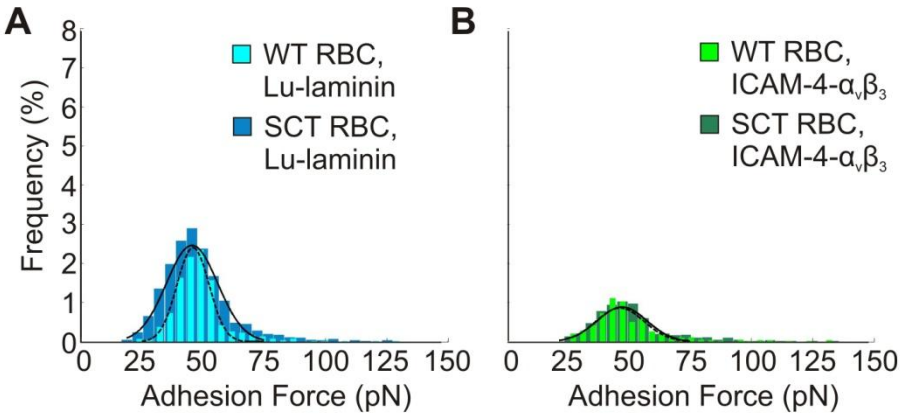

Figure 6.4.4. Measurement of the binding force of the BCAM/Lu-laminin and ICAM-4-$\alpha_v\beta_3$ complexes on erythrocytes. (A) Foreground: Adhesion force histogram obtained from 6,144 force curves (n = 6 cells x 1024 force curves) measured in Alsever's solution between a LAMA5 tip and a wild-type (WT) RBC. The distribution of adhesion forces reveals a maximum value at 46 ± 6 pN, as determined by a Gaussian fit. Background: Adhesion force histogram obtained from 6,144 force curves (n = 6 cells x 1024 force curves) obtained between a LAMA5 tip and a sickle cell trait RBC reveals a distribution of adhesion forces with a maximum value at 46 ± 10 pN. The frequency of adhesion events increased significantly from 10.42% on the wild-type RBC to 16.89% on the SCT RBC ($p < 0.05$). (B) Foreground: Adhesion force histogram obtained from 6,144 force curves (n = 6 cells x 1024 force curves) measured in Alsever's solution between a $\alpha_v\beta_3$ tip and a wild-type RBC. The distribution of adhesion forces reveals a maximum value at 46 ± 10 pN, as determined by a Gaussian fit. Background: Adhesion force histogram (n = 6 cells x 1024 force curves) obtained between a $\alpha_v\beta_3$ tip and a sickle cell trait RBC reveals a distribution of adhesion forces with a maximum value at 47 ± 10 pN. There is a non-significant increase from 5.91% to 7.56% ($p > 0.05$) in the number of adhesion events.

For the measurements of the ICAM-4-$\alpha_v\beta_3$ pair bond strength and local distribution, adhesive forces are extracted from each of the 1024 force curves acquired from tests on n=6 wild-type and n=6 SCT erythrocytes. The average magnitude of the ICAM-4-$\alpha_v\beta_3$ bond is the same for wild-type and SCT (Figure 6.4.4B) erythrocytes, 46 ± 10 pN and 47 ± 10 pN, respectively. This bond strength is also nearly the same as the average rupture force of 47 ± 15 pN (Figure. 6.4.2B) measured between an ICAM-4-coated gold substrate and a functionalized integrin $\alpha_v\beta_3$

probe. The number of observed binding events show an insignificant increase from 5.91% to 7.56% ($p > 0.05$).

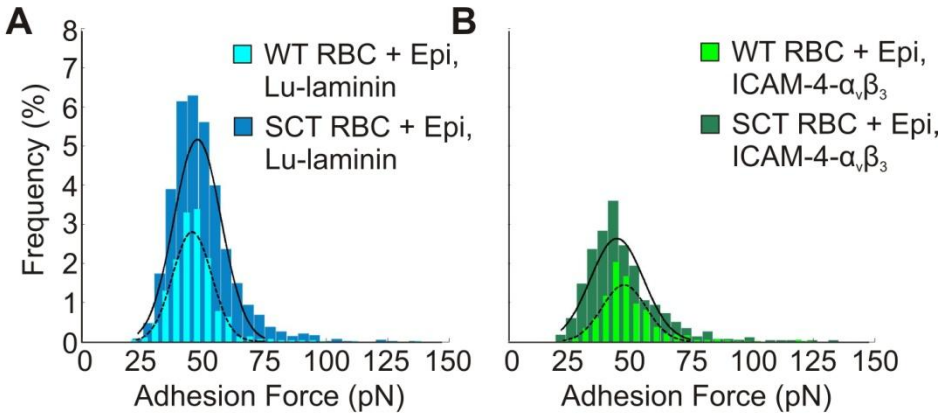

Figure 6.4.5. Measurement of the physiologic implications of epinephrine-stimulated adhesion. (A) Foreground: Adhesion force histogram (n = 6 cells x 1024 force curves) obtained in 10 nM epinephrine between a LAMA5 tip and a wild-type RBC reveals a distribution of adhesion forces with a maximum value at 45 ± 8 pN, comparable to the baseline value. The frequency of adhesion events increased from 10.42% to 14.86% ($p > 0.05$) as compared to baseline measurements of wild-type RBCs. Background: Adhesion force histogram (n = 6 cells x 1024 force curves) obtained between a LAMA5 tip and a SCT RBC. The frequency of adhesion events increased significantly from 16.89% to 35.04% ($p < 0.01$) as compared to baseline measurements of SCT RBCs. The distribution reveals a maximum value at 48 ± 10 pN, comparable to the baseline SCT value. (B) Foreground: Adhesion force histogram (n = 6 cells x 1024 force curves) obtained in 10 nM epinephrine between an integrin $\alpha_v\beta_3$ tip and a wild-type RBC reveals a distribution of adhesion forces with a maximum value at 48 ± 9 pN, comparable to the baseline value. The frequency of adhesion events increased insignificantly from 5.91% to 8.99% ($p > 0.05$) as compared to baseline measurements of wild-type RBCs. Background: Adhesion force histogram (n = 6 cells x 1024 force curves) obtained between a integrin $\alpha_v\beta_3$ tip and a SCT RBC. The frequency of adhesion events increased from 7.56% to 19.89% ($p < 0.05$) as compared to baseline measurements of SCT RBCs. The distribution reveals a maximum value at 45 ± 11 pN, comparable to the baseline value.

Epinephrine-stimulated SCT RBC adhesion to laminin and integrin $\alpha_v\beta_3$

To test the hypothesis that an increase in epinephrine levels results in an increase in the frequency of adhesive interactions, we employed a similar approach. Treatment of wild-type RBCs with 10 nM epinephrine, a physiologically relevant level, induced an insignificant increase from 10.42% to 14.86% ($p > 0.05$) in the frequency of BCAM/Lu-laminin binding events (n = 6, Figure 6.4.5A), and an insignificant increase from 5.91% to 8.99% ($p > 0.05$) in the frequency of

ICAM-4-$\alpha_v\beta_3$ binding events (n = 6, Figure 6.4.5B). There was no notable increase in the bond strength of either pair with epinephrine stimulation. The specificity of the BCAM/Lu-laminin interaction was validated via blocking experiments (Figure 6.4.6). By recording force-distance curves between a LAMA5 tip and wild-type RBCs in Alsever's solution, the number of curves showing adhesion events dramatically reduces to 0.52% from 10.42% ($p < 0.001$).

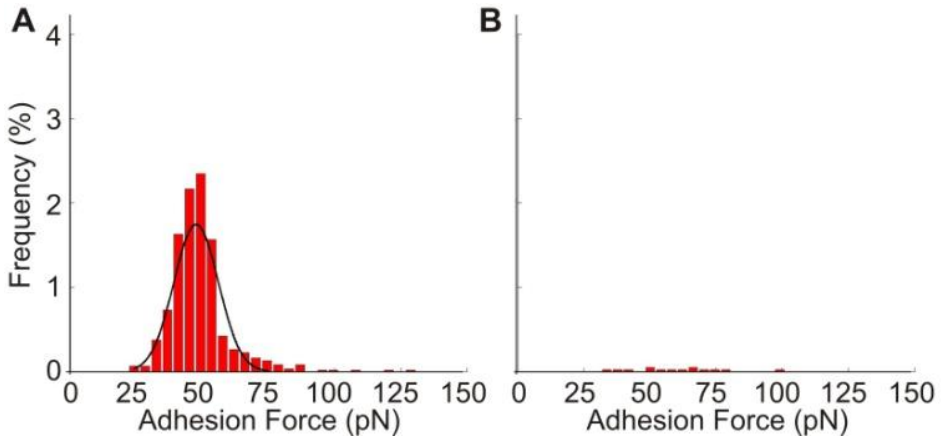

Figure 6.4.6. Validation of the specificity of the BCAM/Lu-laminin interaction on wild-type RBCs. (A) Adhesion force histogram obtained from 6,144 force curves (n = 6 cells x 1024 force curves) measured between a LAMA5 tip and a wild-type RBC. The distribution of adhesion forces reveals a maximum value at 46 ± 6 pN, as determined by a Gaussian fit. (B) Adhesion force histogram (n = 6 cells x 1024 force curves) obtained after injection of free laminin (250 µg/mL) into solution. Force-distance curves were measured in a LAMA5 tip and a wild-type RBC. The dramatic reduction of adhesion frequency to 0.52% from 10.42% on the wild-type in (A) ($p < 0.001$) demonstrates the specificity of the BCAM/Lu-laminin interaction.

Treatment of sickle cell trait RBCs (n = 6) with epinephrine induced an increase in the frequency of BCAM/Lu-laminin binding events from 16.89% to 35.04% ($p < 0.01$) (Figure 6.4.5A). The distribution of the wild-type RBCs with epinephrine has been overlaid on the distribution of the SCT RBCs with epinephrine in Figure 6.4.5A to demonstrate the broadened variability of the Lu/BCAM-laminin adhesion force on the treated SCT erythrocytes. Treatment of sickle trait RBCs (n = 6) with epinephrine induced an increase in the frequency of ICAM-4-$\alpha_v\beta_3$ binding events from 7.56% to 19.89% ($p < 0.05$) (Figure 6.4.5B). The distribution of the wild-type RBCs

with epinephrine has been overlaid on the distribution of the SCT RBCs with epinephrine in Figure 6.4.5D to demonstrate the broadened variability of the ICAM-4-$\alpha_v\beta_3$ adhesion force on the treated SCT erythrocytes.

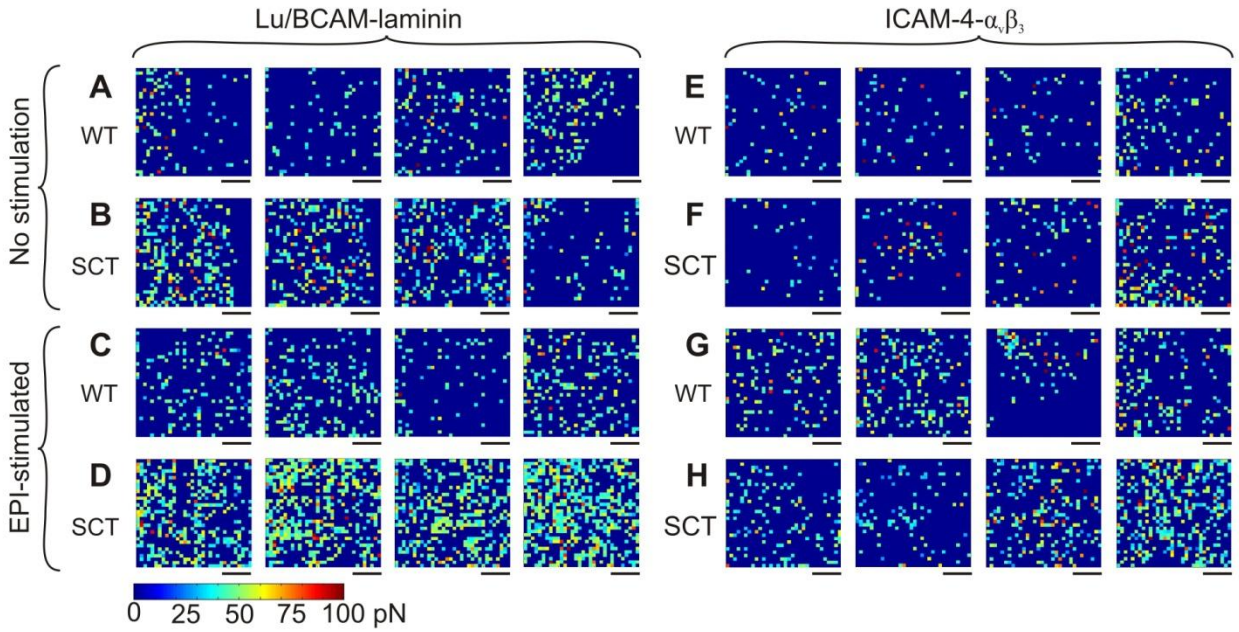

Figure 6.4.7. Distribution of BCAM/Lu and ICAM-4 on the surface of wild-type RBCs and sickle cell trait RBCs using different probes and cell preparations. (A,B) Adhesion force maps (color scale as shown) recorded with LAMA5 functionalized probes over wild-type RBCs (A) and sickle cell trait RBCs (B). (C,D) Adhesion force maps recorded with LAMA5 tips over wild-type RBCs (C) and sickle cell trait RBCs (D) in 10 nM epinephrine. (E,F) Adhesion force maps recorded with integrin $\alpha_v\beta_3$ probes over wild-type RBCs (E) and sickle cell trait RBCs (F). (G,H) Adhesion force maps recorded with integrin $\alpha_v\beta_3$ tips over wild-type RBCs (G) and sickle cell trait RBCs (H) in 10 nM epinephrine. Scale bars, 250 nm.

Notably, 1 µm x 1 µm spatially-resolved adhesion maps revealed that the BCAM/Lu-mediated laminin binding activity is not homogeneously distributed over the SCT RBC surface, but concentrated on nanodomains. These nanodomains, often attributed to membrane rafts, are only observed on SCT RBCs (n = 6) in the presence of epinephrine (Figure 6.4.7D). In contrast, wild-type RBCs (n = 6) stimulated with epinephrine (Figure 6.4.7C) demonstrate a nearly homogeneous distribution of BCAM/Lu receptors. Furthermore, ICAM-4 receptor nanodomains

are also observed, to a lesser degree, on the SCT RBC (n = 6) surface in the presence of epinephrine (Figure 6.4.7H), with a heterogeneous receptor distribution on the wild-type RBC (n = 6) stimulated with epinephrine (Figure 6.4.7G). In the non-stimulated environment, both wild-type (Figure 6.4.7A, 6.4.7E) and sickle cell trait (Figure 6.4.7B, 6.4.7F) RBCs maintain a homogenous distribution of BCAM/Lu and ICAM-4 receptors.

6.5. Discussion

Although it is known that the BCAM/Lu-laminin and ICAM-4-$\alpha_v\beta_3$ binding complexes contribute to SCD vaso-occlusion, the quantitative characteristics of these adhesion interactions has not been explored in SCD or SCT erythrocytes. In wild-type RBCs and sickle cell trait RBCs, the magnitude of the BCAM/Lu-laminin binding complex (46 ± 6 pN and 46 ± 10 pN, respectively) is equal to the average rupture force of 50 ± 11 pN recorded between a functionalized laminin probe and a BCAM/Lu-coated gold substrate. In wild-type RBCs and sickle cell trait RBCs, the magnitude of the ICAM-4-$\alpha_v\beta_3$ binding complex (46 ± 10 pN and 47 ± 10 pN, respectively) is nearly the same as the average rupture force of 47 ± 15 pN recorded between a functionalized integrin $\alpha_v\beta_3$ probe and a ICAM-4-coated gold substrate.

Interactions of receptor molecule cytoplasmic domains with the cytoskeleton can play critical roles in adjusting receptor function. It has been determined that BCAM/Lu has a high degree of connectivity to the erythrocyte membrane cytoskeleton via erythroid spectrin [253-254]. Importantly, disruption of the BCAM/Lu-spectrin linkage is accompanied by enhanced cell adhesion to laminin [254]. A major finding of the current study is that BCAM/Lu adhesion events in SCT erythrocytes increased ($p < 0.05$) as compared to the wild-type. It is known that Hb interacts with the spectrin network via band 3 [40, 151] and the introduction of HbS has recently been found to have an effect on the mechanical properties of SCT erythrocytes [93]. We

conjecture that HbS partially disrupts the spectrin network via its interaction with band 3, indirectly disrupting the BCAM/Lu-spectrin linkage. This results in increased diffusion and aggregation and thus significantly enhanced sickle trait RBC adhesion to ECM laminin.

Epinephrine, acting through the β2-adrenergic receptor, increases Lu-laminin α5 sickle mediated red cell binding via a cAMP and PKA-dependent signaling pathway [72]. Further, the Lu cytoplasmic tail is phosphorylated in epinephrine-stimulated sickle cells, which may be a critical factor in sickle RBC's enhanced adhesion to laminin [83]. The BCAM cytoplasmic tail, which lacks the last 40 amino acids of the sequence, does not undergo phosphorylation. It has been demonstrated that PKA-mediated phosphorylation of the Lu glycoprotein at serine 621 positively regulates the adhesion function of Lu under flow conditions. While the molecular basis for the resulting increased adhesion is not yet understood, it has been hypothesized that phosphorylation of the Lu cytoplasmic tail weakens its interaction with spectrin, enabling the freely-floating transmembrane Lu molecules to cluster and thereby generate a larger adhesive force [83]. A major finding of our current study is the mapping of Lu nanodomains on epinephrine-stimulated SCT erythrocytes, accompanied by an increase in the frequency of binding events ($p < 0.01$) from the baseline SCT erythrocytes. The significant broadening of the bond magnitude distribution agrees with the aggregation of receptors into nanodomains detected in Figure 6.4.7D. While the frequency of adhesive interactions increases on the wild-type RBC in the stress-induced epinephrine environment, this increase (from 10.42% to 14.86%) is not significant and receptor clustering is not observed (see Figure 6.4.7C). This observation strengthens our conjecture that HbS disrupts the spectrin network resulting in aggregation of BCAM/Lu receptors in SCT RBCs. It is noted that, receptor aggregation is not detected in the case of SCT RBCs without epinephrine (see Figure 6.4.7B).

ICAM-4 mediated binding to endothelial cells and leukocytes is also activated by epinephrine via

stimulation of the β2-adrenergic receptor which triggers a cAMP and PKA-dependent signaling pathway [255]. In addition, ICAM-4 on epinephrine-stimulated sickle cells undergo a significant increase in serine phosphorylation, which may be a critical factor in sickle RBC's enhanced adhesion to endothelial integrin $\alpha_v\beta_3$ [249]. It has been hypothesized that phosphorylation-induced changes in the ICAM-4 cytoplasmic domain cause a conformational change in its extracellular domain, thus generating a larger adhesive force. We observed an increase in the frequency of binding events ($p < 0.05$) from the baseline SCT erythrocytes (see Figure 6.4.5D) on epinephrine-stimulated SCT erythrocytes. Another important finding of the present data is the quantification of the insignificant increase ($p > 0.05$) of ICAM-4-$\alpha_v\beta_3$ adhesion events on the wild-type RBCs in the stress-induced epinephrine environment (see Figure 6.4.5B). This is consistent with the known fact that there is minimal ICAM-4 phosphorylation in wild-type RBCs, due to an age-related reduction in the cell's ability to produce cAMP and thereby enhance PKA activity in response to stimulation [72, 256-257]. While the current study tests the effect of epinephrine on single molecule adhesion interactions thought to contribute to vascular blockage in sickle cell vaso-occlusion, epinephrine has also been found to work via increasing RBC trapping in the spleen and liver [255, 258].

6.6. Conclusions

The observed increases in adhesion frequency along with the detected receptor aggregation into nanodomains is significant evidence of the contribution of epinephrine to enhancing BCAM/Lu-laminin and ICAM-4-$\alpha_v\beta_3$ bond interactions. These findings suggest a mechano-adhesive role for epinephrine in the pathophysiology of vaso-occlusive incidents related to sudden death in SCT individuals during strenuous exercise.

Chapter 7. Establishing the Sensitivity of Force Nanoscopy in the Detection of Native SK Channels in Living Neurons

7.1. Abstract

The spatial distribution of ion channels is an important determinant of neuronal excitability. However, there are currently no quantitative techniques to map endogenous ion channels with single-channel resolution in living cells. Here, we demonstrate that integration of pharmacology with single molecule atomic force microscopy (AFM) allows for the high-resolution mapping of native potassium channels in living neurons. We focus on calcium-activated small conductance (SK) potassium channels, which play a critical role in brain physiology. By linking apamin, a toxin that specifically binds to SK channels, to the tip of an AFM cantilever, we are able to detect binding events between the apamin and SK channels. We find that native SK channels from rat hippocampal neurons reside primarily in dendrites as single entities and in pairs. Importantly, we establish the sensitivity of force nanoscopy and show that SK channel dendritic distribution is dynamic and under the control of protein kinase A. Our study demonstrates that integration of toxin pharmacology with single molecule AFM can be used to quantitatively map individual native ion channels in living cells, and thus provides a new tool for the study of ion channels in cellular physiology.

7.2. Introduction

A major challenge in cellular biology is to determine the subcellular distribution of ion channels resident in neurons and other cells in living tissue. In neurons, the differential localization of ion channels specifies the intrinsic excitability and computational properties of the subcellular neuronal compartments (dendrites, soma, axon). The distribution of ion channels is typically

determined using antibodies raised against ion channel subunits together with light, confocal, total internal reflection fluorescence (TIRF) microscopy or electron microscopy (EM). These studies have revealed that ion channels can be polarized within cells and can concentrate in high and low density areas within the plasma membrane [259-260].

Unlike confocal or TIRF microscopy that have an in-plane spatial resolution of ~250 nm, immunogold-EM has a spatial resolution of 20-30 nm making it the highest resolution method to determine the subcellular distribution of ion channels [261-262]. However, it is limited by its inability to map ion channels in living cells. Lately, several advances in super-resolution fluorescence microscopy have made it possible to image proteins in either living or fixed tissue at high spatial resolutions (30-70 nm) [261]. Still, these approaches are generally limited by antibody specificity and/or the use of fluorescent labels that require overexpression of tagged channels in cells.

Recently, single molecule atomic force microscopy (AFM) has been used to localize native proteins in living cells at high resolution (~10 nm) [263]. The technique involves detection of binding events occurring between a cell surface protein and a protein attached to the tip of the AFM cantilever [90]. However, single molecule AFM inherently relies on the specificity and affinity of the protein-protein interactions, which are often unknown. Given the wealth of knowledge available regarding the binding of natural toxins to specific ion channels, we hypothesized that combination of AFM with toxin pharmacology could reveal the localization of endogenous ion channels in neurons with single-channel resolution.

Following neuronal activity, calcium can activate apamin-sensitive SK channels with relatively high affinity [264-266]. Such activation can regulate synaptic plasticity and dendritic neuronal

excitability [267]. SK channels are enriched in dendrites and post-synaptic densities, although other evidence indicates an approximately uniform neuronal distribution [268-272]. Moreover, the spatial organization of these channels within a neuronal compartment is unclear. At least one SK channel isoform (SK2-L) is prone to clustering in heterologous cells [273], raising the possibility that SK channels might not be uniformly distributed on neuronal surfaces, even within a neuronal compartment. To determine SK channel subcellular distribution, we speculated that by attaching apamin molecules to the tip of an AFM cantilever we could detect *binding forces between apamin and single SK channels* on neuronal surfaces of living cells. Apamin is a bee venom toxin that specifically binds to SK channels at their extracellular region with high affinity and with 1:1 stoichiometry [274].

7.3. Materials and Methods

Experiments were carried out according to the guidelines of the University of Connecticut Institutional Animal Care and Use Committee.

Preparation of functionalized cantilever probes

Silicon nitride AFM cantilevers were rinsed with ethanol and 18MΩ water before being treated with 30µL APTES and 10µL triethylamine for 1h. Cantilevers were then added to the PEG-linker solution containing: 0.5mL methylene chloride, 7µL triethylamine, and 7.5µL PEG-linker (Quanta Biodesign) at 4°C for 1h. Probes were rinsed with methylene chloride, ethanol, and 18MΩ water. 50µL of 100 nM apamin was added in contact with the probes for 2h. Cantilevers were rinsed in PBS buffer and stored in PBS at 4°C.

Atomic force microscopy measurements

Binding force maps and force-distance curves were obtained using a MFP-3D-BIO (Asylum

Research) AFM. HEK293T cell measurements were performed in culture media at 25°C. Neuronal cell measurements were performed in neurobasal media stabilized with 30µL of 20 mM HEPES buffer at 25°C. Cells were located via differential interference contrast microscopy and a scan area of 1µm^2 was chosen with a lateral resolution of 31.25nm.

Unless otherwise specified, measurements were recorded with a loading rate of 24000 pN/s, calculated by multiplying the tip retraction velocity (nm/s) by the cantilever spring constant (pN/nm). The nominal spring constant k_c of the employed cantilever was 30 pN/nm, as provided by the manufacturer. Exact values for the cantilever spring constants were obtained via a thermal noise based method implemented by the manufacturer and used in all calculations. This cantilever stiffness was chosen because it is known that when $k_c > 10$ pN/nm, the soft linkage of the protein-protein interaction dominates the behavior of the cantilever-protein effective spring system [104]. Probes had nominal tip radii of 20 nm and nominal angle of 20°.

Electrophysiology

HEK293T cells were transfected with recombinant DNA (0.1 - 3µg) using Lipofectamine 2000 (Invitrogen) and recorded 24-hr post-transfection. SK2 currents were recorded with conventional whole-cell patch-clamp recordings. The recording electrodes were filled with solution containing (in mM): 110 K-gluconate, 10 KCl, 20 KOH, 4 Mg·ATP, 8.73 $CaCl_2$, 20 HEPES, 10 EGTA·KOH (pH 7.2). Based on the Ca-Mg-ATP-EGTA Calculator v1.0 using constants from NIST database #46 v8 the free Ca2+ concentration was 1.1µM. The electrode resistances were 4–5MΩ. The extracellular solution contained (in mM): 144 NaCl, 2.5 KCl, 2.5 $CaCl_2$, 1.2 $MgCl_2$, 10 HEPES, and 22 D-Glucose (pH 7.2). A voltage ramp was applied from a holding potential of -100mV to +20mV (13mV/s). The data were low-pass filtered at 2kHz and sampled at 10kHz. For all recordings, we used a Multiclamp 700B amplifier interfaced to a computer through a Digidata 1440A digitizer (Molecular Devices). Data were acquired with Clampex v10.2 (Molecular

Devices).

Primary hippocampal cultures

Dissociated hippocampal cultures were prepared from Sprague-Dawley pups of either sex as described previously [275].

Molecular biology

SK2-S subcloned into a pEGFP-N1 vector (Clontech) was a gift of Dr. Chul-Seung Park (Gwangju Institute of Science and Technology, Gwangju, Korea) while SK2-L was a gift from John P. Adelman (Vollum Institute, OHSU)

Data Analysis

To detect the distribution of SK2 channels on the cell surface, spatially-resolved binding force maps were recorded using an apamin functionalized probe over 1μm^2 areas. Binding forces were extracted from each of the 1024 force curves acquired from each test. A MATLAB (MathWorks) program was used to create visual binding force maps.

7.4. Results

To test our approach, we functionalized the tip of an AFM cantilever with apamin through a PEG-linker (Figure 7.4.1A) and transiently transfected HEK293T cells with the most commonly used SK2 channel isoform, SK2-S. Force-distance curves were recorded between the apamin-functionalized tips and SK2-S channels. Binding forces are defined as the maximum rupture force associated with the force-distance curves (Figure 7.4.1B). We expected that binding forces would be higher in areas where the apamin-functionalized cantilever made contact with underlying SK channels compared to areas without SK channels, as the attraction between

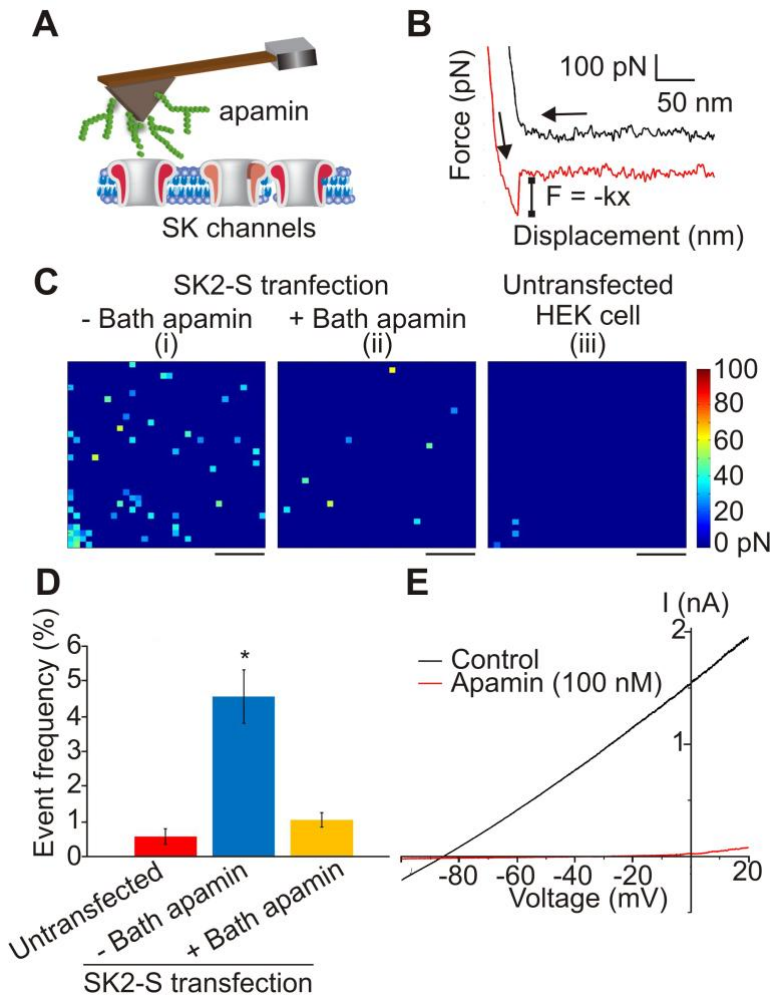

Figure 7.4.1. Detection of SK2 channels on living cells using Atomic Force Microscopy (AFM). (A) AFM cantilever probe is functionalized with apamin, a toxin that specifically binds to SK channels. (B) When apamin attached to the AFM probe adheres to an SK2 channel on the cell surface, the force-displacement curve exhibits an abrupt shift to zero value as shown in the red curve. The shift corresponds to the rupture force. If there is no SK2 channel at the detection point and consequently no binding interaction, the retraction curve is smooth similar to the black curve. The arrow pointing from right-to-left shows the movement of the AFM probe approaching and making contact with the cell surface, while the arrow pointing downward and to the right demonstrates the movement of the AFM probe retracting from the cell surface. (C) Binding force map of a HEK293T cell transfected with SK2-S channels in the absence (i) and presence of 100 nM ambient apamin (ii) to mask SK2 channels apamin binding sites. (iii) Binding force map of an untransfected HEK293T cell probed with an apamin functionalized probe shows minimal attraction. Each pixel corresponds to a rupture force according to the color scale shown. (D) Frequency graph of untransfected and SK2-S transfected cells in the absence or presence of ambient apamin. Star indicates statistical significance of $p<0.01$ (ANOVA Tukey post-hoc test). (F) Expression of SK2-S channels in HEK293T lead to apamin sensitive currents. Scale bars, 250 nm. Color scale as shown.

apamin and the channels would require a higher rupture force compared to apamin interactions with the plasma membrane. Binding forces were measured over a 1μm^2 area of HEK293T plasma membrane in cells transfected with SK2-S. For each recording, 1024 force-distance curves were obtained with a lateral resolution of 31.25nm. Potassium channel width has been reported to be ~10nm [276]. Figure 7.4.1Ci shows an example of a SK2-S binding force map with rupture forces detected between 21.0 to 56.4 pN for events above baseline. Such events were detected in 4.56 ± 0.75% of sampled sites (n=6). We also investigated the dynamics of the apamin SK2-S interaction by recording the force-distance curves at different cantilever retraction rates (2400 pN/s, 32 ± 7 pN; 24000 pN/s, 33 ± 10 pN; 240000 pN/s, 34 ± 10 pN; n=3). The mean binding force did not depend on the retraction rate suggesting that the observed interactions between apamin and SK2-S were at thermodynamic equilibrium [104].

To determine the specificity of the measured binding forces, we repeated experiments in SK2-S transfected cells pre-incubated with apamin as well as untransfected HEK293T cells. As shown in Figure 7.4.1C and 7.4.1D, we found that the frequency of binding force events was not significantly different between SK2-S transfected cells pre-incubated with apamin (Figure 7.4.1Cii) and untransfected cells (Figure 7.4.1Ciii). Events with significant binding forces most likely reflected SK2-S channels that were not bound by bath-applied apamin. Lastly, we measured SK2-S current using patch clamp electrophysiological recordings to verify that the expressed channels were functional and apamin-sensitive (Figure 7.4.1E).

Do the detected events indicate the presence of a single SK channel? To answer this question, we transfected varying concentrations of two SK channel isoforms, SK2-S and SK2-L in HEK293T cells. Previously it has been shown that the SK2-L isoform tends to form clusters possibly due to its cysteine rich N-terminus [273], unlike the SK2-S isoform. We found that increasing the concentration of transfected SK2-S plasmid (0.5 to 3.0 μg) did not substantially

change the mean binding force of detected events (0.5 µg, 27 ± 7 pN; 1.5µg, 32 ± 8 pN; 3.0 µg, 31 ± 10 pN) (Figure 7.4.2A). By plotting a histogram of binding forces, a unimodal Gaussian distribution was obtained for each concentration. The unimodal distribution together with the unchanged mean binding force suggested that we primarily detected a single population of SK2-S channels with no more than one SK2-S channel per 31.25nm.

A different situation was encountered with the SK2-L isoform. Increasing the concentration of transfected SK2-L plasmid from 0.1µg to 3.0µg substantially increased the mean binding force (0.1µg, 27 ± 6 pN; 1.5µg, 44 ± 10 pN; 3.0µg, 43 ± 11 pN) (Figure 7.4.2B). Cells transfected with 0.1µg of SK2-L resulted in force distributions similar to experiments on cells transfected with the SK2-S isoform, suggesting that at this very low concentration single SK2-L channels can be identified. At the higher concentrations of 1.5 and 3.0µg, the mean binding forces for SK2-L were approximately twice as large as the mean force obtained with 0.1µg SK2-L or the non-clustering SK2-S.

Considering that both isoforms share the same apamin binding site sequence [273], the higher mean binding force most likely reflected the presence of two SK2-L channels per recorded site. If this was the case, cells pre-incubated with 20pM apamin should have a similar mean binding force to the value obtained for single SK2-L channels. This is because the dissociation constant (K_D) for apamin binding to SK2 channels is ~10pM [274]. Thus, in the presence of 20pM apamin at least one of the two SK2-L channels in a cluster should be occupied by apamin thereby becoming unavailable for detection by the AFM probe. Indeed, in cells transfected with 3µg SK2-L and in the presence of ambient 20pM apamin, the binding force histogram became bimodal (Figure 7.4.2C) with a major peak at 27 ± 5 pN (n=5), a value similar to that obtained with low plasmid concentrations (27 pN; Figure 7.4.2D). A minor second peak was also recorded (39 ± 9 pN, n=5) likely reflecting remaining clustered channels not bound by the pre-

applied apamin. In summary, our data suggest that the apamin-dependent binding forces measured by AFM are specific and can be used to quantitatively map SK channels on living cell surfaces.

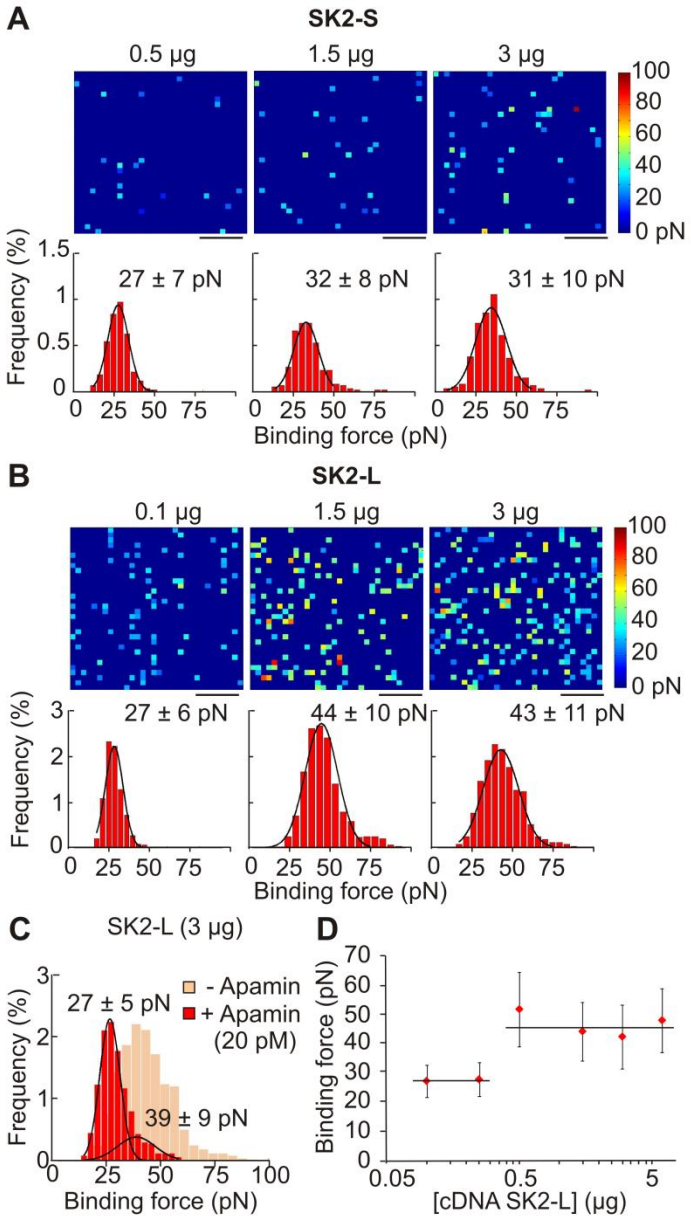

Figure 7.4.2. Counting SK2 channels in living cells. Binding force map and corresponding frequency histograms of HEK293T cells transfected with (A) 3.0 µg SK2-S (n=6), 1.5 µg SK2-S (n=6), and 0.5 µg SK2-S (n=6), (B) 0.1 µg SK2-L (n=6), 1.5 µg SK2-L (n=6), and 3.0 µg SK2-L (n=6). (C) Binding force frequency histograms of HEK293T cells transfected with 3.0 µg SK2-L (n=5) in cells pre-incubated with 20 pM apamin. (D) Summary graph showing the relationship between binding force and increased levels of SK2-L transfection. Scale bars, 250 nm. Color scale as shown.

After establishing the technique in HEK293T cells, we next employed AFM using apamin-functionalized tips to map the subcellular distribution of native SK channels in cultured hippocampal pyramidal neurons. Although SK channels play a critical role in hippocampal neurons, there is no consensus about their subcellular localization with some studies indicating a somatic localization of SK channels [272] whereas others a more dendritic localization of SK channels [268-269]. We probed different 1μm^2 cell surface regions, focusing on the soma and dendrites (Figure 7.4.3). Based on our recordings, SK channel distribution in neurons was polarized with the highest binding event frequency found on dendritic regions furthest from the soma (>30 μm) (6.2 ± 1.1%, n = 11), and the lowest frequency at the soma itself (0.29 ± 0.1%, n = 5), a 20-fold difference (Figure 7.4.3A-C; $p<0.001$ Student's t-test). The frequency of binding events at dendritic areas proximal to the soma (~10-20μm) was 0.70 ± 0.2% (n=7). Interestingly, the binding force distribution at more distal dendritic regions (>30μm) did not follow a unimodal distribution, but instead was best fitted as a mixture of two Gaussians with peaks at 22 ± 6 pN and 41 ± 14 pN (Figure 7.4.3A). These values are similar to those we obtained for single and clustered channels in HEK293T cells (Figure 7.4.2), suggesting that native SK channels are distributed as single channels or as groups of two channels in distal dendritic regions of hippocampal pyramidal neurons. Therefore, the density of SK channels on dendritic surfaces is ~60-90 channels/μm^2, assuming a 6.2% event detection frequency over the 1024 samples in the 1μm^2 area (Figure 7.4.3).

The absence of apamin-sensitive SK channels at the soma was intriguing given that they had been detected in the soma of cultured pyramidal neurons in prior studies [264]. However, this work focused on the localization of transfected SK2-S channels rather than endogenous channels and may have resulted in artificially high levels of SK2 channels throughout the cell. To determine whether overexpression changed the distribution of channels, we overexpressed SK2-S channels in cultured hippocampal pyramidal neurons and repeated measurements with

the apamin functionalized AFM probe. In this situation, binding forces were readily detectable at the soma from SK2-S transfected neurons (Figure 7.4.3D). The binding force histogram could be fitted as a mixture of two Gaussians, with peaks of 40 ± 11 pN and 67 ± 14 pN (Figure 7.4.3D), values approximately two- and three-fold greater than the mean binding force for a single SK channel. This confirms that overexpressed SK2 channels are localized to the soma and suggests that they cluster in groups of two to three channels. However, the absence of significant binding events in the soma of untransfected neurons indicates that native SK channels are minimally expressed in this subcellular compartment.

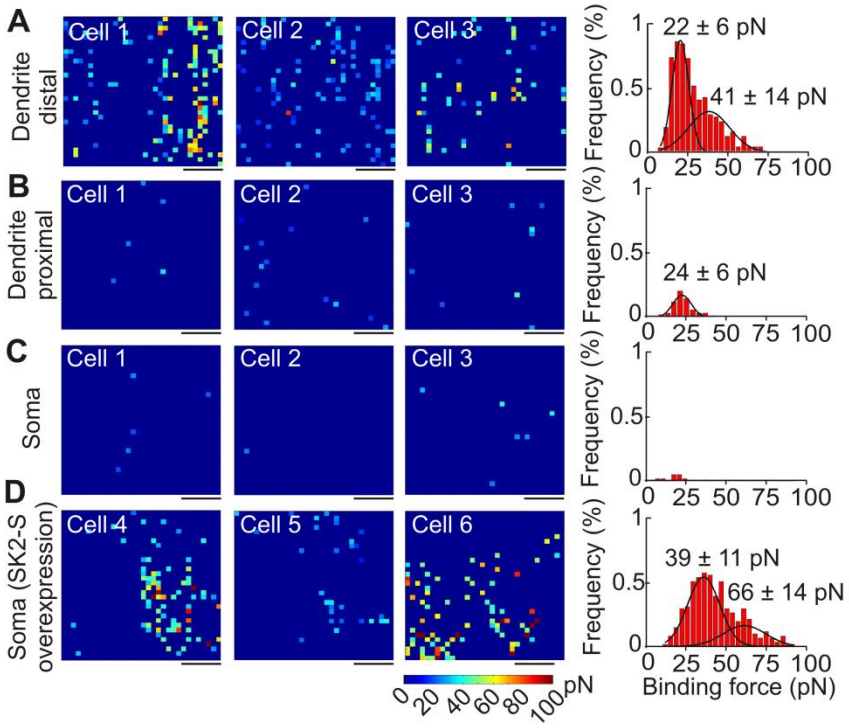

Figure 7.4.3. SK channels are polarized in pyramidal neurons. (A) Binding force maps and corresponding histogram showing detected SK2 channels on the distal region of the dendrite (n=11). (B) Binding force maps and corresponding histogram showing detected SK2 channels on the proximal region of the dendrite (n=7). (C) Binding force maps and corresponding histogram showing the detection of SK2 channels on the soma (n=7). (D) Binding force maps and corresponding histogram showing the detection of SK2 channels on the soma after transfection with SK2 channels (n=6). Scale bars, 250 nm. Color scale as shown.

Finally, we used the quantitative nature of this technique to determine how the dendritic SK channel distribution changes in response to neuromodulation. SK channel activity is affected by multiple neuromodulators, often through generation of cAMP and subsequent activation of protein kinase A (PKA). Studies in neurons and heterologous cells have shown that application of forskolin, a strong PKA activator, causes the internalization of SK2 channels from cell surfaces [277-278]. Therefore, we measured binding events in neurons that had received either 15μM or 30μM forskolin for 15 minutes. Compared to untreated neurons, the more distal dendrites (>30μm from the soma) of forskolin-treated neurons exhibited fewer apamin-dependent binding events (Figure 7.4.4). Interestingly, the mean binding force histograms are different in all three conditions (Figure 7.4.4C): 1) in untreated neurons there is a bimodal histogram with relatively equal peaks at 22 and 44 pN; 2) the histogram for neurons treated with 15 μM FSK is bimodal with a larger peak at 31 pN and a smaller peak at 42 pN; and 3) the apamin binding force histogram follows a unimodal distribution after 30 μM forskolin treatment centered on 27 pN. The peak in the presence of 30 μM forskolin is centered at 27 pN a value in between the two peaks in the untreated neurons, thus making it difficult to conclude whether clusters were preferentially lost. Future studies are needed to explore the effect of FSK on the SK channels subcellular distribution.

7.5. Discussion

In this work we show that integration of single molecule AFM with toxin pharmacology allowed us to map the spatial organization and density of endogenous SK channels in living neurons. By taking advantage of the nanometer resolution of single molecule AFM, we demonstrate that SK channels are highly concentrated on neuronal dendrites. Importantly, we show that SK channels are organized on neuronal membranes as either groups of two or single entities. This differential clustering might represent the distribution of the two SK2 channel isoforms, plasma membrane

diffusional barriers, or areas of exocytosis. Currently, we cannot distinguish between these alternatives.

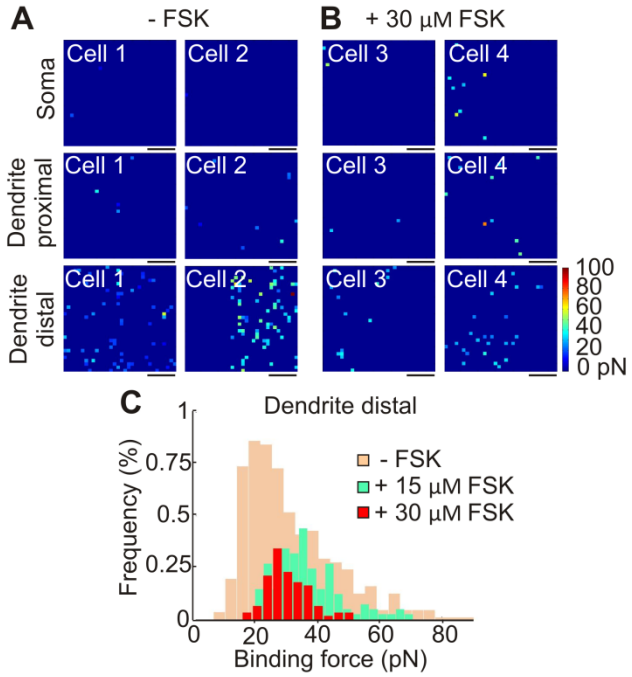

Figure 7.4.4. SK channel maps in pyramidal neurons are dynamic. (A) Binding force maps showing detected SK2 channels without FSK on the soma, proximal dendrite, and outward dendrite. (B) Binding force maps showing a significant decrease in detected SK2 channels after administration of 30 μM FSK for 15 minutes. (C) Binding force histograms showing the distribution of rupture forces in the native state (tan, background) and after 15 μM (green; n=4) and 30 μM FSK administration (red, foreground; n=6). Scale bars, 250 nm. Color scale as shown.

The high density of SK channels in dendrites is also consistent with electrophysiological and imaging work showing that SK channels are critical in regulating dendritic integration [279], controlling the kinetics of excitatory postsynaptic potentials, and induction of long-term potentiation, and learning and memory [267]. But is there a particular advantage for the high SK channel concentration in dendrites? We suggest that high SK channel concentration might increase the gain and reliability of SK channel activation. This might be necessary as SK channels are found in calcium microdomains. That is, SK channels and calcium channels are found within 100-150nm distances from each other, unlike BK channels that are in calcium

nanodomains (10-30nm) [280]. As the calcium concentration decays very rapidly following calcium channel closure, the likelihood of activating SK channels would also decrease quickly. SK channels partly counteract this effect by having high calcium affinity (Km: ~500-700nM) [280]. However, SK channel activation might also be boosted though their high dendritic density. This will further increase their prospect of activation, as more SK channels will be available to capture calcium. Future studies and modeling are required to test this possibility and to examine whether high SK channels density could lead to buffered diffusion of calcium within the SK channel clusters [281]. Calcium buffered diffusion will further increase the probability of SK channel activation.

In conclusion, by using naturally derived toxins that bind with high affinity to ion channels, we can map the subcellular distribution of native ion channels at the cell surface. Over the years, toxins have emerged as an invaluable tool to study ion channels physiology as well as the relationship between their structure and function [282]. Other studies have also used toxins for ion channel localization however, these studies relied on non-living tissue and the use of either radioactive labeled toxins or toxins conjugated with fluorescence probes. Although conjugating toxins with fluorescent dyes would allow for the determination of ion channel density in living neurons, it would be difficult to visualize ion channels on the single channel level without appropriate computational tools. Integration of toxin pharmacology with single molecule AFM bypasses these issues, as it only requires knowledge of the forces between the toxin and the ion channel of interest. We expect our approach to have a significant impact to the study of ion channels and other surface proteins for which high affinity toxins exist.

Chapter 8. AKAP-Dependent Modulation of BCAM/Lu Adhesion on Normal and Sickle Cell Disease RBCs Revealed by Force Nanoscopy

8.1. Abstract

Human normal and sickle red blood cells (RBCs) adhere with high affinity to laminin via the basal cell adhesion molecule/Lutheran (BCAM/Lu) receptor which is implicated in vasoocclusive episodes (VOEs) in sickle cell disease (SCD) and activated through the cyclic adenosine monophosphate (cAMP) signaling pathway. However, the effect of the cAMP pathway on the expression of active BCAM/Lu receptors at the single-molecule level is unknown. We established an *in vitro* technique, based on atomic force microscopy, which enables detection of single BCAM/Lu proteins on the RBC surface and measures the unbinding force between BCAM/Lu and laminin. We showed that the expression of active BCAM/Lu receptors is higher in homozygous sickle RBCs (SS-RBCs) than normal RBCs and that it is critically dependent on the cAMP signaling pathway on both normal and SS-RBCs. Importantly, we illustrated that A-kinase anchoring proteins (AKAPs) are crucial for BCAM/Lu receptor activation. Furthermore, we found that SS-RBCs from hydroxyurea-treated patients show a lower expression of active BCAM/Lu receptors, a lower unbinding force to laminin, and insignificant stimulation by epinephrine as compared to SS-RBCs from untreated patients. These findings may lead to novel anti-adhesive targets for VOEs in SCD.

8.2. Introduction

Red blood cells (RBCs) express several surface adhesion receptors known to modulate cellular physiology [62, 122]. In sickle cell disease (SCD) [28-29], cytoadherence of RBCs to endothelial laminin via the basal cell adhesion molecule/Lutheran (BCAM/Lu) receptor is thought to be a major contributor to and possibly the primary cause of vasoocclusive episodes (VOEs) [64, 71].

On normal and homozygous sickle RBCs (SS-RBCs), the activation of adhesion receptors can be modulated by hormones such as epinephrine [30, 72], pharmaceutical drugs such as hydroxyurea [73, 78], and other biochemical stimuli [283]. Because SCD patients have extensive endothelial damage [80] and elevated plasma levels of laminin [81], RBC adhesion studies have focused on the specific interaction between BCAM/Lu and the α5 chain on laminin (LAMA5), a component of the subendothelial matrix [82-83, 284]. Although it is known that this interaction is mediated by cyclic adenosine monophosphate (cAMP) [72], the effects of the cAMP signaling pathway on the expression of BCAM/Lu receptors and on the interaction between BCAM/Lu and LAMA5 at the single-molecule level are unknown. Further, it is unknown if scaffold or anchoring proteins, such as A-kinase anchoring proteins (AKAPs) [88], play a role in BCAM/Lu receptor activation. It is also unknown, at the single-molecule level, if treatment with hydroxyurea (HU) modulates BCAM/Lu receptor expression or modifies the strength of the bond between BCAM/Lu and LAMA5.

In this paper, we employed single-molecule atomic force microscopy (AFM) [30, 96, 285] to quantitatively study the modulation of BCAM/Lu expression on the membrane of normal and SS-RBCs. Single-molecule AFM measures the unbinding force between a specific ligand and its corresponding receptor on a single cell with piconewton sensitivity [89, 91-92, 132]. We detected the unbinding force between BCAM/Lu and LAMA5, which is interpreted as adhesive force. The generated data are used to calculate the expression of active BCAM/Lu receptors on the RBC surface and their spatial distribution on the membrane at high resolution (~30 nm) [30, 91, 286].

Previous experimental approaches utilizing flow adhesion assays [72] have shown that in SS-RBCs, the interaction between BCAM/Lu and LAMA5 is strongly mediated by cAMP-dependent

protein kinase A (PKA) [72, 83]. Stimulation of the β2-adrenergic receptor (β2-AR) [85-86] activates the G-protein coupled receptor Gαs, which stimulates adenylyl cyclase (AC) [87]. AC then catalyzes the conversion of adenosine triphosphate (ATP) to cAMP, resulting in PKA activation and ensuing BCAM/Lu-laminin adhesion. Normal RBCs, however, adhere minimally to the vascular endothelium [122] and their response to stimulation by epinephrine or forskolin has not been detected by flow adhesion experiments [72]. Here, by using a single-molecule assay, we clearly detected variability in the expression of BCAM/Lu on normal and SS-RBCs as it is modulated by the cAMP signaling pathway.

It is currently unknown if the scaffold protein AKAPs [88] play a role in BCAM/Lu receptor activation by localizing PKA activity to specific subcellular domains within RBCs. In other cell types, it has been found that PKA activity is localized within the cell by attachment of the PKA molecule to an AKAP. Specifically, a PKA tetrameric holoenzyme [79], consisting of two catalytic and two regulatory subunits, binds to an AKAP via its regulatory subunits. The resultant PKA/AKAP complex is localized to a unique subcellular domain due to the AKAP-specific targeting domain [85, 287]. In this work, we showed that AKAPs mediate the activation of BCAM/Lu by PKA in RBCs, signifying that cAMP activates PKA locally, close to the cell membrane.

Hillery et al. [78] first demonstrated that SS-RBCs from patients receiving hydroxyurea undergo a decrease in adhesion to LAMA5. This finding was contrasted by another result [288] showing that the expression of BCAM/Lu receptors on SS-RBCs from HU-treated patients increased. A resolution to this conflicting evidence was offered by a recent work which demonstrated that the reduced adhesion of SS-RBCs to LAMA5 is likely due to inhibition of BCAM/Lu phosphorylation by HU [73]. However, it is still unclear if the lower adhesion is only due to the reduced

expression of active BCAM/Lu receptors as a result of inhibition of BCAM/Lu phosphorylation, or if HU also affects the unbinding force between BCAM/Lu and LAMA5. In our experiments, we measured the expression and unbinding force to LAMA5 of active BCAM/Lu receptors on SS-RBCs from untreated and HU-treated patients. We found that both the expression and adhesive force of active BCAM/Lu molecules is decreased in HU-treated patients. These data demonstrate a very beneficial effect of HU in reducing the propensity of SS-RBCs to adhere to LAMA5.

In summary, we employed single-molecule AFM to investigate interactions between RBCs and the endothelium, and their regulation via cAMP. We quantified cAMP-dependent modulation of active BCAM/Lu receptor expression in normal and SS-RBCs. We are first to demonstrate that AKAPs are crucial for the activation of BCAM/Lu receptors. Lastly, we showed that HU treatment results in decreased erythrocyte adhesion to the endothelium due to lower expression of BCAM/Lu receptors and lower binding forces between BCAM/Lu and LAMA5.

8.3. Methods

Patients and blood samples

Homozygous SCD patients (SS) at steady-state, and age-/race-matched healthy volunteers at least 18 years old were eligible to participate in this study which was approved by the Institutional Review Boards of the UCONN Health Center and UCONN-Storrs. Individuals with SCD were eligible to participate if they had not been transfused in ≥ three months and were not having an acute VOE, suggesting a phenotype of milder severity. A complete blood count test was obtained for each patient. The untreated patients average HbF concentrations of 9.6±4.0% (range: 0%–18.2%), while HU-treated patients average 34.1% (range: 18.1%-56.1%). Reticulocyte percentages average 10.8±2.0% (range: 4.2%-15.7%) for untreated patients and

4.1±0.9% (range: 2.3%-6.7%) for HU-treated patients. Healthy volunteers were eligible to participate if they did not have a blood disorder or hemoglobinopathy, which was confirmed by screening blood samples via hemoglobin electrophoresis. Experiments were performed using fresh-drawn, heparin-anticoagulated venous blood.

Red blood cell preparation

Whole blood was centrifuged at 500*g* for 10min at 4°C to isolate RBCs. The buffy coat was aspirated and discarded. RBCs were washed 3x with Alsever's solution. RBCs were immobilized by incubation on a poly-l-lysine coated glass petri dish for 10min at 37°C and unattached RBCs were removed by rinsing.

Reagents

Human laminin subunit alpha-5 (LAMA5) was obtained from MyBioSource (San Diego, CA), St-Ht31 inhibitor peptide and St-Ht31P control peptide (reconstituted in Alsever's solution) were obtained from Promega (Madison, WI). Alsever's solution, forskolin (*Coleus forskohli*) (reconstituted in DMSO), Rp-Adenosine 3',5'-cyclic monophosphorothioate triethylammonium salt (Rp-cAMPS; reconstituted in DMSO), KT-5720 (reconstituted in methanol), epinephrine (reconstituted in Alsever's solution), bovine serum albumin (BSA; reconstituted in PBS) were purchased from Sigma Aldrich (St. Louis, MO).

Preparation of LAMA5 probes

Silicon nitride cantilevers (Bruker Probes, Camarillo, CA) were silanized with 2% v/v 3-aminopropyltriethoxysilane in acetone (10min), then rinsed with deionized (DI) water and immersed in glutaraldehyde (0.5%, 30min). Cantilevers were rinsed with DI water, incubated in LAMA5 solution (100µg/mL, 30min), rinsed again, and incubated in BSA (100µg/mL, 5min) to

block remaining aldehyde groups. Cantilevers were stored at 4°C and utilized within 48 hours.

Atomic force microscopy assays

Force-distance curves were recorded between laminin-functionalized probes and BCAM/Lu receptors on the RBC surface (Figure 8.3.1A) using the MFP-3D-BIO AFM (Asylum Research, Santa Barbara, CA). An unbinding force is defined as the maximum rupture force associated with the force-distance curve. A representative curve highlighting regions of the approach and retraction cycle is shown in Figure 8.3.1B. On surface regions void of BCAM/Lu receptors, we expected the unbinding force to be approximately zero, while unbinding forces are significantly higher in regions where the laminin-functionalized cantilever made contact with active BCAM/Lu receptors. Unbinding forces were measured on 1μm x 1μm areas of the RBC membrane with a lateral resolution of 31.25nm (1024 sampled sites per experiment). To determine the spatial distribution of BCAM/Lu receptors on the RBC surface, unbinding forces were plotted as a force map (Figure 8.3.1D) using MATLAB (Mathworks) in which the color of each square indicates the magnitude of the corresponding unbinding force obtained from an individual curve [30].

An inverted microscope (Zeiss Axiovert A1) was used to position the AFM cantilever in contact with a chosen RBC (Figure 8.3.1C). Chosen RBCs were less than 10μm in diameter and exhibited a distinct biconcave shape, suggesting RBC maturity. Experiments were performed in Alsever's solution at 37°C, and biochemical modulators were added at least 30min prior to experiments. For each assay, 3 RBCs were tested from each subject's blood. Values reporting "N = " denote the number of unique donors per condition and "n = " denote the total number of tested cells. Measurements were recorded with a loading rate of 24000pN/s [30]. The nominal spring constant of the employed cantilever was 30pN/nm and the exact spring constant value was obtained via a thermal noise-based method and used in all calculations [289].

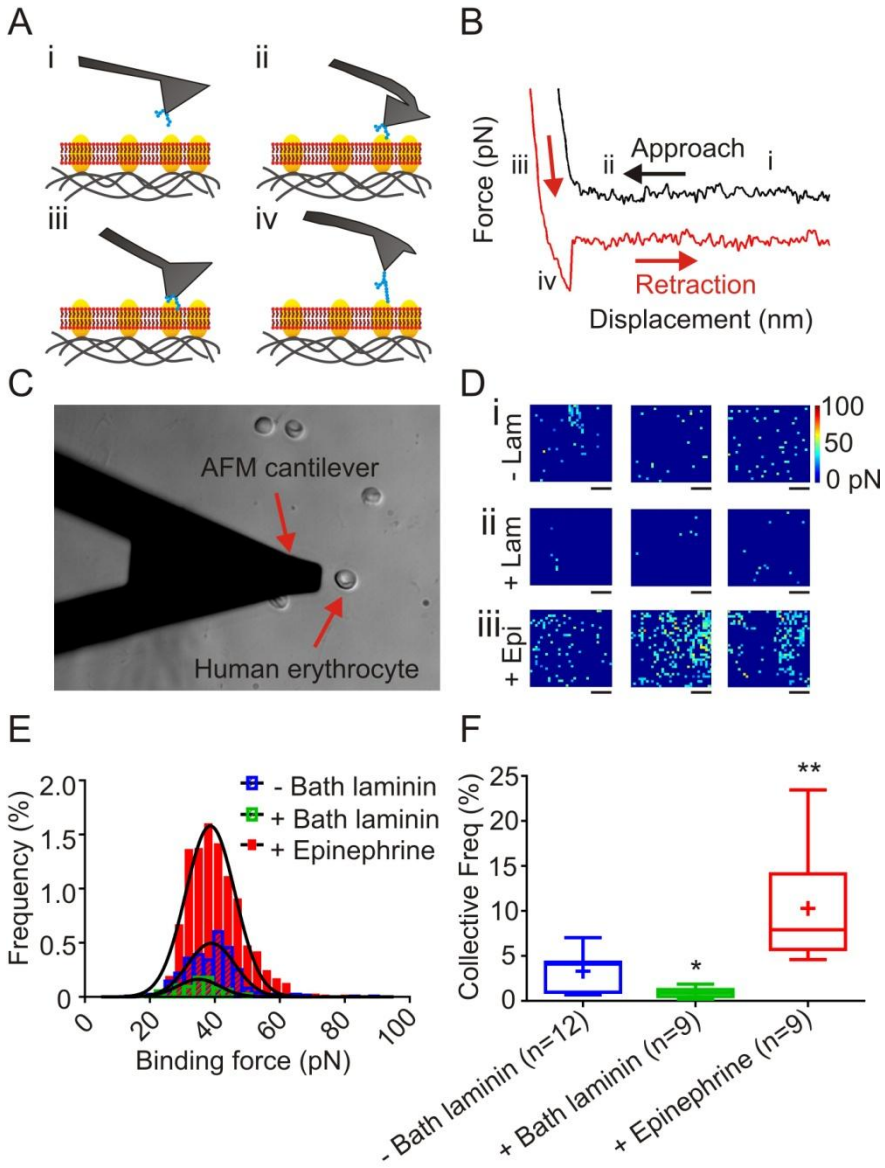

Figure 8.3.1. Measurement of the frequency of active BCAM/Lu surface receptors and the unbinding force with LAMA5 on RBCs using AFM. (A) AFM cantilever probe functionalized with LAMA5. Illustration corresponds to the force curve shown in (B). (B) Force curve obtained from experiments highlighting regions of the approach and withdrawal of the cantilever from the sample. When LAMA5 attached to the AFM probe adheres to a BCAM/Lu receptor on the cell, the force-displacement curve exhibits an abrupt shift to zero which corresponds to the rupture force (red curve). If there is no BCAM/Lu receptor at the detection point and consequently no adhesive interaction, then the retraction curve is similar to the black curve. Specific regions are as follows: (i) No interaction between the tip and cell; (ii) Functionalized cantilever deflects downward towards the cell as a result of van der Waals forces; (iii) Positive deflection of the cantilever due to repulsive forces; (iv) Negative deflection of the cantilever tip as a result of adhesion forces between the tip and the cell. (C) Representative optical microscopy image showing a human RBC and an AFM cantilever probe. (D) Unbinding force maps of single normal RBCs (i) in the absence and (ii) presence of bath laminin to mask BCAM/Lu binding sites. (iii) Unbinding force maps of single normal RBCs in epinephrine (1μM) show an increase

in active BCAM/Lu receptors. Scale bars, 250nm. Color scale as shown. (E) Frequency distributions of measured unbinding forces fit with the Gaussian model to obtain the average unbinding force and (F) box-whisker plot of the collective frequency of detected BCAM/Lu receptors on normal RBCs per experimental condition. Data are presented as median with max and min whiskers and the average denoted as (+).The 'n' on the x-axis indicates the total number of mature RBCs analyzed in each group, obtained from the following numbers of human subjects: – Bath laminin: 4 subjects; + Bath laminin, + Epinephrine: 3 subjects. Significance relative to – bath laminin is denoted as * such that $p<0.05$ and ** such that $p<0.005$ (two-tailed t-test).

Statistical methods

Values for the unbinding force between BCAM/Lu and LAMA5 are reported as average ± standard deviation (SD) as determined by a frequency distribution fit with the Gaussian model (GraphPad Prism). In the frequency (%) distribution, each bin contains the number of unbinding forces with values within the bin's range divided by the total number of sampled sites. We note that the frequency of zero force points is not shown since it is much larger than the frequency of non-zero force points and would obscure the graphs. Collective frequency (%), denoted CF, is defined as the total number of all non-zero force points, without respect to specific unbinding forces, divided by the total number of sampled sites for each experimental condition. It is reported as average ± standard error of the mean (SEM) and is illustrated by box-whisker plots. The collective frequency of active receptors was compared between groups using a one-way ANOVA with the Tukey *post hoc* test, and between two conditions using a two-tailed t-test. Results were considered significant if $p<0.05$.

8.4. Experimental Validation

Immunofluorescence following probe functionalization

Immunofluorescence was used to validate cantilever functionalization with LAMA5. Freshly prepared cantilevers were incubated (1 hour at 25°C) with anti-LAMA5 antibody (200 µg/mL) conjugated to AlexaFluor®488 (EMD Millipore). Fluorescent images were obtained using a

Leica TCS SP2 Confocal Microscope (Figure 8.4.1.). Negative controls were produced using the specific anti- LAMA5 antibody with non-functionalized probes and with probes functionalized with the toxin apamin.

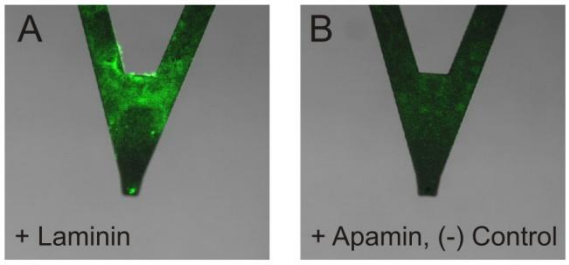

Figure 8.4.1. Immunofluorescence following probe functionalization.

Scan area determination

To determine the ideal scan area for the detection of active BCAM/Lu receptors, we recorded unbinding force maps on 2 μm x 2 μm areas of the RBC membrane with a lateral resolution of 31.25nm (4096 sampled sites per experiment). Multiple cells (n=10) were scanned from one healthy subject. Using a MATLAB script, each 2μm x 2μm binding force map was then divided into areas of the following sizes: 1 μm x 1 μm, 500 nm x 500 nm, and 250 nm x 250 nm.

First, the frequency of detected receptors was calculated for each unbinding force map. For each cell, the total number of force maps is as follows: 2 μm x 2 μm, n = 1; 1 μm x 1 μm, n = 4; 500 nm x 500 nm, n = 16; 250 nm x 250 nm, n = 64. The results are illustrated using a box-whisker plot of the collective frequency of detected BCAM/Lu receptors for each scan size (Figure 8.4.2). The ‘n’ on the x-axis indicates the total number of scan areas analyzed in each group, obtained from n=10 RBCs from one healthy subject. Using a one-way ANOVA with the Tukey *post hoc* test and Bartlett’s test, we find that differences among the standard deviations are statistically significant ($p < 0.0001$). As expected, there is no difference among the means. Analysis was also performed on individual cells, yielding the same result. To validate this result,

the D'Agostino-Pearson omnibus test was employed to determine if the collective frequency values exhibit normality. It was determined that 500 nm x 500 nm and 250 nm x 250 nm unbinding force maps do not exhibit normality ($p<0.0001$). To make experimental testing more efficient, we performed all atomic force microscopy tests on 1µm x 1µm areas of the RBC membrane.

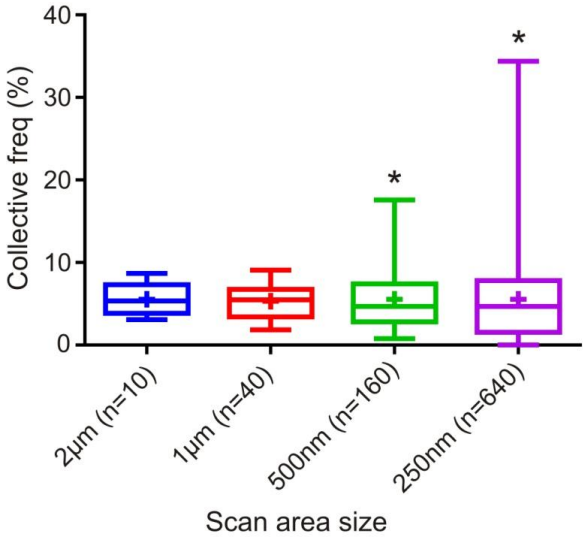

Figure 8.4.2. Scan area size determination. Box-whisker plot of the collective frequency of detected BCAM/Lu receptors for each scan size. Data are presented as median with max and min whiskers. The 'n' on the x-axis indicates the total number of scan areas analyzed in each group, obtained from n=10 RBCs from one healthy subject.

Specificity of experimental assay

To determine the specificity of the measured unbinding forces, we performed experiments on normal RBCs at baseline and on normal RBCs pre-incubated with laminin. As shown in Figure 8.4.3, we found that the frequency of binding force events significantly decreased on RBCs pre-incubated with laminin ($p < 0.01$, from 4.23 ± 1.27% to 0.868 ± 0.197%). Furthermore, the unbinding force decreased in the presence of bath laminin (from 43.45 ± 9.64 pN to 35.42 ± 6.72 pN) Events with significant binding forces most likely reflected BCAM/Lu receptors that were not bound by bath-applied laminin.

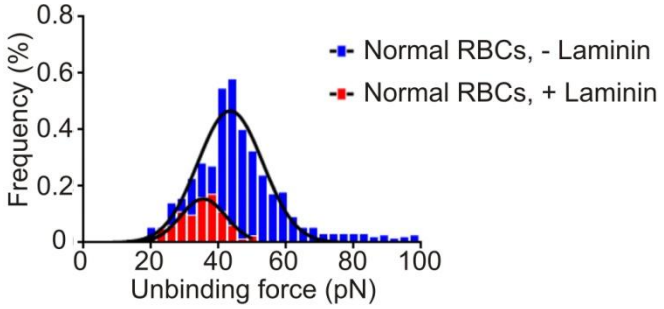

Figure 8.4.3. Specificity of unbinding forces.

8.5. Results

Single-molecule measurement of active BCAM/Lu receptors on normal RBCs

We first performed experiments on normal RBCs in Alsever's solution to determine the baseline frequency (- bath laminin) of active BCAM/Lu receptors and the unbinding force of BCAM/Lu to LAMA5. Figure 8.3.1D(i) shows representative BCAM/Lu-LAMA5 force maps with forces detected between 21.66 and 65.39pN. The frequency of non-zero unbinding forces detected on normal RBCs is shown in Figure 8.3.1E. By accumulating all of the non-zero unbinding forces per cell we obtained the collective frequency, as explained in the methods. The results, illustrated using a box-whisker plot, show that unbinding forces were detected in 3.31±0.67% of sampled sites (Figure 8.3.1F).

To determine the specificity of measured unbinding forces, we repeated experiments on normal samples preincubated with laminin. As shown in Figures 8.3.1D(ii),F, the CF of events detecting unbinding forces on RBCs preincubated with laminin (+ bath laminin) was 0.89±0.21%, which is significantly lower ($p<0.01$) than the baseline frequency (- bath laminin, CF: 3.31±0.67%). Recorded unbinding forces likely reflected BCAM/Lu receptors that were not bound by bath

laminin. To establish that the assay can detect variations in the number of active BCAM/Lu receptors, we preincubated RBCs with epinephrine (1μM), a β-AR agonist known to increase BCAM/Lu binding to LAMA5, and found that events were detected in 10.27±2.02% of sampled sites, a significant increase ($p<0.001$) in the CF from baseline (Figure 8.3.1D(iii),F). Frequency distributions (Figure 8.3.1E) show that while the average unbinding force between BCAM/Lu and LAMA5 did not change in these experimental conditions, the frequency of detected events changed significantly. Further, the data in Figure 8.3.1F illustrate that the AFM-based assay can detect differences in the collective frequency of active BCAM/Lu receptors on normal RBCs at baseline and preincubated with laminin or epinephrine.

BCAM/Lu adhesion of normal RBCs to endothelial laminin is PKA-dependent

Taking advantage of the high-resolution and high-sensitivity of single-molecule AFM, we investigated changes in the frequency of active BCAM/Lu receptors on normal and SS-RBCs via pharmacologic modulation of the cAMP-PKA pathway. First, we treated normal RBCs with forskolin (30μM, FSK), a strong AC activator that stimulates cAMP production, subsequently activating PKA. Compared to untreated RBCs, forskolin-treated RBCs exhibited significantly more unbinding events as shown by the frequency distribution and box-whisker plots (Figure 8.5.1A,C; CF: 18.19±4.68%; $p<0.001$). Previous evidence suggests that the interaction between BCAM/Lu and LAMA5 is stimulated significantly by FSK in SS-RBCs but insignificantly in normal RBCs [72]. These studies used a FSK concentration (80μM) much higher than that currently used (30μM). To understand the discrepancy between ours and previous results, we

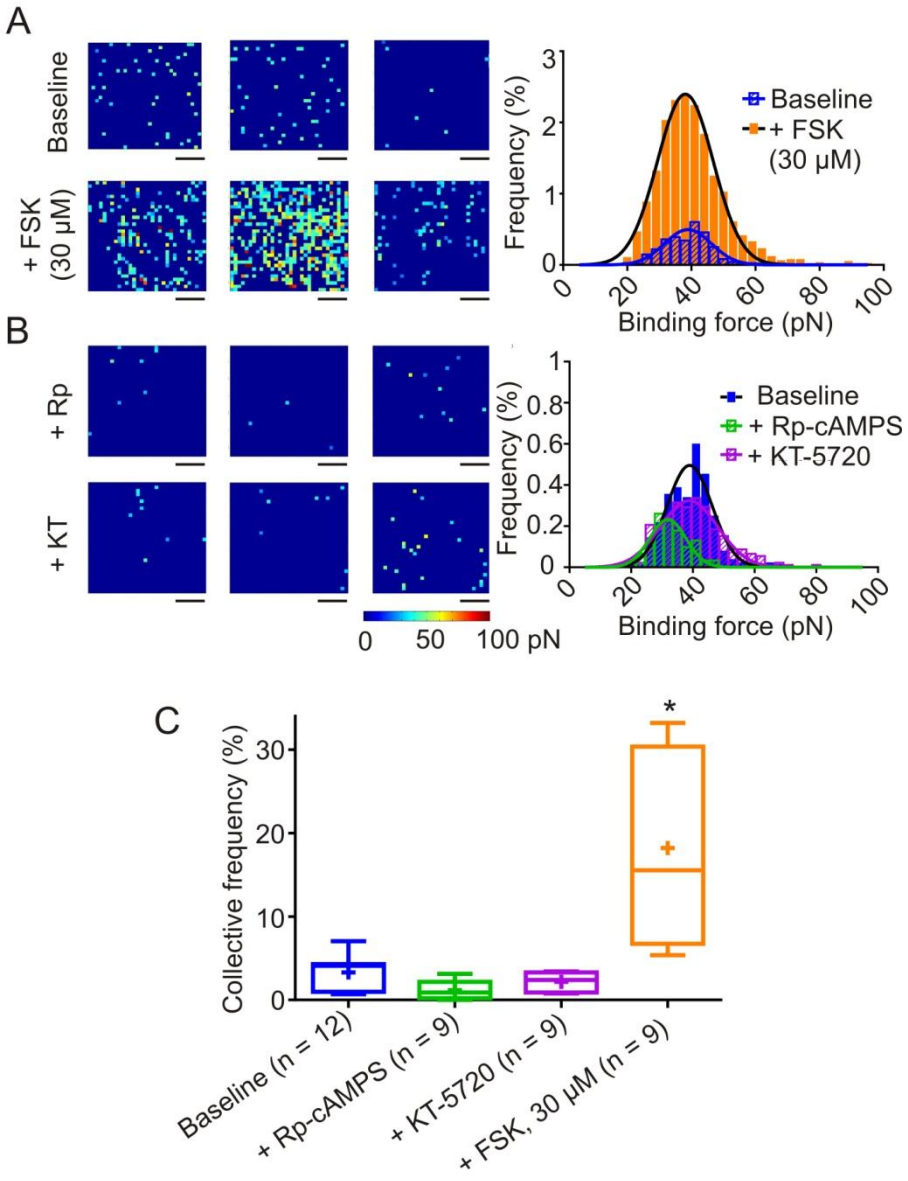

Figure 8.5.1. Distribution of BCAM/Lu on normal RBCs and unbinding force of BCAM/Lu to LAMA5. (A) Unbinding force maps and corresponding unbinding force frequency histograms of normal RBCs measured at baseline and after treatment with 30μM FSK, and (B) measured in the presence of the PKA inhibitors Rp-cAMPS and KT-5720. (C) Box-whisker plot showing the collective frequency of detected BCAM/Lu receptors on normal RBCs for the biochemical modulators indicated on the x-axis, presented as in Figure 8.3.1. The 'n' on the x-axis indicates the total number of mature RBCs analyzed in each group, obtained from the following numbers of human subjects: Baseline: 4 subjects; FSK (30μM), Rp-cAMPS, KT-5720: 3 subjects. Significance relative to baseline is denoted as * such that $p<0.001$ (ANOVA, Tukey *post hoc* test).

used the higher concentration of FSK employed in the previous study [72]. In this case, we found that the interaction between BCAM/Lu and LAMA5 was stimulated (data not shown; CF: 10.10±1.89%, N=3, n=9) significantly more than normal RBCs at baseline ($p<0.05$), albeit not significantly more than those treated with 30μm FSK. It is possible that flow adhesion assays, which measure the average adhesion of a large number of erythrocytes to a functionalized-substrate under flow-induced shear stress, are not sensitive enough to detect increases in the overall low adhesion of normal RBCs.

To quantify the effect of PKA inhibition on the frequency of active BCAM/Lu receptors, we treated RBCs with Rp-cAMPS (100μM), a strong inhibitor of PKA activation by cAMP. RBCs pretreated with Rp-cAMPS exhibited fewer unbinding events (Figure 8.5.1B-C; CF: 1.17±0.47%) than normal RBCs at baseline. An apparent decrease in the unbinding force following preincubation with Rp-cAMPS compared to baseline results is statistically insignificant. Next, we directly inhibited PKA using KT-5720 (1μM) and recorded a decrease in the unbinding event frequency (Figure 8.5.1B-C; CF: 2.16±0.41%), albeit not as large as with Rp-cAMPS. Figure 8.5.1C shows a box-whisker plot summarizing changes in the collective frequency of active BCAM/Lu receptors on normal RBCs in response to cAMP-dependent pathway modulation. It is clear that there is a significant increase in the collective frequency of active BCAM/Lu receptors resulting from 30μM forskolin, demonstrating that our system can detect changes in the adhesive properties of human RBCs in response to increases in intracellular cAMP.

SS-RBCs demonstrate greater PKA-dependence of BCAM/Lu adhesion to endothelial laminin than normal RBCs

After establishing our single-molecule AFM technique on normal RBCs and confirming that we can detect differences in the frequency of active BCAM/Lu in response to cAMP-dependent

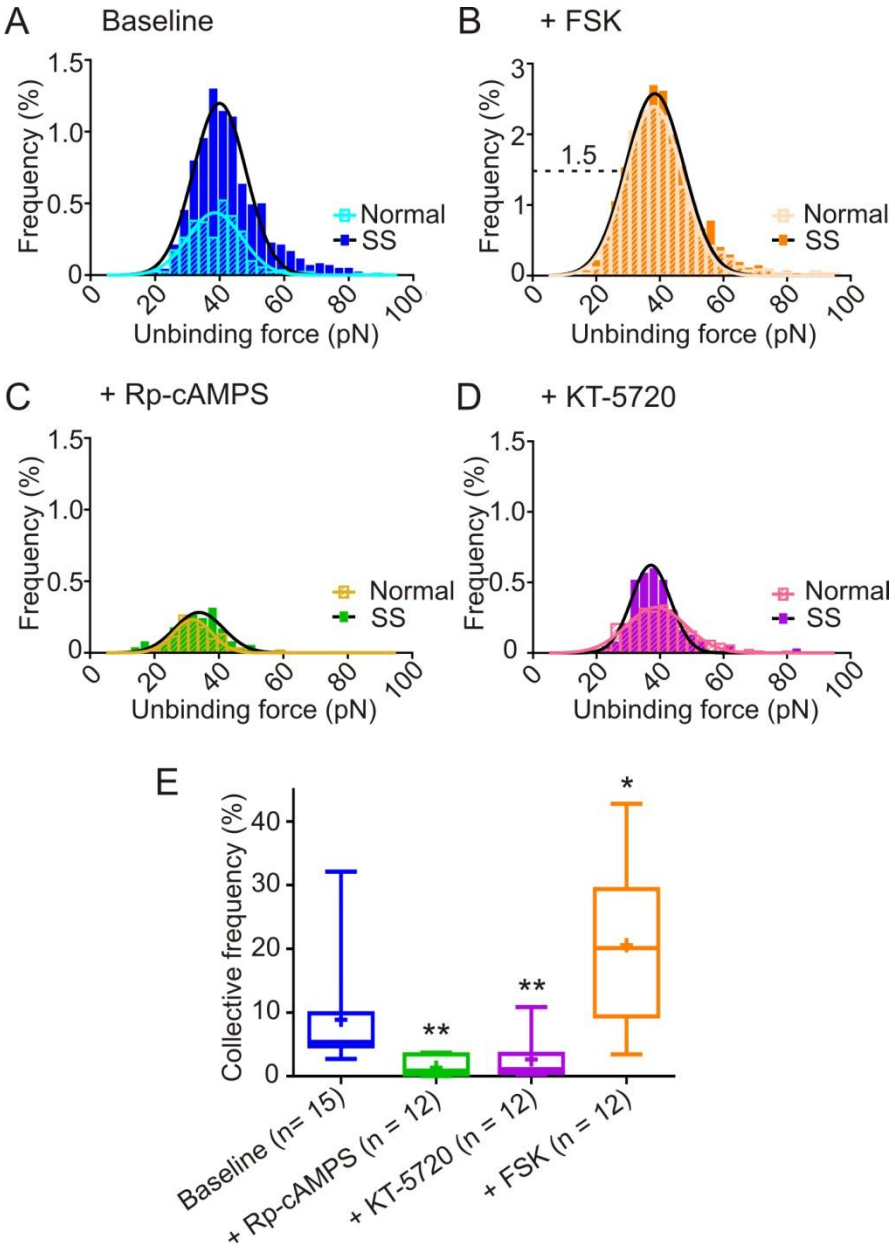

Figure 8.5.2. Distribution of BCAM/Lu on SS-RBCs and unbinding force of BCAM/Lu to LAMA5. (A) SS-RBCs show a significantly greater number of BCAM/Lu surface receptors than normal RBCs at baseline. Measurement after treatment with (B) 30μM FSK, (C) 100μM Rp-cAMPS, and (D) 1μM KT-5720 indicate that SS-RBCs behave similar to normal RBCs upon cAMP-PKA pathway modulation. (E) Box-whisker plot of the collective frequency of detected BCAM/Lu receptors on SS-RBCs for the biochemical modulators indicated on the x-axis. The 'n' on the x-axis indicates the total number of mature RBCs analyzed in each group, obtained from the following numbers of human subjects: Baseline: 5 subjects; FSK (30μM), Rp-cAMPS, KT-5720: 4 subjects. Significance relative to baseline is denoted as * such that $p<0.05$ and ** such that $p<0.01$ (ANOVA, Tukey *post hoc* test).

pathway modulators, we applied the same experimental approach to SS-RBCs. In agreement with previous reports [72, 122], we measured a significant increase in the frequency of BCAM/Lu receptors on SS-RBCs (Figure 8.5.2A,E; CF: 8.89±2.05%) as compared to normal RBCs ($p<0.01$). Next, we quantified changes in the frequency of active BCAM/Lu receptors on SS-RBCs in response to cAMP-dependent pathway modulation. Following preincubation with FSK (30μM), we observed an increase in the CF to 20.56±3.63% on SS-RBCs, which was significantly greater than that measured at baseline (Figure 8.5.2E; $p<0.01$) and similar to that observed on normal RBCs (Figure 8.5.2B). Importantly, when treated with Rp-cAMPS, the adhesion level of SS-RBCs reduced to that of normal RBCs treated with Rp-cAMPS. However, preincubation with KT-5720 (Figure 8.5.2D) did not decrease the BCAM/Lu receptor frequency on SS-RBCs to the adhesion level of normal RBCs, but still significantly decreased below the baseline measurement to 2.66±1.02% (Figure 8.5.2E; $p<0.05$). Frequency distributions illustrate that the response to modulation of BCAM/Lu on SS-RBCs was analogous to that on normal RBCs (Figure 8.5.2B-D). Further, the collective frequency of detected BCAM/Lu receptors was highly sensitive to cAMP-dependent pathway modulators (Figure 8.5.2E).

A-kinase anchoring proteins regulate BCAM/Lu adhesion

After establishing that our assay can detect cAMP-dependent modulation of active BCAM/Lu receptors on normal and SS-RBCs, we investigated the possibility of localized BCAM/Lu activation via AKAPs [85, 287]. To detect the presence of AKAPs on normal and SS-RBCs, cells were treated with St-Ht31 peptide (5μM), which inhibits binding of PKA to AKAPs. Our experiments revealed that following pretreatment with St-Ht31, the CF of active BCAM/Lu receptors decreased significantly in normal RBCs (Figure 8.5.3A-B; CF: 5.71±1.23% to 3.15±1.09%; $p<0.05$) and in SS-RBCs (Figure 8.5.3C-D; CF: 7.19±1.42% to 2.02±0.37%; $p<0.005$). As a negative control, RBCs were pretreated with St-Ht31P control peptide (5μM),

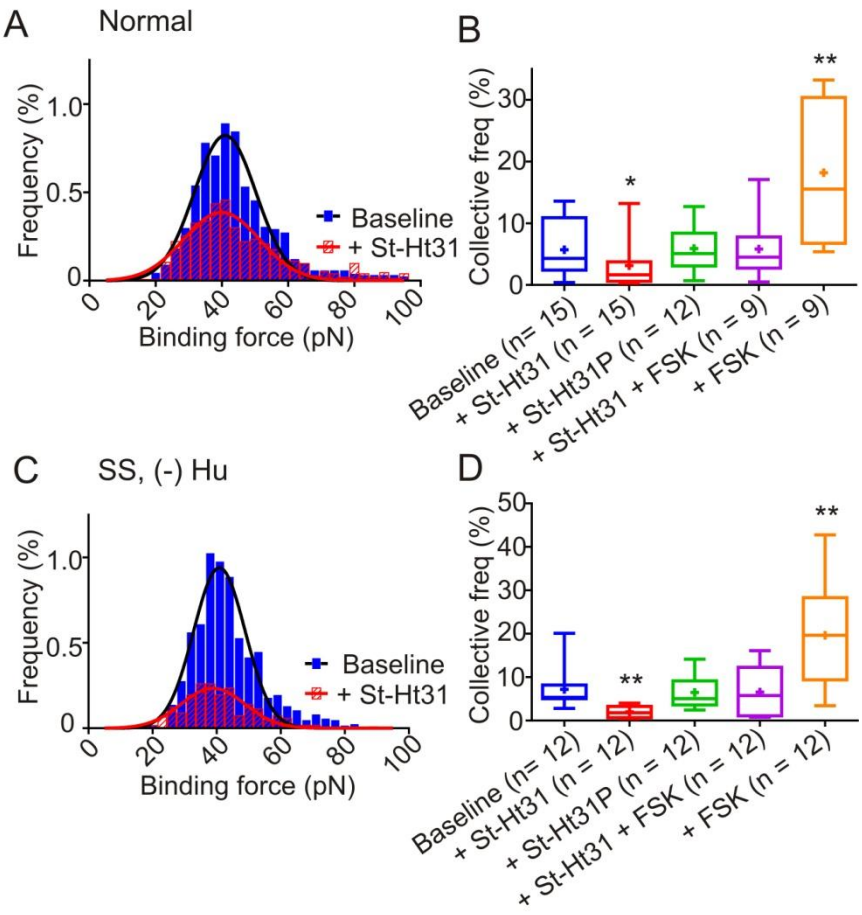

Figure 8.5.3. Modulation of BCAM/Lu via AKAPs on the RBC membrane. (A) Measurements in 5μM St-Ht31 inhibitor peptide demonstrate the presence of AKAPs on normal RBC membranes as revealed by the reduction of the frequency of active BCAM/Lu receptors. (B) Box-whisker plot of the collective frequency of detected BCAM/Lu receptors on normal RBCs for the biochemical modulators indicated on the x-axis, presented as in Figure 8.3.1. The 'n' on the x-axis indicates the total number of mature RBCs analyzed in each group, obtained from the following numbers of human subjects: Baseline, St-Ht31: 5 subjects; St-Ht31P: 4 subjects; St-Ht31 + FSK (30μM): 3 subjects. Significance relative to baseline is denoted as * such that $p<0.05$ and ** such that $p<0.005$ (ANOVA, Tukey *post hoc* test). (C) Measurements in 5μM St-Ht31 inhibitor peptide demonstrates the presence of AKAPs on SS-RBC membranes as revealed by the reduction of active BCAM/Lu receptors. (D) Box-whisker plot of the collective frequency of detected BCAM/Lu receptors on SS-RBCs for the biochemical modulators indicated on the x-axis, presented as in Figure 8.3.1. The 'n' on the x-axis indicates the total number of mature RBCs analyzed in each group, obtained from the following numbers of human subjects: Baseline, St-Ht31, St-Ht31P, St-Ht31 + FSK (30μM): 4 subjects. Significance denoted as in (B).

which did not alter the collective frequency of active BCAM/Lu receptors in normal RBCs (Figure 8.5.3B; CF: 5.92±1.09%) or in SS-RBCs (Figure 8.5.3D; CF: 6.49±1.27%) as compared to baseline measurements. To ensure that AKAP inhibition would block BCAM/Lu receptor activation, RBCs were treated with St-Ht31 (5μM) and subsequently with FSK (30μM). On normal RBCs, the CF of active BCAM/Lu receptors was measured to be 5.83±1.65% versus 18.19±4.68% following only FSK stimulation (Figure 8.5.3B; $p<0.005$). Similarly, on SS-RBCs the CF of active BCAM/Lu receptors was measured to be 6.57±1.60% in this case versus 19.63±3.44% following only FSK stimulation (Figure 8.5.3D; $p<0.005$). This indicates the presence of AKAPs in the RBC membrane and suggests their importance in the mediation of RBC cytoadherence to the endothelium in both normal and SS-RBCs.

Hydroxyurea decreases the frequency and the strength of BCAM/Lu-dependent adhesion events on SS-RBCs

Hydroxyurea is currently the only pharmacologic treatment to reduce the frequency of VOEs in SCD, yet only two-thirds of patients respond favorably to the drug [74]. The drug has specifically been found to inhibit phosphorylation of BCAM/Lu receptors and consequently to decrease SS-RBC adhesion to laminin [73, 78]. Here, we investigated the quantitative effect of HU treatment on the frequency of active BCAM/Lu receptors and on the magnitude of the unbinding force between BCAM/Lu and LAMA5, which could be another reason for the reduced adhesion of SS-RBCs to laminin. Our experiments showed that SS-RBCs from HU-treated patients have a significantly lower frequency of active BCAM/Lu receptors than SS-RBCs from untreated patients (Figure 8.5.4A; CF: 8.89±2.05% to 2.43±0.51%; $p<0.001$). Importantly, we also detected that the unbinding force between BCAM/Lu and LAMA5 was lower on SS-RBCs from HU-treated patients (Figure 8.5.4B; CF: 35.14±7.18pN versus 40.00±8.12pN; $p<0.0001$). Next, the physiologic implication of epinephrine-stimulated adhesion of HU-treated SS-RBCs was

studied. We treated SS-RBCs with epinephrine and found that for SS-RBCs from patients undergoing HU-treatment, the frequency of BCAM/Lu did not increase significantly. Figure 8.5.4C shows that while the CF of BCAM/Lu receptors increased significantly following treatment with epinephrine on both normal RBCs and untreated SS-RBCs, there was no significant increase in hydroxyurea-treated SS-RBCs.

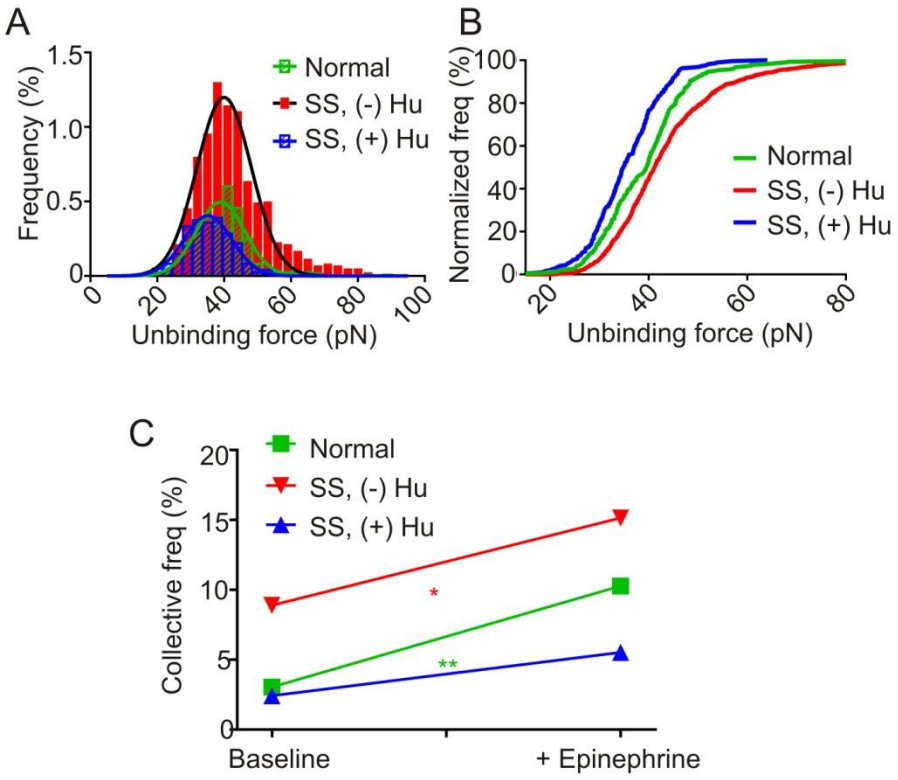

Figure 8.5.4. Modulation of the collective frequency of BCAM/Lu receptors on SS-RBCs from HU-treated patients. (A) SS-RBCs from HU-treated patients (N=4, n=12) have a significantly lower frequency of BCAM/Lu receptors than SS-RBCs from untreated patients (N=5, n=15) and healthy subjects (N=4, n=12). (B) Normalized cumulative distribution clearly shows significant shift in the unbinding force of BCAM/Lu and laminin on SS-RBCs from HU-treated patients ($p<0.0001$). (C) Preincubation with epinephrine causes a significant increase in the collective frequency of BCAM/Lu receptors on both normal RBCs (N=3, n=9) and SS-RBCs from untreated patients (N=5, n=15) but not on SS-RBCs from HU-treated patients (N=4, n=12). Significance is denoted as * such that $p<0.05$ and ** such that $p<0.005$ as computed using the t-test.

8.6. Discussion

In this work, we established a technique, based on AFM, which enables the detection of single BCAM/Lu molecules on the RBC surface and measures the unbinding force between BCAM/Lu and LAMA5. The technique is used to study the effect of the cAMP signaling pathway on the activation of BCAM/Lu receptors at the single-molecule level. Importantly, we demonstrate that AKAPs are essential for BCAM/Lu receptor activation, and that the collective frequency of BCAM/Lu receptors, present on both the normal and SS-RBC membrane, is critically dependent on the cAMP pathway. Lastly, we found that SS-RBCs from hydroxyurea-treated patients have a lower frequency of active BCAM/Lu receptors than SS-RBCs from untreated patients, and undergo insignificant stimulation by epinephrine. We also demonstrated that the unbinding force between BCAM/Lu and LAMA5 in hydroxyurea-treated patients is lower than in untreated patients.

cAMP-dependent modulation of BCAM/Lu on normal RBCs

We first determined how the frequency of active BCAM/Lu receptors changes in response to cAMP signaling. Forskolin activates AC which raises levels of cAMP and subsequently activates the cAMP-dependent pathway. Normal RBCs treated with FSK (30μM) showed an increase in the frequency of active BCAM/Lu receptors significantly above baseline, in accordance with established cAMP-dependent pathway modulation. However, previous studies based on flow adhesion assays showed that adhesion of normal RBCs via BCAM/Lu is not mediated significantly by forskolin, likely due to low levels of intracellular cAMP [72]. In contrast, our results indicate that normal RBC adhesion to LAMA5 via the BCAM/Lu receptor is significantly modulated by the cAMP-dependent pathway. This difference is due to two reasons. First, previous studies used a forskolin concentration of 80μM, which is more than 2x greater than the concentration we initially employed (30μM). When normal RBCs were treated with 80μM FSK,

the frequency of active BCAM/Lu receptors did not increase as significantly above the baseline as in the case of 30μM FSK. This suggests that high concentrations of FSK may desensitize BCAM/Lu to cAMP-dependent pathway signaling, as shown for the ICAM-4 receptor on RBCs and signaling receptors on other cell types [249, 290-291]. Second, because the adhesiveness of normal RBCs is low, the high-sensitivity of AFM allows for a more precise detection of active adhesion receptors than traditional flow adhesion assays. We also note that flow adhesion assays did not detect adhesion of non-stimulated normal RBCs to laminin [72-73].

cAMP-dependent modulation of BCAM/Lu on SS-RBCs

While the pathway by which cAMP mediates BCAM/Lu receptor activation is well-established, the possibility that AKAPs are involved in the localization of cAMP close to the RBC membrane has not been investigated. In the current work, we used specific biochemical modulators to investigate the subcellular targeting of the cAMP-dependent PKA [79]. PKA activity can be mediated by AKAPs, which sequester PKA to specific subcellular sites through binding to its regulatory subunits [85, 287, 292]. Each AKAP contains two classes of binding sites: an anchoring motif, which binds to the regulatory subunit of PKA, and a targeting domain, which directs the subcellular localization of the PKA-AKAP complex through association with structural proteins, membranes, or other cell elements [287]. BCAM/Lu-mediated SS-RBC adhesion to LAMA5 is activated by the phosphorylation of serine 621 in the BCAM/Lu cytoplasmic domain, but this phosphorylation does not occur as readily in normal RBCs [83]. We conjecture that this is due to the presence of more PKA-AKAP complexes in SS-RBCs, and resultant AKAP assistance in the phosphorylation of BCAM/Lu on RBCs. Also, because protein activation is highly selective despite the high cAMP diffusion constant of 270-280 $\mu m^2/s$, it is likely that the cAMP is compartmentalized [293-294] and has a basal effect on normal RBCs which only requires increases in cAMP near the membrane. This may explain why we detected modulation

of BCAM/Lu via the cAMP-dependent pathway despite low levels of cAMP in normal RBCs [72].

Hydroxyurea reduces the adhesion of SS-RBCs via the BCAM/Lu receptor

Hydroxyurea, a pharmacologic treatment for SCD VOEs, is known to stimulate an increase in HbF [75-76] synthesis, and may also alter RBC signaling [73, 77-78]. The drug has been found to decrease SS-RBC adhesion to laminin [73, 78], although it increases BCAM/Lu surface expression [73, 288]. Hillery et al. [78] first demonstrated that RBCs from SCD patients receiving HU undergo a decrease in adhesion to laminin. Recently it was shown that although BCAM/Lu receptor expression is increased on SS-RBCs from HU-treated patients, SS-RBC adhesion to laminin is decreased because of inhibition of cAMP phosphorylation [73, 288]. In our experiments, we measured a lower frequency of active BCAM/Lu receptors on SS-RBCs from HU-treated patients versus SS-RBCs from untreated patients. In addition, AFM measurements revealed a lower unbinding force between BCAM/Lu on SS-RBCs from HU-treated patients with LAMA5 as compared to untreated patients. The lower unbinding force between BCAM/Lu and LAMA5 in conjunction with the lower frequency of active BCAM/Lu receptors on SS-RBCs from HU-treated patients demonstrate the beneficial effect of HU in reducing SS-RBC adherence to LAMA5, a mechanism thought to be critical to VOE genesis.

To determine the physiological implications of cAMP-stimulated adhesion of HU-treated RBCs, we preincubated SS-RBCs from untreated and HU-treated patients with epinephrine, a hormone released during stress and known to stimulate the β2-AR [30, 72]. Our results indicate that epinephrine does not significantly increase the frequency of active BCAM/Lu receptors on the surface of SS-RBCs from HU-treated patients. Further, because we did not detect a difference in the unbinding force or the receptor frequency, we conjecture that HU modifies the β2-AR pathway thereby reducing the ability for epinephrine-stimulation. Consistent with previous

studies related to the phenotypic variability of SCD [72], we also found that the patient response to epinephrine was variable.

A determinant of clinical phenotype in SCD is the adhesive property of RBCs, defined by the subcellular density and distribution of adhesion receptors, and the unbinding force associated with specific ligands. In this work, single-molecule AFM was employed to quantify the response to cAMP-dependent pathway modulation via measurement of specific ligand-receptor unbinding forces and the CF of active adhesion receptors on the RBC. Importantly, we detected the presence of AKAPs on the membrane of both normal and SS-RBCs, and revealed that these proteins play a significant role in the modulation of BCAM/Lu via the cAMP pathway. Lastly, we demonstrated that HU-treatment reduces the ability for stimulation by epinephrine suggesting that HU modifies the β2-pathway. The study shows new, important implications for AFM cytoadhesion assays in evaluating the pharmacologic response of adhesion receptors on RBCs.

Chapter 9. Single-Cell Force Spectroscopy as a Technique to Quantify Human Red Blood Cell Adhesion to Subendothelial Laminin

9.1. Abstract

Single-cell force spectroscopy (SCFS), an atomic force microscopy (AFM)-based assay, enables quantitative study of cell adhesion while maintaining the native state of surface receptors in physiological conditions. Human healthy and pathological red blood cells (RBCs) express a large number of surface proteins which mediate cell-cell interactions, or cell adhesion to the extracellular matrix. In particular, RBCs adhere with high affinity to subendothelial matrix laminin via the basal cell adhesion molecule and Lutheran protein (BCAM/Lu). Here, we established SCFS as an *in vitro* technique to study human RBC adhesion at baseline and following biochemical treatment. Using blood obtained from healthy human subjects, we recorded adhesion forces from single RBCs attached to AFM cantilevers as the cell was pulled-off of substrates coated with laminin protein. We found that an increase of the overall cell adhesion measured via SCFS is correlated with an increase in the resultant total force measured on 1 μm^2 areas of the RBC membrane. Further, we showed that SCFS can detect significant changes in the adhesive response of RBCs to modulation of the cyclic adenosine monophosphate (cAMP) and protein kinase A (PKA) pathway. Lastly, we identified variability in the RBC adhesion force to laminin amongst the human subjects, suggesting that RBCs maintain diverse levels of active BCAM/Lu adhesion receptors. By using single-cell measurements, we established a powerful new method for the quantitative measurement of the adhesion of single RBCs with specific receptor-mediated binding.

9.2. Introduction

Although red blood cells (RBCs) are generally considered to be relatively inactive due to their

lack of a nucleus and other organelles, they express several surface adhesion receptors which modulate cellular function [62]. Many of these receptors mediate cell-cell interactions, or adhesion, on both healthy and pathological RBCs. Knowledge of cytoadhesion is necessary to understand normal physiology, the pathophysiology of disease, and the cellular-level effects of pharmacotherapies. Atomic force microscopy (AFM) [89] has introduced a wide range of novel approaches for imaging and manipulating biological systems in their native environment [132, 144, 157, 286, 295-296]. AFM allows for measurements of native biological samples under physiological conditions [30, 92] while avoiding complex sample preparation procedures and the artifacts accompanying them. In this paper, we present single-cell force spectroscopy (SCFS) as a new tool [130, 134-135] which enables the quantitative study of RBC adhesion while maintaining surface receptors in their native state. The technique is performed by measuring the adhesion between a single RBC attached to an AFM cantilever and a surface coated with either purified proteins or other cells.

In the past, RBC adhesion was traditionally investigated via large-scale flow adhesion assays [122-125], which measure the average adherence of a large number of RBCs to a functionalized-substrate under flow-induced shear stress [126-127]. These measurements provide only estimates of the adhesion force to which cells are subjected because the shear force exerted on cells depends on parameters such as cell size and shape, as well as the viscoelastic and elastic properties of the cells [128-130]. For example, it is known that RBCs from sickle cell disease (SCD) patients show variability in their viscoelastic and elastic properties [100, 119], and these properties can change after biochemical or pharmacologic treatment [87]. Further, flow adhesion assays are unable to provide information regarding receptor activity, including detachment forces, receptor localization, and changes in the number of active receptors upon biochemical stimulation. To obtain more controlled and quantitative

measurements of RBC adhesion, single-molecule and single-cell methods must be employed.

AFM studies of RBC adhesion have been utilized to provide quantitative evidence of changes in surface receptor distribution and values for the unbinding forces with specific ligands [30]. A technique known as single-molecule force spectroscopy (SMFS) utilizes cantilever tips functionalized with specific ligands to probe the cell surface. SMFS measures the unbinding, or detachment force, between a specific ligand on the AFM tip and its corresponding receptor on the membrane of a single cell with piconewton sensitivity [30, 91-92, 131-132]. Because SMFS is broadly used in conjunction with optical microscopy, the user has the ability to choose a RBC of interest for measurements. SMFS operates by collecting a set of force-distance curves of the approach-retract cycle of the functionalized tip from the cell surface. Specifically, the retraction curve, obtained when the functionalized probe pulls away from the RBC surface, gives the detachment force. Individual approach/retract curves can be obtained at many points on a RBC surface to create a two-dimensional map of detected surface adhesion receptors [30, 297]. Forces probed by SMFS reflect interactions between molecules [91]. Specifically, this technique allows for (i) quantifying the detachment force of specific receptor-ligand bonds, (ii) mapping the distribution of active receptors on cellular surfaces with high resolution, and (iii) calculating the density of active receptors on the cell surface [94, 96-98]. While SMFS is a very powerful technique to study RBC adhesion at the single-molecule level, it cannot provide the overall adhesion of a living cell to a substrate or to another living cell. Further, it is currently unknown how SMFS measurements compare to whole cell measurements.

To overcome these limitations, SCFS assays which use a living cell as a probe were developed [130, 134-138]. This AFM-based method is highly versatile because of its ability to measure a wide range of forces, from ~5 pN to ~100 nN [130]. In SCFS, a RBC attached to an AFM

cantilever is positioned above a functionalized substrate or another living cell. Similar to SMFS measurements, SCFS also records force-distance curves of an approach/retract cycle between the RBC probe and the functionalized substrate or cell. The RBC is lowered onto the substrate until a preset contact force is reached, and then held stationary for a defined time. Subsequently, the cell is withdrawn from the substrate at a constant speed and bonds between the cell and substrate break until the two entities are completely separated. In this case, the maximum detachment force is characterized as the force required to fully disengage the RBC from the functionalized substrate.

The adhesion of single RBCs is central to disease pathology. In this work, we established the technique of single-cell force spectroscopy as a method to probe RBC adhesion, specifically with subendothelial laminin proteins. Importantly, we found a significant correlation between SMFS measurements and SCFS measurements. To our knowledge, these two measurement techniques had not been directly compared until now. Finally, we showed that SCFS can detect significant changes in the adhesive response of RBCs to modulation of the cyclic adenosine monophosphate (cAMP) pathway. Based on these measurements, we identified variability in the RBC adhesion force to laminin amongst the human subjects, suggesting that RBCs maintain diverse intracellular levels of tonic protein kinase A (PKA). This is especially important in the case of blood pathologies in which specific blood cell adhesion receptors are targeted for anti-adhesive therapies, suggesting that individual treatment remedies may be needed.

9.3. Methods

Human subjects, blood samples, and blood preparation

Healthy volunteers at least 18 years old were eligible to participate in this study if they did not have a blood disorder or hemoglobinopathy, which was confirmed by screening blood samples

via complete blood count and hemoglobin electrophoresis. This study was approved by the Institutional Review Boards of the UCONN Health Center and UCONN-Storrs. Written informed consent was obtained from all subjects. Whole blood was centrifuged at 500*g* for 10min at 4°C to isolate the RBCs. The buffy coat and plasma were discarded and RBCs were washed 3x with Alsever's solution.

Reagents

Alsever's solution, laminin, glutaraldehyde, biotinamido-caproyl-labeled bovine serum albumin (biotin-BSA, reconstituted in PBS), streptavidin (reconstituted in PBS), biotinylated concanavalin A (ConA, reconstituted in PBS), 3-aminopropyltriethoxysilane (APTES, reconstituted in acetone), forskolin (*Coleus forskohli*, reconstituted in DMSO), KT-5720 (reconstituted in methanol), epinephrine (reconstituted in Alsever's solution), bovine serum albumin (reconstituted in PBS), were purchased from Sigma Aldrich (St. Louis, MO). Anti-laminin-5 antibody conjugated to AlexaFluor®488 was obtained from EMD Millipore (Billerica, MA). BCAM protein was obtained from Novus Biologicals (Littleton, CO).

Surface coating with laminin

Clean glass petri dishes (Ted Pella, Inc., Redding, CA) were divided using a hydrophobic PAP pen (Sigma Aldrich, St. Louis, MO) enabling us to separate RBCs from the laminin surface (Figure 9.3.1a). One half of the glass surface was silanized with 2% v/v 3-APTES for 10min, then rinsed with deionized (DI) water and treated with 0.5% glutaraldehyde for 30min. Surfaces were rinsed with DI water, incubated in laminin solution for 30min, rinsed again, and incubated in bovine serum albumin (100μg/mL) for 5min to block remaining aldehyde groups. Dishes were prepared on the same day of use.

Preparation of cantilevers

Tipless silicon nitride AFM cantilevers (NanoWorld, Neuchâtel, Switzerland) were cleaned in ethanol and thoroughly rinsed with DI water. Cantilevers were then soaked in acetone for 5min, and UV irradiated for 15min. Next, cantilevers were incubated overnight in 0.5 mg/ml biotin-BSA at 37°C. After rinsing with PBS, cantilevers were fixed in 1% glutaraldehyde for 30s. Cantilevers were rinsed again, then incubated in 0.5 mg/ml streptavidin for 10min at 25°C, rinsed, and finally incubated in 0.5 mg/ml biotinylated Con A (in PBS) for 10min at room temperature.

Silicon nitride cantilevers (Bruker Probes, Camarillo, CA) for single-molecule experiments were functionalized with BCAM protein as follows. Cantilevers were silanized with 2% v/v APTES for 10min, then rinsed with DI water and immersed in 0.5% glutaraldehyde for 30min. Cantilevers were rinsed with DI water, incubated in BCAM solution (100µg/mL) for 30min, rinsed again, and incubated in bovine serum albumin (100µg/mL) for 5min to block remaining aldehyde groups. Cantilevers were stored at 4°C and utilized within 48 hours.

Cell capture and experimental setup

Cells were allowed to weakly bind to the non-functionalized region of the glass substrate via incubation at 37°C for 10min followed by rinsing with Alsever's solution. This gentle immobilization on the glass substrate allowed for engagement of the tipless cantilever on a chosen RBC. Single cells were captured by positioning the ConA-functionalized cantilever above the center of a cell (Figure 9.3.1a) and gently lowering it onto the cell for ~30 s with a contact force of 1nN. Cells were precisely attached at the very end of the tipless cantilevers (Figure 9.3.1c) to prevent the cantilever surface (incubated with ConA) from interacting with the laminin substrate. The cell was lifted from the surface and allowed to establish firm adhesion on the cantilever for 1min before being moved to the laminin-functionalized area of the glass dish.

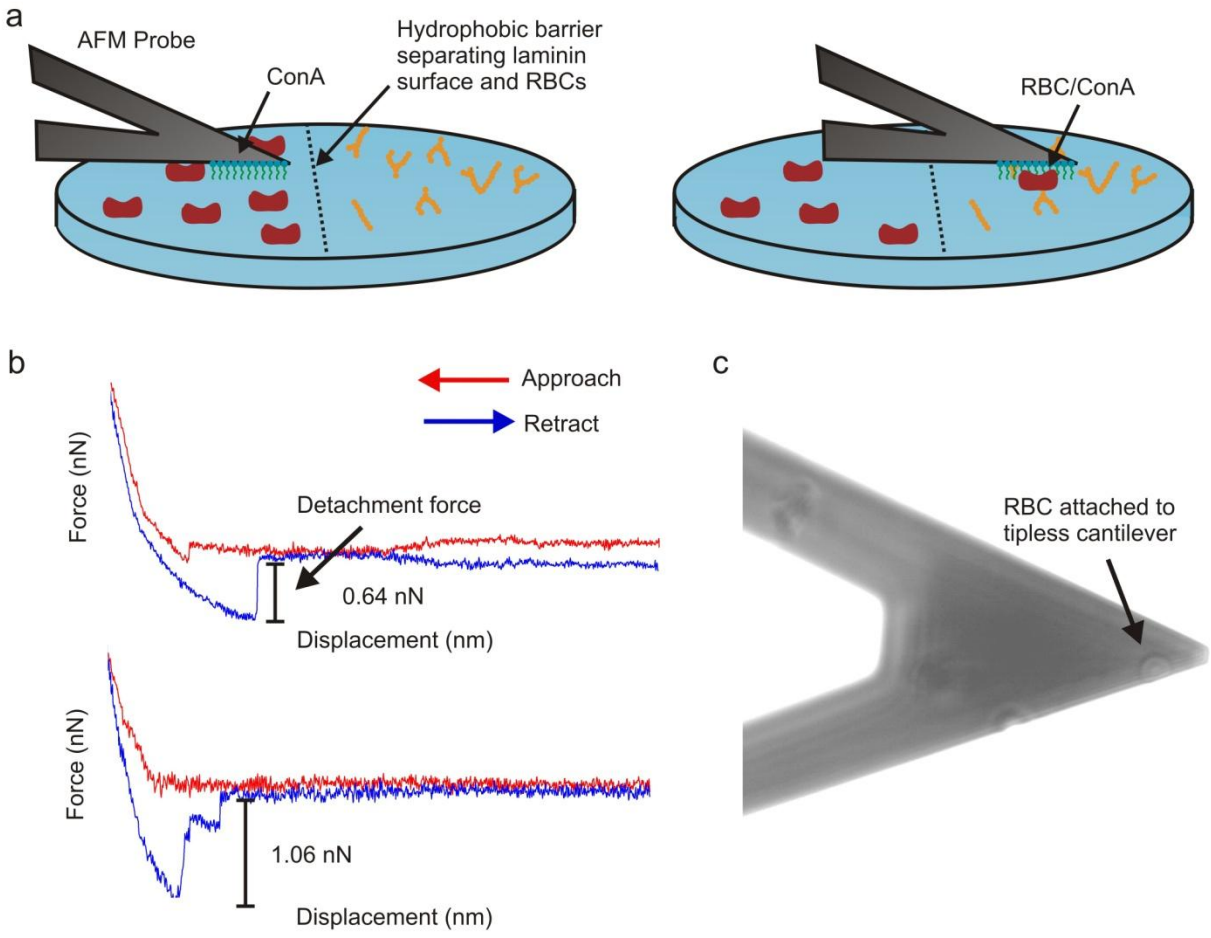

Figure 9.3.1. Measurement of red blood cell adhesion to subendothelial matrix laminin using single-cell force spectroscopy. (a) The apex of a tipless ConA-functionalized AFM cantilever is positioned above a RBC. It is then gently pushed (~1 nN) for 30 s onto the cell. The cantilever-bound RBC is separated from the substrate and allowed to establish firm adhesion to the cantilever for 1 min. The cantilever is then slowly moved to the functionalized segment of the petri dish to perform adhesion measurements. (b) Representative force-distance curves obtained from experiments for an RBC probing a laminin substrate. The measured detachment forces are 0.64 nN in the first curve which shows a single rupture and 1.06 nN in the second curve which shows multiple rupture events. (c) Optical microscopy image showing a human RBC attached to the apex of a ConA-functionalized cantilever.

AFM setup for SCFS

SCFS experiments were conducted using the MFP-3D-BIO AFM (Asylum Research, Santa Barbara, CA) mounted on an inverted optical microscope (Zeiss Axiovert A1). The nominal

spring constant of the employed cantilever was 80 mN/m and the effective spring constant was obtained via a thermal noise-based method prior to cell capture and used in all calculations [289]. The effective cantilever stiffness was lower than then nominal spring constant for each functionalized cantilever, as expected [298-299]. All experiments were performed in Alsever's solution at 37°C, and biochemical modulators were added 30min prior to experiments. For each assay, 5 RBCs were tested from each subject's blood. Values reporting "N = " denote the number of unique donors per condition and "n = " denote the total number of tested cells.

Each measuring session involved testing a single RBC probe attached to a previously calibrated cantilever for 100 approach/retraction cycles on a laminin-functionalized glass substrate. As monitored by optical microscopy, the captured cells rarely detached from the cantilever during pulling. Tests were performed with a preset trigger force of 500 pN. After the approach and a contact time of 0.1 s (unless otherwise noted), the cantilever was retracted at 800 nm/s until the RBC completely detached from the laminin substrate. Recorded force-distance curves were used to determine the detachment force of the RBC from the laminin substrate. A detachment force is defined as the maximum rupture force associated with the force-distance curve. Two representative curves are shown in Figure 9.3.1b. A relatively high number of curves exhibited single rupture events, as shown in the first curve. The experiments also resulted in curves compatible with multiple rupture events as shown in the second curve.

Statistical methods

Values for the detachment forces are reported as average ± standard deviation (SD) as determined by a frequency (%) distribution fit with the Gaussian function (GraphPad Prism). In the frequency (%) distribution, each bin contains the number of detachment forces with values within the bin's range divided by the total number of approach/retraction cycles. For SMFS,

frequency (%) is defined as the total number of all non-zero force points divided by the total number of sampled sites for each experimental condition. It is reported as average ± standard error of the mean (SEM).

9.4. Results and Discussion

Surface density of laminin for functionalized substrates

To obtain the experimental parameters used in our SCFS assay, we first needed to determine the appropriate solution concentration of laminin to be used for functionalization of the glass substrate. SMFS experiments were performed using a BCAM-functionalized probe against a laminin substrate. Substrates were prepared with various solution concentrations of laminin (1 µg/ml, 5 µg/ml, 10 µg/ml, 25 µg/ml, 50 µg/ml, and 100 µg/ml) and three 1 µm x 1 µm areas of each substrate were scanned with a lateral resolution of 31.25 nm yielding a total of 3072 measurements for each laminin solution concentration.

The average detachment force of BCAM with laminin was nearly constant across all solution concentrations, measuring 105 ± 11 pN (Figure 9.4.1a,b). Interestingly, this detachment force was approximately double what our lab had previously measured for the inverse interaction between BCAM on the RBC and laminin on the AFM probe using SMFS [30, 300]. In this case, we conjectured that more BCAM proteins attached to the AFM tip make contact with multiple laminin proteins on the substrate. BCAM proteins are approximately 6nm [301-302], whereas laminin is a cruciform structure with four arms of lengths ranging between 40 nm and 80 nm [303], therefore it is possible for multiple BCAM proteins to attach to multiple laminin binding sites. Upon functionalizing a substrate with BCAM and measuring the detachment force using a laminin-functionalized probe, we confirmed that the bond force is 43 ± 13 pN, in agreement with our previous measurements (Figure 9.4.1a).

For laminin-functionalized substrates, the percentage of sampled sites where a detachment force was detected increased with higher laminin concentrations (Figure 9.4.1c; 1 µg/ml: 35.22 ± 6.28%; 5 µg/ml: 60.19 ± 5.47%; 10 µg/ml: 51.66 ± 6.45%; 25 µg/ml: 73.21 ± 7.63%; 50 µg/ml: 63.93 ± 7.09%; 100 µg/ml: 71.13 ± 2.53%; $p < 0.01$, one-way ANOVA with Tukey *post hoc*). Variability reflects different substrate and probe preparations. To determine background noise, measurements were recorded on a substrate in which the laminin functionalization step was omitted (0 µg/ml). For the 0 µg/ml laminin substrate, interactions were detected in 4.1 ± 0.65% of sampled sites. The substrate density appeared to reach a plateau at 25 µg/ml, suggesting that 25 µg/ml, 50 µg/ml, or 100 µg/ml were suitable for our assay.

We next determined the effect of different laminin solution concentrations on the adherence of RBC probes to the laminin substrate. RBCs were attached to ConA-functionalized tipless AFM cantilevers (Figure 9.3.1a,c). Five cells from each healthy human subject were used as a probe and pressed onto laminin substrates with a contact time of 0.1 s and the cantilever was subsequently retracted until the cell was completely detached from the laminin substrate. Background noise was quantified by using a RBC to probe a substrate in which the laminin step was omitted from the functionalization procedure. Small forces of 73 ± 23 pN were detected in 25.70 ± 7.43% of sampled curves. The specificity of the interaction is demonstrated by performing experiments in a bath solution of 100 µg/mL laminin, thus blocking the BCAM/Lu receptors prior to interaction with the laminin functionalized substrate. By recording approach/retraction cycles between RBC probes and a substrate functionalized with 50 µg/ml laminin, the number of curves showing detachment forces dramatically reduced from 88% to 8% ($p < 0.0001$, Figure 9.4.1d). Further, detachment forces recorded in bath laminin decreased five-fold, from 511 ± 216 pN to 106 ± 23 pN ($p < 0.0001$) reflecting bath laminin bound to many BCAM/Lu receptors and thereby significantly reducing the propensity for binding of the RBC

probe to the laminin substrate.

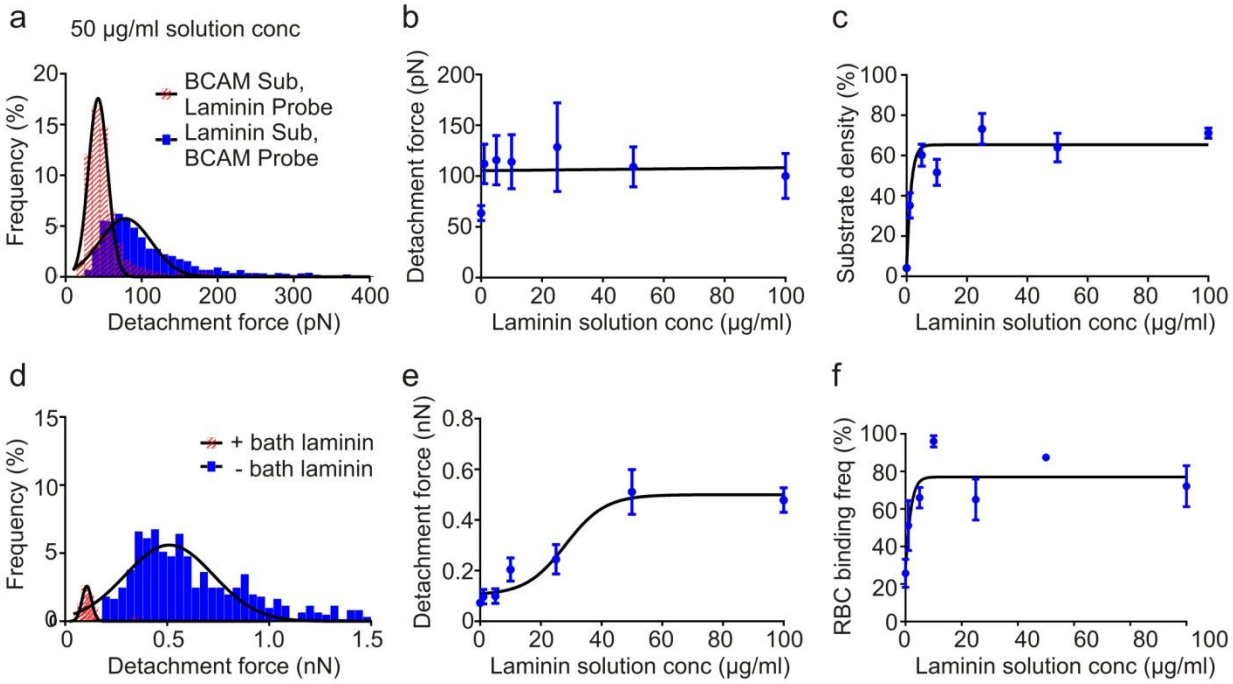

Figure 9.4.1. Determination of laminin solution concentration to be employed in SCFS assay. (a) Frequency distributions obtained from SMFS experiments of measured detachment forces between (i) a substrate coated with laminin (50 µg/ml) and a BCAM/Lu probe, and (ii) a substrate coated with BCAM (50 µg/ml) and a laminin probe. (b) Plot of the average detachment force measured at each tested laminin solution concentration shows the values are nearly consistent (1 µg/ml: 111 ± 33 pN; 5 µg/ml: 116 ± 41 pN; 10 µg/ml: 114 ± 46 pN; 25 µg/ml: 129 ± 93; 50 µg/ml: 78 ± 34 pN; 100 µg/ml: 100 ± 38). (c) Plot of the substrate density measured at each tested laminin concentration shows that the density appears to reach a plateau at 25 µg/ml (1 µg/ml: 35.22 ± 6.28%; 5 µg/ml: 60.19 ± 5.47%; 10 µg/ml: 51.66 ± 6.45%; 25 µg/ml: 73.21 ± 7.63%; 50 µg/ml: 63.93 ± 7.09%; 100 µg/ml: 71.13 ± 2.53%; $p < 0.01$, one-way ANOVA with Tukey *post hoc*). (d) Frequency distributions obtained from SCFS experiments of detachment forces between a RBC probe and laminin substrate (50 µg/ml) measured in the (i) absence and (ii) presence of bath laminin. The significant reduction in the number of curves showing detachment forces, from 99% to 8% ($p < 0.0001$) demonstrates the specificity of the measurements. (e) Plot of mean detachment force for human RBC probes (N=2, n=10) at each laminin solution concentration. Detachment forces were found to increase with higher laminin concentrations (1 µg/ml: 97 ± 49 pN; 5 µg/ml: 100 ± 49 pN; 10 µg/ml: 205 ± 79 pN; 25 µg/ml: 245 ± 142 pN; 50 µg/ml: 511 ± 216 pN; 100 µg/ml: 479 ± 118 pN; $p < 0.0001$), appearing to plateau at the 50 µg/ml concentration. (f) Plot of RBC binding frequency shows an increase in binding as laminin substrate concentration increases (1 µg/ml: 51.16 ± 13.31%; 5 µg/ml: 66.01 ± 5.43%; 10 µg/ml: 96.04 ± 2.97%; 25 µg/ml: 65.02 ± 10.91%; 50 µg/ml: 87.46 ± 1.78%; 100 µg/ml: 72.11 ± 10.90%; $p < 0.0001$).

After confirming the specificity of the measured interaction, RBC probes were used to record forces against each laminin substrate. Detachment forces were found to increase with higher laminin solution concentrations (1 μg/ml: 97 ± 49 pN; 5 μg/ml: 100 ± 49 pN; 10 μg/ml: 205 ± 79 pN; 25 μg/ml: 245 ± 142 pN; 50 μg/ml: 511 ± 216 pN; 100 μg/ml: 479 ± 118 pN; $p < 0.0001$), appearing to stabilize around the 50 μg/ml concentration (Figure 9.4.1e). For the 50 μg/ml concentration, we obtained force curves characterized by maximal detachment forces up to 3.4 nN. In contrast, the 1, 5, 10, and 25 μg/ml concentrations resulted in maximal detachment forces of less than 2.2 nN reflecting the need for a denser laminin concentration on the substrate to maximize BCAM/Lu receptor binding. These detachment force values are comparable to those observed for RBCs in other experiments [136]. Moreover, the frequency of RBC binding to the laminin substrate, or the percentage of approach/retract cycles which recorded detachment forces, also increased with higher laminin concentrations (Figure 9.4.1f) confirming the need for a higher density of laminin (1 μg/ml: 51.16 ± 13.31%; 5 μg/ml: 66.01 ± 5.43%; 10 μg/ml: 96.04 ± 2.97%; 25 μg/ml: 65.02 ± 10.91%; 50 μg/ml: 87.46 ± 1.78%; 100 μg/ml: 72.11 ± 10.90%; $p < 0.0001$).

From the experiments employed to determine the appropriate solution concentration of laminin to be used for substrate functionalization, and the effect of different concentrations on RBC detachment forces, we found that detachment forces appear to reach a plateau at the 50 μg/ml laminin concentration (Figure 9.4.1e), whereas the surface density detected via SMFS appears to reach a plateau at the 25 μg/ml laminin concentration (Figure 9.4.1c). Tethered polymer layers are comprised of polymer molecules attached to a surface, with a density high enough that the chains must stretch away from the surface [304-305]. By maximizing the brush height, the free-energy cost per chain is minimized, thus minimizing the strength of repulsion between

chains. This situation may have a large effect on the binding of tested cells and molecules to proteins attached to a surface. The surface distribution of a tethered polymer layer can be characterized by the distance between attachment points, D. As D approaches the radius of gyration, R_g, of the polymer chain, the molecules interact and the polymer layer structure gradually passes from the single-chain (mushroom) regime to the brush regime. In the 'mushroom' regime the reduced tethered density, $\Sigma = \sigma\pi R_g^2$, where $\sigma = 1/D^2$, is $\Sigma < 1$, the 'mushroom-to-brush' transition regime occurs for $1 < \Sigma < 5$, and the transition to 'brush' regime occurs at $\Sigma = 5$. The value $\Sigma = 1$ corresponds to $D = D_1 = \sqrt{\pi}R_g$ [306]. For the case of laminin, where $R_g \cong 80\,nm$ [307-308], the 'mushroom' regime appears for $D_1 > 140\,nm$ and the transition to 'brush' regime occurs at $D = D_2 = D_1/\sqrt{5} \cong 63\,nm$ [306]. Because the lateral step size was 31.25 nm during our SMFS experiments, after we reach the first transition point, from 'mushroom' to 'mushroom-to-brush' regime, it is difficult to distinguish between different surface densities. Based on Figure 9.4.1c, we conjecture that the transition point was reached at approximately 25 μg/ml laminin solution concentration. This conclusion is reinforced by the fact that the binding frequency for SCFS experiments plateau at the same laminin concentration (25 μg/ml), meaning that at this concentration, most of the substrate is covered with laminin chains in the 'mushroom' form. We found however, that the detachment force reaches a plateau at approximately 50 μg/ml solution concentration, meaning that the binding between all active RBC adhesion receptors and laminin molecules reaches equilibrium at this concentration. We conjecture that this is the second transition point, from 'mushroom-to-brush' to 'brush' regime, and determined the corresponding concentration of 50 μg/ml to be most suitable for SCFS assays of human RBCs.

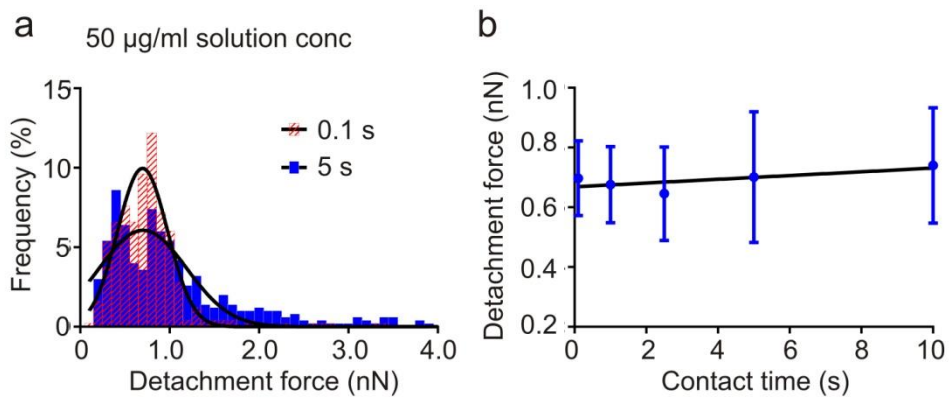

Figure 9.4.2. Human RBC adhesion to laminin substrates (50 µg/ml) at increasing contact times (N=2, n=10). (a) Frequency distributions show that the mean detachment force for RBCs from laminin substrates are the same for 0.1 s and 5 s contact times, however the range of measured detachment forces increases. (b) Plot shows that the mean detachment force does not significantly change with increasing contact time, however the deviation increases (0.1 s: 0.70 ± 0.28 nN; 1 s: 0.68 ± 0.28 nN; 2.5 s: 0.65 ± 0.35 nN; 5 s: 0.70 ± 0.49 nN; 10 s: 0.74 ± 0.43 nN).

Dependence of BCAM/Lu-mediated RBC adhesion on contact time

To investigate the time dependence of cell adhesion formation in more detail, we varied the contact time of RBCs with 50 µg/ml laminin substrates between 0.1 and 10 s and determined the respective detachment forces. It should be noted that the maximal contact time that can be achieved with our AFM system is 10 s. For each contact time interval, 5 cells were analyzed and 100 approach/retraction cycles were recorded per cell at each interval. For the 0.1 s contact time, RBCs required forces of several hundred piconewtons for laminin detachment (Figure 9.4.2a). As the contact time increased to 10 s, we recorded a minor increase in the mean detachment forces (Figure 9.4.2b), however the range of forces increased significantly, with a maximal detachment force of 3.3 nN at 0.1 s and 13.7 nN at 10 s. Because the result is similar across the different time scales, we opted to use the 0.1 s contact time for experimental convenience. At higher time scales, the RBC had a greater probability to detach from the probe prior to the completion of 100 approach/retraction cycles leading to experimental failure.

Increases in SCFS detachment forces correlates with increases in total forces recorded by SMFS on 1 μm^2 membrane regions

To determine the relationship between single-molecule measurements and single-cell measurements, we performed both assays using 5 cells from healthy human subjects (N = 3). In contrast to SMFS experiments, which probe specific receptor-ligand adhesion events on a small area on the cell membrane with high resolution, SCFS obtains the detachment force of cell probes from a functionalized substrate, or another cell. The method of SCFS is more readily comparable to flow adhesion assays, which measure the average adhesion of a large number of RBCs to a functionalized-substrate under flow-induced shear stress. Further, the measurements of SCFS are able to specifically quantify the detachment of cells from endothelial proteins found in capillaries and blood vessels, giving substantial insight into cytoadhesion events in the body.

SMFS experiments probed 1 μm x 1 μm areas of the RBC surface with a lateral resolution of 31.25 nm, enabling us to measure single-rupture events. The details of the technique along with the protocols we follow and the calibration tests are explained elsewhere [30, 300]. For the SCFS assay, RBCs probed a laminin-functionalized substrate (50 μg/ml laminin solution concentration) with a contact time of 0.1 s. For comparison of SMFS to SCFS, the resultant total force associated with each 1 μm x 1 μm membrane area was calculated as the product of the frequency of detected events and the mean detachment force. For example, an area with a mean detachment force of 39.51 pN detected in 2.83% of sampled sites yields a total force of 1.15 nN, while an area with a mean detachment force of 46.98 pN detected in 3.52% of sampled sites yields a total force of 1.69 nN. Resultant total forces measured on 1 μm x 1 μm areas of the RBC ranged from 0.77 nN to 3.92 nN (Figure 9.4.3a). In contrast, detachment forces obtained between single RBCs with a laminin substrate were lower, averaging 0.61 ± 0.27 nN and ranging from 0.24 nN to 1.38 nN (Figure 9.4.3a). The mean detachment force for

an entire RBC corresponds to the simultaneous formation of approximately 15-20 active bonds between BCAM/Lu molecules expressed on the RBC surface and laminin added to the substrate. This was calculated by dividing the average single cell detachment force by the average single-molecule detachment force, where the detachment force of one BCAM/Lu receptor from laminin is taken to be 40.24 pN, as determined by fitting the Gaussian model to a frequency (%) distribution of all SMFS measured detachment forces.

Since multiple cells (n = 5) were tested from each subject (N = 3), detachment forces could be compared between subjects. The Pearson correlation test was used to determine the strength of relationship between single-molecule and single-cell force spectroscopy assays (Figure 9.4.3b). We found that SMFS total force (1 µm x 1 µm area) correlated strongly with the whole cell force obtained via SCFS (Pearson correlation test; $r = 0.96$, $R^2 = 0.93$). Due to the fact that SCFS measurements reflect the percentage of bonds that are currently active, as well as innate cellular features, they can be used as an innovative tool to study RBC adhesion. However, it is important to note that detachment of the cell from the substrate is a complicated process, and the detachment force obtained is a result not only of receptor-ligand binding strength and spatial distribution of receptors on the cell membrane but also of other factors such as membrane fluctuations, cellular elasticity, and cell shape [130, 309-310].

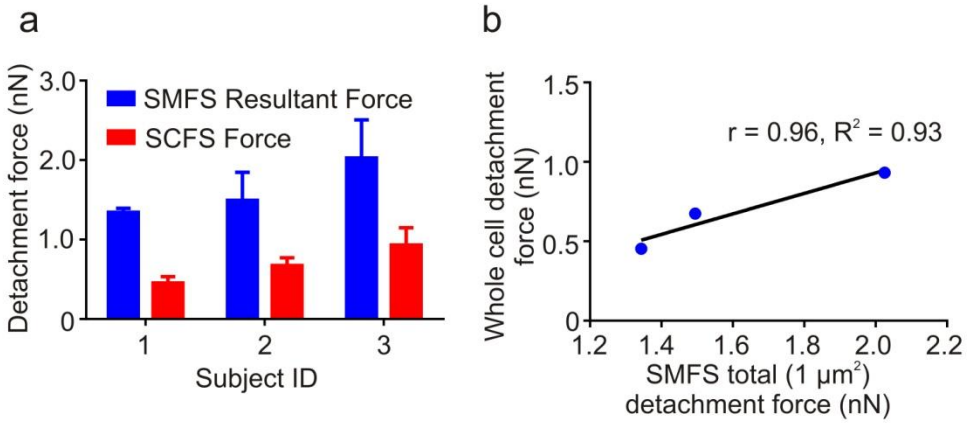

Figure 9.4.3. Correlation of single-cell measurements with traditional SMFS measurements. (a) Plot of the mean detachment forces from SMFS and SCFS assays. Experiments were performed on 5 cells from each human sample (N=3). SCFS experiments used single RBCs to probe a laminin functionalized substrate (50 µg/ml) with a contact time of 0.1 s. SMFS experiments probed BCAM/Lu receptors on 1 µm x 1 µm areas of the RBC surface with a laminin-functionalized probe. The resultant total force for each area was calculated as the product of the frequency of detected events and the mean detachment force. Error bars represent SEM. (b) Correlation of the resultant total force on 1 µm x 1 µm areas of the RBC surface obtained via SMFS with the mean detachment force obtained via SCFS measurements (Pearson correlation test; r = 0.96, R^2 = 0.93). Each plotted point represents 5 tested cells from one healthy subject.

Increases in RBC compliance may allow the cell to spread, leading to an increased number of ligand-receptor interactions and in effect, greater detachment forces measured via SCFS [138]. Because our experiments were conducted using RBCs from healthy subjects (N = 3, n = 5), the samples had a similar Young's modulus and we found that there was not a significant correlation between the mean effective Young's modulus of tested samples [30, 100] and the mean detachment force of RBCs (Pearson correlation test; r = -0.62, R^2 = 0.39).

cAMP-dependent modulation of red blood cell adhesion to laminin via BCAM/Lu

To establish the sensitivity of the assay in the detection of variations in the adhesion of BCAM/Lu to laminin based primarily on the number of active receptors, we investigated changes in the detachment force between single RBCs and the laminin substrate via

pharmacologic modulation of the cAMP signaling pathway. Quantitative understanding of RBC cytoadherence mediated by the second messenger cAMP is necessary to fully elucidate the mechanism of RBC adhesion. Previous experimental approaches utilizing flow adhesion assays have shown that the interaction between BCAM/Lu and laminin is mediated by cAMP-dependent PKA [30, 83]. Stimulation of the β2-adrenergic receptor (β2-AR) [85-86] activates the G-protein coupled receptor Gαs, which stimulates adenylyl cyclase (AC) [87]. AC then catalyzes the conversion of adenosine triphosphate (ATP) to cAMP, resulting in PKA activation and ensuing BCAM/Lu-laminin adhesion. In human RBCs, basal intracellular cAMP levels are controlled through the activity of phosphodiesterases [224, 293], which limit not only the signaling lifespan of cAMP but also the distance it can diffuse from its site of production [311].

First, we treated RBCs with forskolin (30μM, FSK), a strong AC activator that stimulates cAMP production, subsequently activating PKA. Compared to untreated RBCs, forskolin-treated RBCs exhibited significantly higher detachment forces shown by the shift in the frequency distribution and bar graph (Figure 9.4.4a,b,e; $p < 0.0001$, one-way ANOVA with Tukey *post hoc*). To quantify the effect of direct PKA inhibition on the detachment force of the RBC with laminin, RBCs were treated with KT-5720 (1μM), a PKA inhibitor, which resulted in a significant decrease in the detachment force from baseline measurements (Figure 9.4.4c; $p < 0.01$). PKA is a key regulator of BCAM/Lu receptor activation on human RBCs. Based on the results obtained in the presence of KT-5720 and FSK, PKA inhibitor and activator respectively, we conjecture that RBCs maintain varying intracellular levels of tonic PKA [311-312]. We further speculate that this tonic PKA is modulated by cAMP levels and must be raised for activation of BCAM/Lu receptors to occur, resulting in elevated adhesion to subendothelial laminin. Indeed, inhibition of PKA activity with KT-5720 was sufficient to reduce the number of active BCAM/Lu receptors on the RBC surface, reflected by the significant decrease in detachment forces. This

is suggestive of a tonic drive because even in the absence of PKA inhibitors and activators, PKA exerts a sustained, steady-state activation of BCAM/Lu receptors. Finally, the physiologic implication of cAMP-stimulated adhesion was studied by treating RBCs with epinephrine (1μM), a hormone released during stress and strenuous exercise which is known to stimulate the β2-AR. Treatment with epinephrine resulted in a significant increase in the detachment force as compared to baseline (Figure 9.4.4d; $p < 0.0005$). These data demonstrate that the single-cell AFM assay can detect differences in the detachment of whole RBCs from a laminin substrate in response to pharmacologic modulation (Figure 9.4.4e). Because a single-cell technique was used to measure 5 cells each from several human subjects (N=3), we also showed the individual results of detachment forces for each subject. Figure 9.4.4f shows the mean detachment force for each subject measured in each condition. Interpatient variations in baseline measurements showed that the sustained steady-state activation of BCAM/Lu receptors by PKA is not identical among human subjects.

It should be noted that previous experiments using flow adhesion assays did not detect adhesion of non-stimulated normal RBCs to laminin [72-73] nor an increase in adhesion upon FSK stimulation [72]. It is highly possible that flow adhesion assays, which measure the average adhesion of a large number of erythrocytes to a functionalized-substrate under flow-induced shear stress, are not sensitive enough to detect increases in the overall low adhesion of normal RBCs.

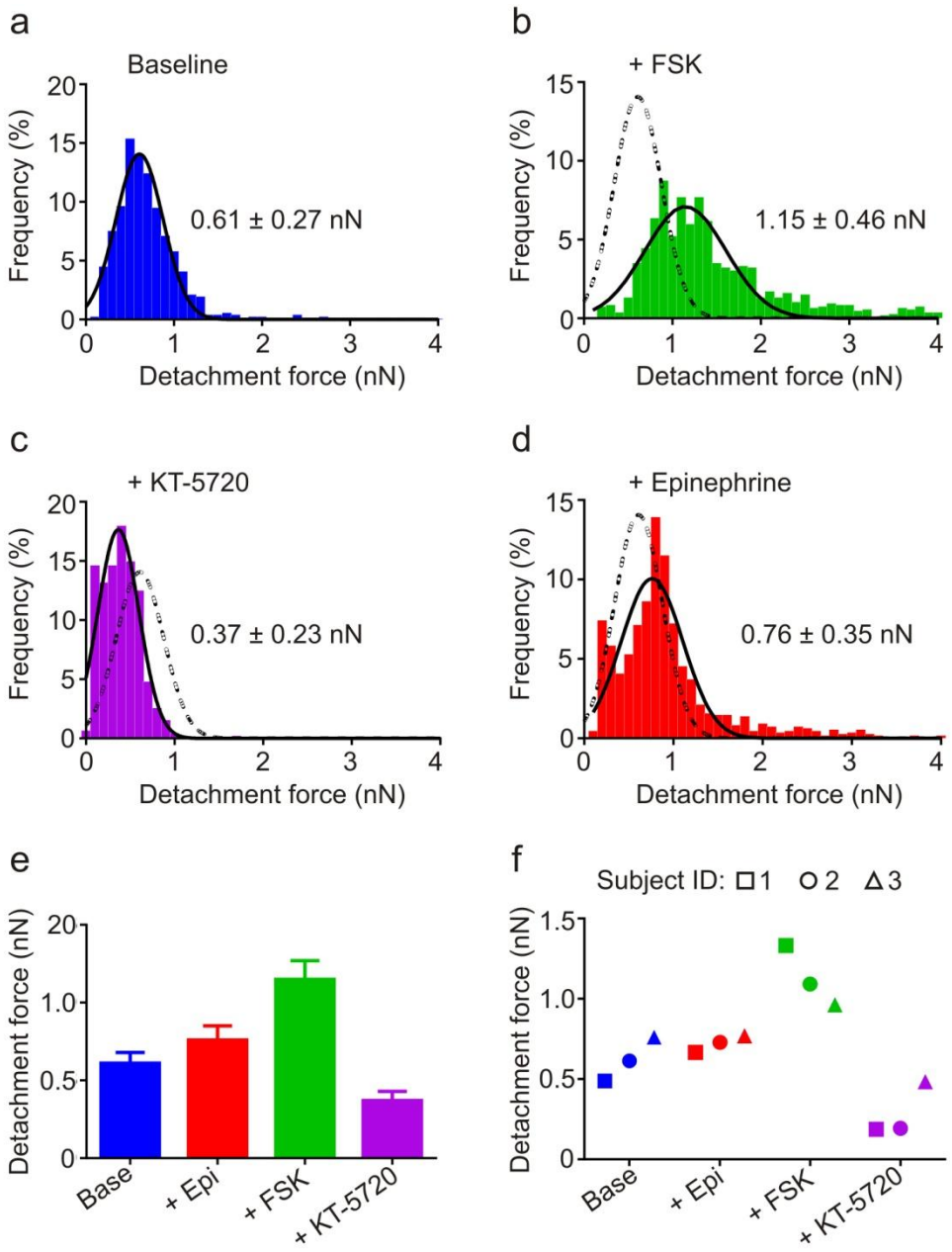

Figure 9.4.4. Single-cell force spectroscopy can clearly detect significant changes in RBC adhesion to laminin substrates (50 µg/ml) following treatment with biochemical agents modulating the cAMP-dependent pathway. (a) Frequency distribution of the mean detachment force associated with healthy RBCs at baseline (N=3, n=15) shows a mean force of 0.61 ± 0.27 nN. (b) Measurement in FSK (30 µM) indicates a significant increase in the mean detachment force to 1.15 ± 0.46 nN ($p < 0.0001$, one-way ANOVA with Tukey *post hoc*). Dotted distribution represents frequency distribution of the mean detachment force measured at baseline. (c) Measurement in KT-5720 (1 µM) indicates a significant decrease in the mean detachment force to 0.37 ± 0.23 nN ($p < 0.01$). (d) The physiologic implication of cAMP-stimulated adhesion was studied. Measurement in epinephrine (1 µM) indicates a significant increase in the mean detachment force to 0.76 ± 0.35 nN ($p < 0.0005$). (e) Summary of mean detachment forces

obtained for healthy RBCs from laminin substrates in the presence and absence of biochemical agents known to modulate cAMP-dependent adhesion. (f) Variability in mean detachment force amongst patient samples under different conditions.

9.5. Conclusion

In this work, SCFS was established as a method to quantify the strength and modulation of adhesion of human RBCs to functionalized substrates. We first determined the appropriate solution concentration of laminin to utilize for substrate functionalization via SMFS to determine the density of protein adsorption to the substrate. Subsequently, single-cell experiments were performed to measure variation in the detachment force associated with different laminin concentrations. From these tests, we determined the 50 µg/ml solution concentration of laminin to be most effective for our assay. Next, we probed laminin substrates with RBCs using various contact times, with a minimum contact time 0.1 s, and a maximum contact time of 10 s. While the mean detachment forces did not increase significantly, we observed an increase in the range of measured detachment forces. At 10 s, there was an increased probability of experimental failure resulting when the RBC would detach from the probe prior to the completion of 100 approach/retract cycles. Therefore, we chose 0.1 s for experimental convenience and for comparison between single-molecule and single-cell detachment forces. We found a significant correlation between results from SMFS measurements probing BCAM/Lu with a laminin-functionalized probe and SCFS measurements probing a laminin substrate with an RBC probe. Finally, we established that SCFS can detect variations in the detachment force of RBCs to laminin based primarily on the number of active BCAM/Lu receptors, which was modulated via biochemicals affecting the cAMP-PKA pathway. This study shows new, important implications for AFM-based SCFS measurements in understanding and evaluating the pharmacologic response of adhesion receptors on RBCs. Further, this method can easily be employed to measure the adhesive interactions of various cell types with functionalized substrates or other cells.

Chapter 10. Epilogue

The pathogenesis of vasculopathy in sickle cell disease is a multi-faceted biological process resulting from red cell sickling, inflammation and adhesion biology, coagulation activation, stasis, deficient bioavailability and excessive consumption of NO, excessive oxidation, and reperfusion injury physiology [2]. VOEs account for much of the morbidity and mortality in SCD and also with exercise-induced collapse and sudden death in SCT. The biomechanical properties of increased erythrocyte stiffness and abnormal cytoadherence to endothelial components were investigated to gain insight into the cascade of events involved in the pathogenesis of complications in SCD and SCT. AFM is appropriate for measuring the biomechanical and adhesive properties of living cells due to its high force sensitivity and ability to measure local and overall properties of individual cells in physiological conditions. In particular, the effective Young's modulus was quantified for RBCs from healthy, SCT, and SCD subjects, as well as RBC adhesive properties, defined by 1) the subcellular density and distribution of adhesion receptors, and 2) the unbinding force associated with specific ligands.

Three-dimensional topographic images were recorded for human RBCs from healthy subjects, SCT subjects, and SCD subjects using AFM. The characteristic biconcave shape was observed for normal erythrocytes while SCT erythrocytes deviated from this morphology by means of a decrease in the diameter and height, likely due to increased membrane stiffness and dehydration. In contrast to normal and SCT RBCs, erythrocytes from patients with SCD substantially deviated from the characteristic biconcave shape and possessed highly irregular morphologies characterized by protrusions, elongation, bumps, and enlargement associated with aggregation of HbS fibers.

The biomechanical properties of human RBCs from healthy subjects, SCT subjects, and SCD subjects were investigated. A systematic force-displacement curve analysis based on the Hertz model was established to quantify the effective Young's modulus of RBCs from human subjects via AFM microindentation measurements. Consistent with the Hertz model, no adhesion was observed between the indenter and the tested cell. It was determined that sickle RBCs possess Young's modulus values between 1-60 kPa depending on their degree of oxygenation and, we conjecture, the percentage of HbS present in the RBCs. Both oxygenated and deoxygenated samples of RBCs from patients with SCD maintained a bimodal distribution with peaks representative of normal RBCs (E_1 = 1.0 kPa ± 1.1 kPa) and SCT RBCs (E_2 = 3.0 ± 2.7 kPa). Significantly higher Young's modulus values resulting in peaks at E = 15 kPa for oxygenated sickle RBCs and E = 40 kPa for deoxygenated sickle RBCs were likely a result of the presence of polymerized HbS. This significant increase in the Young's modulus upon full deoxygenation can present major problems in SCD vasculopathy because rigid RBCs have a greater propensity to occlude the microvasculature, resulting in severe VOEs. Small Young's modulus values for both oxygenated and deoxygenated SCD erythrocytes are likely due to treatment with the drug hydroxyurea, a variable in the obtained clinical samples. Hydroxyurea is the only approved medication for the treatment of VOEs in SCD for adults which works by stimulating the production of HbF and inhibits sickling by preventing effective contact between HbS molecules.

The AFM technique used to measure the stiffness of normal and pathological RBCs was then employed in the study of RBCs from mice with SCD. In an effort to rectify the increased stiffness of sickle RBCs, mice were fed a diet supplemented with DHA, an omega-3 fatty acid. To date, studies of omega-3 fatty acids in human SCD showed a decrease in acute painful VOEs, but have not carefully assessed the effect of DHA on sickle RBC structural and functional characteristics. Although individuals with SCD are known to have increased daily pain and

allodynia, effects of omega-3 fatty acid supplementation on chronic or neuropathic pain in SCD have not been reported. Our findings indicate that DHA supplementation improves RBC membrane flexibility measured via AFM and reduces irreversibly sickled cells in mice with SCD. The increased RBC flexibility and decrease in irreversibly sickled RBCs found in this study at steady state suggest that the RBCs in SCD DHA mice may be more resistant to acute sickling events and resultant tissue injury, such as can be induced using hypoxia-reoxygenation in SCD mice. Therefore, dietary supplementation with omega-3 fatty acids may provide a safe and effective way to ameliorate pathologies associated with VOEs in human and murine SCD.

As previously mentioned, the abnormal cytoadherence of RBCs to the endothelium is thought to be a chief contributor to the complicated biological processes causing the pathogenesis of vasculopathy in SCD and SCT. It is known that the BCAM/Lu-laminin and ICAM-4-$\alpha_v\beta_3$ binding complexes contribute to VOEs, yet the single-molecule characteristics of these adhesive interactions were previously unknown for SCT and SCD erythrocytes. To establish the single-molecule force spectroscopy technique which measures adhesive interactions, experiments were performed using a functionalized laminin probe and a BCAM/Lu-coated gold substrate. In wild-type and SCT RBCs, the magnitude of the BCAM/Lu-laminin binding complex (46 ± 6 pN and 46 ± 10 pN, respectively) was found to be equal to the average rupture force of 50 ± 11 pN recorded between a functionalized laminin probe and a BCAM/Lu-coated gold substrate. Similarly, in wild-type RBCs and sickle cell trait RBCs, the magnitude of the ICAM-4-$\alpha_v\beta_3$ binding complex (46 ± 10 pN and 47 ± 10 pN, respectively) is nearly the same as the average rupture force of 47 ± 15 pN recorded between a functionalized integrin $\alpha_v\beta_3$ probe and a ICAM-4-coated gold substrate. Further, the observed increase in adhesive frequency, in conjunction with the detected receptor aggregation into nanodomains, is significant evidence of the contribution of epinephrine to enhancing BCAM/Lu-laminin and ICAM-4-$\alpha_v\beta_3$ adhesive interactions. These findings suggest a mechano-adhesive role for epinephrine in the

pathophysiology of VOEs related to collapse and sudden death in SCT individuals during strenuous exercise.

The sensitivity of the SMFS system was validated in a neuronal system to quantitatively map SK channels. Because the activation of adhesion receptors on RBCs and other cells can be modulated by various biochemical stimuli, it was important to assure that the technique could detect changes in the population of membrane components such as adhesion receptors or ion channels. We showed that integration of single-molecule force spectroscopy with toxin pharmacology allowed us to map the spatial organization and density of endogenous SK channels in living neurons. By taking advantage of the nanometer resolution of single-molecule AFM, we demonstrated that SK channels are highly concentrated on neuronal dendrites and are organized on neuronal membranes as either groups of two or single entities. To establish the technique's sensitivity, forskolin was used to show that SK channel dendritic distribution is dynamic and under the control of PKA.

SMFS was employed to investigate the effects of subcellular cAMP pathway targeting on the activation of BCAM/Lu receptors at the single-molecule level on normal and SCD RBCs. In SCD, cytoadherence of RBCs to endothelial and subendothelial matrix components is thought to be a major contributor to and possibly the primary cause of VOEs. A determinant of clinical phenotype in SCD is the adhesive properties of RBCs, defined by the subcellular density and distribution of adhesion receptors, and the unbinding force associated with specific ligands. Importantly, we demonstrate that AKAPs are essential for BCAM/Lu receptor activation, and that the collective frequency of BCAM/Lu receptors, present on both the normal and SS-RBC membrane, is critically dependent on the cAMP pathway. HU-treatment was also found to reduce the ability for BCAM/Lu receptor stimulation by epinephrine suggesting that HU modifies β2-AR signaling. We also measured that the unbinding force between BCAM/Lu and laminin in

hydroxyurea-treated patients is lower than in untreated patients. The study shows new, important implications for AFM cytoadhesion assays in evaluating the pharmacologic response of adhesion receptors on RBCs.

To examine the relevance of results based on SMFS in the cytoadhesion of entire RBCs, SCFS was established to measure the adhesion of whole cells with a functionalized substrate. We first determined the appropriate solution concentration of laminin to utilize for substrate functionalization by employing both SMFS and SCFS experiments. It was determined that the 50 µg/ml solution concentration of laminin is most effective for this assay. Laminin substrates were then probed with RBCs using various contact times, ranging from 0.1 s to 10 s. While the mean detachment forces did not increase significantly, we observed an increase in the range of measured detachment forces with increased contact time. It was determined that elevated overall cell adhesion measured via SCFS coincided with a rise in the resultant force measured on 1μm^2 areas of the RBC membrane via SMFS. To establish the sensitivity of the technique, RBCs were treated with biochemicals affecting the cAMP-PKA pathway and we indeed found that SCFS can detect variations in the detachment force of RBCs to laminin based primarily on the number of active BCAM/Lu receptors. This study shows new, important implication for AFM-based SCFS measurements in understanding and evaluating the pharmacologic response of adhesion receptors on RBCs.

Chapter 11. References

1. Rees, D. C., T. N. Williams, and M. T. Gladwin. 2010. Sickle-cell disease. The Lancet 376:2018-2031.
2. Hebbel, R. P., G. M. Vercellotti, and K. A. Nath. 2009. A systems biology consideration of the vasculopathy of sickle cell anemia: the need for multi-modality chemo-prophylaxis. Cardiovascular & hematological disorders drug targets 9:271.
3. Odièvre, M.-H., E. Verger, A. C. Silva-Pinto, and J. Elion. 2011. Pathophysiological insights in sickle cell disease. The Indian journal of medical research 134:532.
4. Hassell, K. L. 2010. Population estimates of sickle cell disease in the US. American Journal of Preventive Medicine 38:S512-S521.
5. Piel, F. B., S. I. Hay, S. Gupta, D. J. Weatherall, and T. N. Williams. 2013. Global Burden of Sickle Cell Anaemia in Children under Five, 2010–2050: Modelling Based on Demographics, Excess Mortality, and Interventions. PLoS Med 10:e1001484.
6. Makani, J., S. E. Cox, D. Soka, A. N. Komba, J. Oruo, H. Mwamtemi, P. Magesa, S. Rwezaula, E. Meda, J. Mgaya, B. Lowe, D. Muturi, D. J. Roberts, T. N. Williams, K. Pallangyo, J. Kitundu, G. Fegan, F. J. Kirkham, K. Marsh, and C. R. Newton. 2011. Mortality in Sickle Cell Anemia in Africa: A Prospective Cohort Study in Tanzania. PLoS ONE 6:e14699.
7. Strouse, J. J., S. Lanzkron, M. C. Beach, C. Haywood, H. Park, C. Witkop, R. F. Wilson, E. B. Bass, and J. B. Segal. 2008. Hydroxyurea for Sickle Cell Disease: A Systematic Review for Efficacy and Toxicity in Children. Pediatrics 122:1332-1342.
8. Makani, J., T. Williams, and K. Marsh. 2007. Sickle cell disease in Africa: burden and research priorities. Annals of Tropical Medicine and Parasitology 101:3-14.
9. Tsaras, G., A. Owusu-Ansah, F. O. Boateng, and Y. Amoateng-Adjepong. 2009. Complications Associated with Sickle Cell Trait: A Brief Narrative Review. The American Journal of Medicine 122:507-512.
10. Roach, E. S., M. R. Golomb, R. Adams, J. Biller, S. Daniels, G. Deveber, D. Ferriero, B. V. Jones, F. J. Kirkham, R. M. Scott, and E. R. Smith. 2008. Management of stroke in infants and children - A scientific statement from a special writing group of the American Heart Association Stroke Council and the Council on Cardiovascular Disease in the young. Stroke 39:2644-2691.
11. Switzer, J. A., D. C. Hess, F. T. Nichols, and R. J. Adams. 2006. Pathophysiology and treatment of stroke in sickle-cell disease: present and future. Lancet Neurology 5:501-512.
12. Hillery, C. A., and J. A. Panepinto. 2004. Pathophysiology of stroke in sickle cell disease. Microcirculation 11:195-208.
13. DeBaun, M. R., C. P. Derdeyn, and R. C. McKinstry. 2006. Etiology of strokes in children with sickle cell anemia. Mental Retardation and Developmental Disabilities Research Reviews 12:192-199.
14. Mehta, S. H., and R. J. Adams. 2006. Treatment and prevention of stroke in children with sickle cell disease. Curr Treat Options Neurol 8:503-512.
15. Abboud, M. R., and G. F. Atweh. 2006. Prevention and management of strokes in patients with sickle cell disease. Curr Hematol Rep 5:15-22.
16. Qureshi, N., B. Lubin, and M. C. Walters. 2006. The prevention and management of stroke in sickle cell anaemia. Expert Opinion on Biological Therapy 6:1087-1098.
17. Wang, W. C. 2007. The pathophysiology, prevention, and treatment of stroke in sickle cell disease. Current Opinion in Hematology 14:191-197.
18. Ohene-Frempong, K., S. J. Weiner, L. A. Sleeper, S. T. Miller, S. Embury, J. W. Moohr, D. L. Wethers, C. H. Pegelow, F. M. Gill, and D. Cooperative Study Sickle Cell. 1998. Cerebrovascular accidents in sickle cell disease: Rates and risk factors. Blood 91:288-

294.
19. Silva, G. S., P. Vicari, M. S. Figueiredo, H. Carrete, Junior, M. H. Idagawa, and A. R. Massaro. 2009. Brain Magnetic Resonance Imaging Abnormalities in Adult Patients With Sickle Cell Disease: Correlation With Transcranial Doppler Findings. Stroke 40:2408-2412.
20. Kwiatkowski, J. L., R. A. Zimmerman, A. N. Pollock, W. Seto, K. Smith-Whitley, J. Shults, A. Blackwood-Chirchir, and K. Ohene-Frempong. 2009. Silent infarcts in young children with sickle cell disease. British Journal of Haematology 146:300-305.
21. Wang, W., P. Naidu, L. Wynn, R. Smrt, M. Cancio, G. Hankins, G. Steen, and K. Helton. 2003. Abnormal magnetic resonance imaging of the brain in very young children with sickle cell disease is associated with new overt and silent infarcts after extended follow-up. Blood 102:409.
22. Casella, J. F., A. A. King, B. Barton, D. A. White, M. J. Noetzel, R. N. Ichord, C. Terrill, D. Hirtz, R. C. McKinstry, J. J. Strouse, T. H. Howard, T. D. Coates, C. P. Minniti, A. D. Campbell, B. A. Vendt, H. Lehmann, and M. R. DeBaun. 2010. DESIGN OF THE SILENT CEREBRAL INFARCT TRANSFUSION (SIT) TRIAL. Pediatric Hematology and Oncology 27:69-89.
23. Hulbert, M. L., R. C. McKinstry, J. L. Lacey, C. J. Moran, J. A. Panepinto, A. A. Thompson, S. A. Sarnaik, G. M. Woods, J. F. Casella, B. Inusa, J. Howard, F. J. Kirkham, K. A. Anie, J. E. Mullin, R. Ichord, M. Noetzel, Y. Yan, M. Rodeghier, and M. R. DeBaun. 2010. Silent cerebral infarcts occur despite regular blood transfusion therapy after first stroke in children with sickle cell disease. Blood:blood-2010-2001-261123.
24. Miller, S. T., E. A. Macklin, C. H. Pegelow, T. R. Kinney, L. A. Sleeper, J. A. Bello, L. D. DeWill, D. M. Gallagher, L. Guarini, F. G. Moser, K. Obene-Frempong, N. Sanchez, E. P. Vichinsky, W. C. Wang, D. L. Wethers, D. P. Younkin, R. A. Zimmerman, M. R. DeBaun, and D. Cooperative Study of Sickle Cell. 2001. Silent infarction as a risk factor for overt stroke in children with sickle cell anemia: A report from the Cooperative Study of Sickle Cell Disease. Journal of Pediatrics 139:385-390.
25. Pegelow, C. H., E. A. Macklin, F. G. Moser, W. C. Wang, J. A. Bello, S. T. Miller, E. P. Vichinsky, M. R. DeBaun, L. Guarini, R. A. Zimmerman, D. P. Younkin, D. M. Gallagher, and T. R. Kinney. 2002. Longitudinal changes in brain magnetic resonance imaging findings in children with sickle cell disease. Blood 99:3014-3018.
26. Kinney, T. R., L. A. Sleeper, W. C. Wang, R. A. Zimmerman, C. H. Pegelow, K. Ohene-Frempong, D. L. Wethers, J. A. Bello, E. P. Vichinsky, F. G. Moser, D. M. Gallagher, M. R. DeBaun, O. S. Platt, and S. T. Miller. 1999. Silent cerebral infarcts in sickle cell anemia: A risk factor analysis. Pediatrics 103:640-645.
27. Dowling, M. M., C. T. Quinn, Z. R. Rogers, and G. R. Buchanan. 2010. Acute Silent Cerebral Infarction in Children with Sickle Cell Anemia. Pediatric Blood & Cancer 54:461-464.
28. Pauling, L., H. A. Itano, S. J. Singer, and I. C. Wells. 1949. Sickle Cell Anemia, a Molecular Disease. Science 110:543-548.
29. Steinberg, M. H., and G. P. Rodgers. 2001. Pathophysiology of sickle cell disease: Role of cellular and genetic modifiers. Seminars in Hematology 38:299-306.
30. Maciaszek, J. L., B. Andemariam, G. Huber, and G. Lykotrafitis. 2012. Epinephrine Modulates BCAM/Lu and ICAM-4 Expression on the Sickle Cell Trait Red Blood Cell Membrane. Biophysical Journal 102:1137-1143.
31. Embury, S. H. 1986. The Clinical Pathophysiology of Sickle Cell Disease. Annual Review of Medicine 37:361-376.
32. Rosse, W. F., M. Narla, L. D. Petz, and M. H. Steinberg. 2000. New Views of Sickle Cell Disease Pathophysiology and Treatment. Hematology 2000:2-17.
33. Ferrone, F. A. 2004. Polymerization and sickle cell disease: A molecular view.

Microcirculation 11:115-128.
34. Hebbel, R. P., R. Osarogiagbon, and D. Kaul. 2004. The endothelial biology of sickle cell disease: Inflammation and a chronic vasculopathy. Microcirculation 11:129-151.
35. Noguchi, C. T., and A. N. Schechter. 1985. Sickle Hemoglobin Polymerization in Solution and in Cells. Annual Review of Biophysics and Biophysical Chemistry 14:239-263.
36. Turner, M. S., J. C. Wang, C. W. Jones, F. A. Ferrone, R. Josephs, and R. W. Briehl. 2002. Fluctuations in self-assembled sickle hemoglobin fibers. Langmuir 18:7182-7187.
37. Christoph, G. W., J. Hofrichter, and W. A. Eaton. 2005. Understanding the shape of sickled red cells. Biophysical Journal 88:1371-1376.
38. Connes, P., H. Reid, M. D. Hardy-Dessources, E. Morrison, and O. Hue. 2008. Physiological Responses of Sickle Cell Trait Carriers during Exercise. Sports Medicine 38:931-946.
39. Charache, S. 1990. Fetal hemoglobin, sickling, and sickle cell disease. Adv Pediatr 37:1-31.
40. Fortier, N., L. M. Snyder, F. Garver, C. Kiefer, J. McKenney, and N. Mohandas. 1988. The Relationship Between Invivo Generated Hemoglobin Skeletal Protein Complex and Increased Red-Cell Membrane Rigidity. Blood 71:1427-1431.
41. Higgins, J. M., D. T. Eddington, S. N. Bhatia, and L. Mahadevan. 2007. Sickle cell vasoocclusion and rescue in a microfluidic device. Proceedings of the National Academy of Sciences of the United States of America 104:20496-20500.
42. Li, H., and G. Lykotrafitis. 2011. A coarse-grain molecular dynamics model for sickle hemoglobin fibers. Journal of the Mechanical Behavior of Biomedical Materials 4:162-173.
43. Lorey, F. W., J. Arnopp, and G. C. Cunningham. 1996. Distribution of hemoglobinopathy variants by ethnicity in a multiethnic state. Genetic Epidemiology 13:501-512.
44. Neel, J. V., I. C. Wells, and H. A. Itano. 1951. FAMILIAL DIFFERENCES IN THE PROPORTION OF ABNORMAL HEMOGLOBIN PRESENT IN THE SICKLE CELL TRAIT. Journal of Clinical Investigation 30:1120-1124.
45. Wells, I. C., and H. A. Itano. 1951. Ratio of sickle-cell anemia hemoglobin to normal hemoglobin in sicklemics. J Biol Chem 188:65-74.
46. Kark, J. A. 2000. Sickle Cell Trait. Washington, D.C.
47. Neel, J. V. 1949. The Inheritance of Sickle Cell Anemia. Science 110:64-66.
48. Strasser, B. J. 1999. Molecular medicine - "Sickle cell anemia, a molecular disease". Science 286:1488-1490.
49. Jones SR, B. R., Donowho EM. 1970. Sudden Death in Sickle Cell Trait. N Engl J Med 282:323-325.
50. Kark, J. A., D. M. Posey, and H. R. Schumacher. 1987. Sickle-Cell Trait as a Risk Factor for Sudden Death in Physical Training. N Engl J Med 317:781-787.
51. Martin, T. W., I. M. Weisman, R. J. Zeballos, and S. R. Stephenson. 1989. Exercise and Hypoxia Increase Sickling in Venous-Blood from an Exercising Limb in Individuals with Sickle-Cell Trait. American Journal of Medicine 87:48-56.
52. Connes, P., O. Hue, J. Tripette, and M. D. Hardy-Dessources. 2008. Blood rheology abnormalities and vascular cell adhesion mechanisms in sickle cell trait carriers during exercise. Clinical Hemorheology and Microcirculation 39:179-184.
53. Kark, J. A., and F. T. Ward. 1994. Exercise and Hemoglobin-S. Seminars in Hematology 31:181-225.
54. Tripette, J., P. Connes, E. Beltan, T. Chalabi, L. Marlin, R. Chout, O. K. Baskurt, O. Hue, and M. D. Hardy-Dessources. 2010. Red blood cell deformability and aggregation, cell adhesion molecules, oxidative stress and nitric oxide markers after a short term, submaximal, exercise in sickle cell trait carriers. Clinical Hemorheology and

Microcirculation 45:39-52.
55. Stuart, M. J., and R. L. Nagel. 2004. Sickle-cell disease. Lancet 364:1343-1360.
56. Acharya, K., C. W. Lang, and L. F. Ross. 2009. A Pilot Study to Explore Knowledge, Attitudes, and Beliefs about-Sickle Cell Trait and Disease. Journal of the National Medical Association 101:1163-1172.
57. Sears, D. A. 1978. Morbidity of Sickle-Cell Trait - Review of Literature. American Journal of Medicine 64:1021-1036.
58. Shemin, D., and D. Rittenberg. 1946. The life span of the human red blood cell. Journal of Biological Chemistry 166:627-636.
59. Alberts, B., D. Bray, J. Lewis, M. Raff, K. Roberts, and J. D. Watson. 2002. Molecular Biology of the Cell.
60. Mohandas, N., and P. G. Gallagher. 2008. Red cell membrane: past, present, and future. Blood 112:3939-3948.
61. Li, J., M. Dao, C. T. Lim, and S. Suresh. 2005. Spectrin-level modeling of the cytoskeleton and optical tweezers stretching of the erythrocyte. Biophysical Journal 88:3707-3719.
62. Telen, M. J. 2000. Red blood cell surface adhesion molecules: Their possible roles in normal human physiology and disease. Seminars in Hematology 37:130-142.
63. Telen, M. J. 2005. Erythrocyte adhesion receptors: Blood group antigens and related molecules. Transfusion Medicine Reviews 19:32-44.
64. Ballas, S. K., and N. Mohandas. 1996. Pathophysiology of vaso-occlusion. Hematology-Oncology Clinics of North America 10:1221-&.
65. Chiang, E. Y., and P. S. Frenette. 2005. Sickle Cell Vaso-Occlusion. Hematology/Oncology Clinics of North America 19:771-784.
66. Conran, N., C. F. Franco-Penteado, and F. F. Costa. 2009. Newer Aspects of the Pathophysiology of Sickle Cell Disease Vaso-Occlusion. Hemoglobin 33:1-16.
67. Kaul, D. K., M. E. Fabry, and R. L. Nagel. 1996. The pathophysiology of vascular obstruction in the sickle syndromes. Blood Reviews 10:29-44.
68. Brittain, H. A., J. R. Eckman, R. A. Swerlick, R. J. Howard, and T. M. Wick. 1993. Thrombospondin from activated platelets promotes sickle erythrocyte adherence to human microvascular endothelium under physiological flow - a potential role for platelet activation in sickle-cell vasoocclusion. Blood 81:2137-2143.
69. Aprelev, A., M. A. Rotter, Z. Etzion, R. M. Bookchin, R. W. Briehl, and F. A. Ferrone. 2005. The effects of erythrocyte membranes on the nucleation of sickle hemoglobin. Biophysical Journal 88:2815-2822.
70. Wu, Y. Z., Y. Hu, J. Y. Cai, S. Y. Ma, X. P. Wang, Y. Chen, and Y. L. Pan. 2009. Time-dependent surface adhesive force and morphology of RBC measured by AFM. Micron 40:359-364.
71. Hebbel, R. P., O. Yamada, C. F. Moldow, H. S. Jacob, J. G. White, and J. W. Eaton. 1980. Abnormal adherence of sickle erythrocytes to cultured vascular endothelium: possible mechanism for microvascular occlusion in sickle cell disease. The Journal of Clinical Investigation 65:154-160.
72. Hines, P. C., Q. Zen, S. N. Burney, D. A. Shea, K. I. Ataga, E. P. Orringer, M. J. Telen, and L. V. Parise. 2003. Novel epinephrine and cyclic AMP-mediated activation of BCAM/Lu-dependent sickle (SS) RBC adhesion. Blood 101:3281-3287.
73. Bartolucci, P., V. Chaar, J. Picot, D. Bachir, A. Habibi, C. Fauroux, F. Galactéros, Y. Colin, C. Le Van Kim, and W. El Nemer. 2010. Decreased sickle red blood cell adhesion to laminin by hydroxyurea is associated with inhibition of Lu/BCAM protein phosphorylation. Blood 116:2152-2159.
74. Fathallah, H., and G. F. Atweh. 2006. Induction of fetal hemoglobin in the treatment of sickle cell disease. Hematology Am Soc Hematol Educ Program:58-62.

75. Charache, S. 1997. Mechanism of action of hydroxyurea in the management of sickle cell anemia in adults. Seminars in Hematology 34:15-21.
76. Platt, O. S. 2008. Hydroxyurea for the treatment of sickle cell anemia. New England Journal of Medicine 358:1362-1369.
77. Halsey, C., and I. A. G. Roberts. 2003. The role of hydroxyurea in sickle cell disease. British Journal of Haematology 120:177-186.
78. Hillery, C. A., M. C. Du, W. C. Wang, and J. P. Scott. 2000. Hydroxyurea therapy decreases the in vitro adhesion of sickle erythrocytes to thrombospondin and laminin. British Journal of Haematology 109:322-327.
79. Taylor, S. S., J. A. Buechler, and W. Yonemoto. 1990. Camp-Dependent Protein Kinase: Framework for a Diverse Family of Regulatory Enzymes. Annual Review of Biochemistry 59:971-1005.
80. Solovey, A., Y. Lin, P. Browne, S. Choong, E. Wayner, and R. P. Hebbel. 1997. Circulating Activated Endothelial Cells in Sickle Cell Anemia. New England Journal of Medicine 337:1584-1590.
81. Bolarin, D. M., P. Swerdlow, A. M. Wallace, and L. Littsey. 1998. Serum concentrations of laminin P1 and aminoterminal propeptide of type III procollagen in sickle cell disease. Haematologia 29:51.
82. Zen, Q., M. Cottman, G. Truskey, R. Fraser, and M. J. Telen. 1999. Critical factors in basal cell adhesion molecule/Lutheran-mediated adhesion to laminin. Journal of Biological Chemistry 274:728-734.
83. Gauthier, E., C. Rahuel, M. P. Wautier, W. El Nemer, P. Gane, J. L. Wautier, J. P. Cartron, Y. Colin, and C. Le Van Kim. 2005. Protein kinase A-dependent phosphorylation of lutheran/basal cell adhesion molecule glycoprotein regulates cell adhesion to laminin alpha 5. Journal of Biological Chemistry 280:30055-30062.
84. Murphy, M. M., M. A. Zayed, A. Evans, C. E. Parker, K. I. Ataga, M. J. Telen, and L. V. Parise. 2005. Role of Rap1 in promoting sickle red blood cell adhesion to laminin via BCAM/LU. Blood 105:3322-3329.
85. Benovic, J. L. 2002. Novel β2-adrenergic receptor signaling pathways. Journal of Allergy and Clinical Immunology 110:S229-S235.
86. Eyler, C. E., T. Jackson, L. E. Elliott, L. M. De Castro, J. Jonassaint, A. Ashley-Koch, and M. J. Telen. 2007. b2-Adrenergic receptor and adenylate cyclase gene polymorphisms affect sickle red cell adhesion. British Journal of Haematology:105-108.
87. Muravyov, A. V., V. B. Koshelev, O. E. Fadukova, I. A. Tikhomirova, A. A. Maimistova, and S. V. Bulaeva. 2011. The role of red blood cell adenylyl cyclase activation in changes of erythrocyte membrane microrheological properties. Biochem. Moscow Suppl. Ser. A 5:128-134.
88. Wong, W., and J. D. Scott. 2004. AKAP signalling complexes: focal points in space and time. Nature Reviews Molecular Cell Biology 5:959-970.
89. Binnig, G., C. F. Quate, and C. Gerber. 1986. Atomic force microscope. Phys Rev Lett 56:930-933.
90. Dufrene, Y. F., and P. Hinterdorfer. 2008. Recent progress in AFM molecular recognition studies. Pflugers Archiv-European Journal of Physiology 456:237-245.
91. Müller, D. J., and Y. F. Dufrêne. 2011. Force nanoscopy of living cells. Current biology : CB 21:R212-R216.
92. Alessandrini, A., and P. Facci. 2005. AFM: a versatile tool in biophysics. Meas. Sci. Technol. 16:R65-R92.
93. Maciaszek, J. L., and G. Lykotrafitis. 2011. Sickle cell trait human erythrocytes are significantly stiffer than normal. Journal of Biomechanics 44:657-661.
94. Dupres, V., F. D. Menozzi, C. Locht, B. H. Clare, N. L. Abbott, S. Cuenot, C. Bompard, D. Raze, and Y. F. Dufrene. 2005. Nanoscale mapping and functional analysis of

individual adhesins on living bacteria. Nature Methods 2:515-520.
95. Lee, S., J. Mandic, and K. J. Van Vliet. 2007. Chemomechanical mapping of ligand-receptor binding kinetics on cells. Proceedings of the National Academy of Sciences of the United States of America 104:9609-9614.
96. Lim, T. S., S. R. K. Vedula, P. J. Kausalya, W. Hunziker, and C. T. Lim. 2008. Single-molecular-level study of claudin-1-mediated adhesion. Langmuir 24:490-495.
97. Hinterdorfer, P., W. Baumgartner, H. J. Gruber, K. Schilcher, and H. Schindler. 1996. Detection and localization of individual antibody-antigen recognition events by atomic force microscopy. Proceedings of the National Academy of Sciences of the United States of America 93:3477-3481.
98. Baumgartner, W., P. Hinterdorfer, W. Ness, A. Raab, D. Vestweber, H. Schindler, and D. Drenckhahn. 2000. Cadherin interaction probed by atomic force microscopy. Proceedings of the National Academy of Sciences of the United States of America 97:4005-4010.
99. Asylum. 2011. Asylum Research MFP-3D-BIO.
100. Maciaszek, J. L., B. Andemariam, and G. Lykotrafitis. 2011. Microelasticity of red blood cells in sickle cell disease. The Journal of Strain Analysis for Engineering Design 46:368-379.
101. Radmacher, M. 1997. Measuring the elastic properties of biological samples with the AFM. Ieee Engineering in Medicine and Biology Magazine 16:47-57.
102. Rico, F., P. Roca-Cusachs, N. Gavara, R. Farre, M. Rotger, and D. Navajas. 2005. Probing mechanical properties of living cells by atomic force microscopy with blunted pyramidal cantilever tips. Phys Rev E 72:-.
103. Vinckier, A., and G. Semenza. 1998. Measuring elasticity of biological materials by atomic force microscopy. FEBS Lett. 430:12-16.
104. Evans, E. 2001. Probing the relation between force - Lifetime - and chemistry in single molecular bonds. Annu Rev Bioph Biom 30:105-128.
105. Timoshenko, S. P., and J. N. Goodier. 1970. Theory of Elasticity. McGraw-Hill, New York.
106. Hertz. 1881. On the contact of elastic solids. J. Reine und Angew. Math. 92:156-171.
107. Sneddon, I. 1965. The relation between load and penetration in axisymmetric Boussinesq problem for a punch of arbitrary profile. Int J Eng Sci 3:47-57.
108. Barber, J. R., and D. A. Billings. 1990. An Approximate Solution for the Contact Area Elastic Compliance of a Smooth Punch of Arbitrary Shape. Int J Mech Sci 32:991-997.
109. Barber, J. R. 1974. Determining the contact area in elastic-indentation problems. J. Strain Anal 9:230-232.
110. Giannakopoulos, A. E. 2006. Elastic and viscoelastic indentation of flat surfaces by pyramid indentors. Journal of the Mechanics and Physics of Solids 54:1305-1332.
111. Dulinska, I., M. Targosz, W. Strojny, M. Lekka, P. Czuba, W. Balwierz, and M. Szymonski. 2006. Stiffness of normal and pathological erythrocytes studied by means of atomic force microscopy. J. Biochem. Biophys. Methods 66:1-11.
112. Hategan, A., R. Law, S. Kahn, and D. E. Discher. 2003. Adhesively-tensed cell membranes: Lysis kinetics and atomic force microscopy probing. Biophysical Journal 85:2746-2759.
113. Kuznetsova, T. G., M. N. Starodubtseva, N. I. Yegorenkov, S. A. Chizhik, and R. I. Zhdanov. 2007. Atomic force microscopy probing of cell elasticity. Micron 38:824-833.
114. Bilodeau, G. G. 1992. Regular Pyramid Punch Problem. Journal of Applied Mechanics 59:519-523.
115. Alcaraz, J., L. Buscemi, M. Grabulosa, X. Trepat, B. Fabry, R. Farre, and D. Navajas. 2003. Microrheology of human lung epithelial cells measured by atomic force microscopy. Biophysical Journal 84:2071-2079.

116. Mahaffy, R. E., C. K. Shih, F. C. MacKintosh, and J. Kas. 2000. Scanning probe-based frequency-dependent microrheology of polymer gels and biological cells. Physical Review Letters 85:880-883.
117. Dimitriadis, E. K., F. Horkay, J. Maresca, B. Kachar, and R. S. Chadwick. 2002. Determination of elastic moduli of thin layers of soft material using the atomic force microscope. Biophysical Journal 82:2798-2810.
118. Johnson, K. L., K. Kendall, and A. D. Roberts. 1971. Surface Energy and the Contact of Elastic Solids. Proceedings of the Royal Society of London. Series A, Mathematical and Physical Sciences 324:301-313.
119. Puig-De-Morales-Marinkovic, M., K. T. Turner, J. P. Butler, J. J. Fredberg, and S. Suresh. 2007. Viscoelasticity of the human red blood cell. American Journal of Physiology-Cell Physiology 293:C597-C605.
120. Heuberger, M., G. Dietler, and L. Schlapbach. 1995. MAPPING THE LOCAL YOUNGS MODULUS BY ANALYSIS OF THE ELASTIC DEFORMATIONS OCCURRING IN ATOMIC-FORCE MICROSCOPY. Nanotechnology 6:12-23.
121. Vanlandingham, M. R., S. H. McKnight, G. R. Palmese, J. R. Elings, X. Huang, T. A. Bogetti, R. F. Eduljee, and J. W. Gillespie. 1997. Nanoscale indentation of polymer systems using the atomic force microscope. Journal of Adhesion 64:31-59.
122. Hillery, C. A., M. C. Du, R. R. Montgomery, and J. P. Scott. 1996. Increased adhesion of erythrocytes to components of the extracellular matrix: Isolation and characterization of a red blood cell lipid that binds thrombospondin and laminin. Blood 87:4879-4886.
123. Cooke, B. M., S. J. Rogerson, G. V. Brown, and R. L. Coppel. 1996. Adhesion of malaria-infected red blood cells to chondroitin sulfate A under flow conditions. Blood 88:4040-4044.
124. Brittain, J. E., K. J. Mlinar, C. S. Anderson, E. P. Orringer, and L. V. Parise. 2001. Activation of sickle red blood cell adhesion via integrin-associated protein/CD47–induced signal transduction. Journal of Clinical Investigation 107:1555-1562.
125. Setty, B., and M. J. Stuart. 1996. Vascular cell adhesion molecule-1 is involved in mediating hypoxia-induced sickle red blood cell adherence to endothelium: potential role in sickle cell disease. Blood 88:2311-2320.
126. Soyer, M., and G. Duménil. 2012. A Laminar-Flow Chamber Assay for Measuring Bacterial Adhesion Under Shear Stress. In Neisseria meningitidis. Springer. 185-195.
127. Kucik, D. F. 2009. Measurement of adhesion under flow conditions. Current Protocols in Cell Biology:9.6. 1-9.6. 10.
128. Qian, J., and H. Gao. 2010. Soft Matrices Suppress Cooperative Behaviors among Receptor-Ligand Bonds in Cell Adhesion. PLoS ONE 5:e12342.
129. Sato, M., N. Ohshima, and R. Nerem. 1996. Viscoelastic properties of cultured porcine aortic endothelial cells exposed to shear stress. Journal of Biomechanics 29:461-467.
130. Helenius, J., C.-P. Heisenberg, H. E. Gaub, and D. J. Muller. 2008. Single-cell force spectroscopy. Journal of Cell Science 121:1785-1791.
131. Sen, S., S. Subramanian, and D. E. Discher. 2005. Indentation and Adhesive Probing of a Cell Membrane with AFM: Theoretical Model and Experiments. Biophysical Journal 89:3203-3213.
132. Brown André, E. X., R. I. Litvinov, D. E. Discher, and J. W. Weisel. 2007. Forced Unfolding of Coiled-Coils in Fibrinogen by Single-Molecule AFM. Biophysical Journal 92:L39-L41.
133. Müller, D. J., and Y. F. Dufrene. 2008. Atomic force microscopy as a multifunctional molecular toolbox in nanobiotechnology. Nature Nanotechnology 3:261-269.
134. Friedrichs, J., J. Helenius, and D. J. Muller. 2010. Quantifying cellular adhesion to extracellular matrix components by single-cell force spectroscopy. Nature Protocols 5:1353-1361.

135. Taubenberger, A., D. A. Cisneros, J. Friedrichs, P.-H. Puech, D. J. Muller, and C. M. Franz. 2007. Revealing early steps of α2β1 integrin-mediated adhesion to collagen type I by using single-cell force spectroscopy. Molecular biology of the cell 18:1634-1644.
136. Carvalho, P. A., M. Diez-Silva, H. Chen, M. Dao, and S. Suresh. 2013. Cytoadherence of erythrocytes invaded by Plasmodium falciparum: Quantitative contact-probing of a human malaria receptor. Acta Biomaterialia 9:6349-6359.
137. Simon, A., and M.-C. Durrieu. 2006. Strategies and results of atomic force microscopy in the study of cellular adhesion. Micron 37:1-13.
138. Wojcikiewicz, E. P., X. Zhang, A. Chen, and V. T. Moy. 2003. Contributions of molecular binding events and cellular compliance to the modulation of leukocyte adhesion. Journal of Cell Science 116:2531-2539.
139. Janmey, P. A. 1998. The cytoskeleton and cell signaling: Component localization and mechanical coupling. Physiological Reviews 78:763-781.
140. Huang, S., and D. E. Ingber. 1999. The structural and mechanical complexity of cell-growth control. Nature Cell Biology 1:E131-E138.
141. Suresh, S. 2007. Nanomedicine - Elastic clues in cancer detection. Nature Nanotechnology 2:748-749.
142. Rotsch, C., F. Braet, E. Wisse, and M. Radmacher. 1997. AFM imaging and elasticity measurements on living rat liver macrophages. Cell Biology International 21:685-696.
143. Radmacher, M., M. Fritz, C. M. Kacher, J. P. Cleveland, and P. K. Hansma. 1996. Measuring the viscoelastic properties of human platelets with the atomic force microscope. Biophysical Journal 70:556-567.
144. Cross, S. E., Y. S. Jin, J. Rao, and J. K. Gimzewski. 2007. Nanomechanical analysis of cells from cancer patients. Nature Nanotechnology 2:780-783.
145. Iyer, S., R. M. Gaikwad, V. Subba-Rao, C. D. Woodworth, and I. Sokolov. 2009. Atomic force microscopy detects differences in the surface brush of normal and cancerous cells. Nature Nanotechnology 4:389-393.
146. Li, Q. S., G. Y. H. Lee, C. N. Ong, and C. T. Lim. 2008. AFM indentation study of breast cancer cells. Biochemical and Biophysical Research Communications 374:609-613.
147. Buehler, M. J., and Y. C. Yung. 2009. Deformation and failure of protein materials in physiologically extreme conditions and disease. Nature Materials 8:175-188.
148. Steinberg, M. H., and C. Brugnara. 2003. Pathophysiological-Based Approaches to Treatment of Sickle Cell Disease. Annual Review of Medicine 54:89.
149. Mohandas, N., and E. Evans. 1994. Mechanical-Properties of the Red-Cell Membrane in Relation to Molecular-Structure and Genetic-Defects. Annu Rev Bioph Biom 23:787-818.
150. Statius van Eps, L. W. 1999. Sickle Cell Disease. Current Medicine, Inc, Philadelphia, PA.
151. Snyder, L. M., L. Leb, J. Piotrowski, N. Sauberman, S. C. Liu, and N. L. Fortier. 1983. Irreversible Spectrin Hemoglobin Crosslinking In Vivo - A Marker for Red-Cell Senescence. British Journal of Haematology 53:379-384.
152. Walder, J. A., R. Chatterjee, T. L. Steck, P. S. Low, G. F. Musso, E. T. Kaiser, P. H. Rogers, and A. Arnone. 1984. The Interaction of Hemoglobin with the Cytoplasmic Domain of Band-3 of the Human-Erythrocyte Membrane. Journal of Biological Chemistry 259:238-246.
153. Tuvia, S., S. Levin, and R. Korenstein. 1992. OXYGENATION-DEOXYGENATION CYCLE OF ERYTHROCYTES MODULATES SUBMICRON CELL-MEMBRANE FLUCTUATIONS. Biophysical Journal 63:599-602.
154. Dao, M., C. T. Lim, and S. Suresh. 2003. Mechanics of the human red blood cell deformed by optical tweezers. Journal of the Mechanics and Physics of Solids 51:2259-2280.
155. Gray, D. E. 1972. American Institute of Physics Handbook. McGraw-Hill, New York.

156. Fung, Y. C. 1981. Biomechanics: mechanical properties of living tissues. Biomechanics: mechanical properties of living tissues.:i-xii, 1-433.
157. Cai, X. F., X. B. Xing, J. Y. Cai, Q. Chen, S. X. Wu, and F. C. Huang. 2010. Connection between biomechanics and cytoskeleton structure of lymphocyte and Jurkat cells: An AFM study. Micron 41:257-262.
158. Cai, X. F., X. X. Yang, J. Y. Cai, S. X. Wu, and Q. Chen. 2010. Atomic Force Microscope-Related Study Membrane-Associated Cytotoxicity in Human Pterygium Fibroblasts Induced by Mitomycin C. J. Phys. Chem. B 114:3833-3839.
159. Schafer, A., and M. Radmacher. 2005. Influence of myosin II activity on stiffness of fibroblast cells. Acta Biomaterialia 1:273-280.
160. Yim, E. K. F., E. M. Darling, K. Kulangara, F. Guilak, and K. W. Leong. 2010. Nanotopography-induced changes in focal adhesions, cytoskeletal organization, and mechanical properties of human mesenchymal stem cells. Biomaterials 31:1299-1306.
161. Domke, J., S. Dannohl, W. J. Parak, O. Muller, W. K. Aicher, and M. Radmacher. 2000. Substrate dependent differences in morphology and elasticity of living osteoblasts investigated by atomic force microscopy. Colloids and Surfaces B-Biointerfaces 19:367-379.
162. Simon, A., T. Cohen-Bouhacina, M. C. Porte, J. P. Aime, J. Amedee, R. Bareille, and C. Baquey. 2003. Characterization of dynamic cellular adhesion of osteoblasts using atomic force microscopy. Cytometry Part A 54A:36-47.
163. Takai, E., K. D. Costa, A. Shaheen, C. T. Hung, and X. E. Guo. 2005. Osteoblast elastic modulus measured by atomic force microscopy is substrate dependent. Annals of Biomedical Engineering 33:963-971.
164. Turner, M. S., R. W. Briehl, J. C. Wang, F. A. Ferrone, and R. Josephs. 2006. Anisotropy in sickle hemoglobin fibers from variations in bending and twist. Journal of Molecular Biology 357:1422-1427.
165. vonRuckmann, B., T. Jons, F. Dolle, D. Drenckhahn, and D. Schubert. 1997. Cytoskeleton-membrane connections in the human erythrocyte membrane: band 4.1 binds to tetrameric band 3 protein. Biochim. Biophys. Acta-Biomembr. 1325:226-234.
166. Brugnara, C. 2001. Red cell Membrane in sickle cell disease. In Disorders of Hemoglobin. B. F. MH Steinberg, DR Higgs, RL Nagel, editor. Cambridge University Press, New York.
167. Charache, S., G. J. Dover, R. D. Moore, S. Eckert, S. K. Ballas, M. Koshy, P. F. A. Milner, E. P. Orringer, G. Phillips, O. S. Platt, and G. H. Thomas. 1992. HYDROXYUREA - EFFECTS ON HEMOGLOBIN-F PRODUCTION IN PATIENTS WITH SICKLE-CELL-ANEMIA. Blood 79:2555-2565.
168. Austin, H., N. S. Key, J. M. Benson, C. Lally, N. F. Dowling, C. Whitsett, and W. C. Hooper. 2007. Sickle cell trait and the risk of venous thromboembolism among blacks. Blood 110:908-912.
169. Li, J., G. Lykotrafitis, M. Dao, and S. Suresh. 2007. Cytoskeletal dynamics of human erythrocyte. Proceedings of the National Academy of Sciences of the United States of America 104:4937-4942.
170. Cartron, J. P., P. Bailly, C. Le van Kim, B. Cherif-Zahar, G. Matassi, O. Bertrand, and Y. Colin. 1998. Insights into the structure and function of membrane polypeptides carrying blood group antigens. Vox Sang. 74:29-64.
171. Iolascon, A., S. Perrotta, and G. W. Stewart. 2003. Red blood cell membrane defects. Rev Clin Exp Hematol 7:22-56.
172. Tse, W. T., and S. E. Lux. 1999. Red blood cell membrane disorders. British Journal of Haematology 104:2-13.
173. Glenister, F. K., R. L. Coppel, A. F. Cowman, N. Mohandas, and B. M. Cooke. 2002. Contribution of parasite proteins to altered mechanical properties of malaria-infected red

blood cells. Blood 99:1060-1063.
174. Evans, E. A. 1973. NEW MEMBRANE CONCEPT APPLIED TO ANALYSIS OF FLUID SHEAR-DEFORMED AND MICROPIPET-DEFORMED RED BLOOD-CELLS. Biophysical Journal 13:941-954.
175. Daily, B., E. L. Elson, and G. I. Zahalak. 1984. CELL POKING - DETERMINATION OF THE ELASTIC AREA COMPRESSIBILITY MODULUS OF THE ERYTHROCYTE-MEMBRANE. Biophysical Journal 45:671-682.
176. Lenormand, G., S. Henon, A. Richert, J. Simeon, and F. Gallet. 2001. Direct measurement of the area expansion and shear moduli of the human red blood cell membrane skeleton. Biophysical Journal 81:43-56.
177. Dao, M., J. Li, and S. Suresh. 2006. Molecularly based analysis of deformation of spectrin network and human erythrocyte. Mat Sci Eng C-Bio S 26:1232-1244.
178. Gu, M., S. Kuriakose, and X. S. Gan. 2007. A single beam near-field laser trap for optical stretching, folding and rotation of erythrocytes. Optics Express 15:1369-1375.
179. Marinkovic, M., M. Diez-Silva, I. Pantic, J. J. Fredberg, S. Suresh, and J. P. Butler. 2009. Febrile temperature leads to significant stiffening of Plasmodium falciparum parasitized erythrocytes. American Journal of Physiology-Cell Physiology 296:C59-C64.
180. Musielak, M. 2009. Red blood cell-deformability measurement: Review of techniques. Clinical Hemorheology and Microcirculation 42:47-64.
181. Haga, H., S. Sasaki, K. Kawabata, E. Ito, T. Ushiki, and T. Sambongi. 2000. Elasticity mapping of living fibroblasts by AFM and immunofluorescence observation of the cytoskeleton. Ultramicroscopy 82:253-258.
182. Nowakowski, R., P. Luckham, and P. Winlove. 2001. Imaging erythrocytes under physiological conditions by atomic force microscopy. Biochim. Biophys. Acta-Biomembr. 1514:170-176.
183. Ikai A, X. X., Mitsui K. 1997. Measurements of mechanical parameters of biological structures with atomic force microscope. Scanning Microscopy 12:585-596.
184. Lekka, M., P. Laidler, D. Gil, J. Lekki, Z. Stachura, and A. Z. Hrynkiewicz. 1999. Elasticity of normal and cancerous human bladder cells studied by scanning force microscopy. Eur. Biophys. J. Biophys. Lett. 28:312-316.
185. Suresh, S. 2006. Mechanical response of human red blood cells in health and disease: Some structure-property-function relationships. Journal of Materials Research 21:1871-1877.
186. Liu, F., H. Mizukami, S. Sarnaik, and A. Ostafin. 2005. Calcium-dependent human erythrocyte cytoskeleton stability analysis through atomic force microscopy. Journal of Structural Biology 150:200-210.
187. Takakuwa, Y. 2000. Protein 4.1, a multifunctional protein of the erythrocyte membrane skeleton: Structure and functions in erythrocytes and nonerythroid cells. Int. J. Hematol. 72:298-309.
188. Maher, A. D., and P. W. Kuchel. 2003. The Gardos channel: a review of the Ca2+-activated K+ channel in human erythrocytes. International Journal of Biochemistry & Cell Biology 35:1182-1197.
189. Stocker, J. W., L. De Franceschi, G. A. McNaughton-Smith, R. Corrocher, Y. Beuzard, and C. Brugnara. 2003. ICA-17043, a novel Gardos channel blocker, prevents sickled red blood cell dehydration in vitro and in vivo in SAD mice. Blood 101:2412-2418.
190. Hebbel, R. P. 2004. Special issue of microcirculation: examination of the vascular pathobiology of sickle cell anemia. Microcirculation 11:99-100.
191. Epstein, F. H., and H. F. Bunn. 1997. Pathogenesis and treatment of sickle cell disease. New England Journal of Medicine 337:762-769.
192. Belhassen, L., G. Pelle, S. d. Sediame, D. Bachir, C. Carville, C. Bucherer, C. Lacombe, F. Galacteros, and S. Adnot. 2001. Endothelial dysfunction in patients with sickle cell

disease is related to selective impairment of shear stress–mediated vasodilation. Blood 97:1584-1589.
193. Aslan, M., T. M. Ryan, B. Adler, T. M. Townes, D. A. Parks, J. A. Thompson, A. Tousson, M. T. Gladwin, R. P. Patel, and M. M. Tarpey. 2001. Oxygen radical inhibition of nitric oxide-dependent vascular function in sickle cell disease. Proceedings of the National Academy of Sciences 98:15215-15220.
194. Brandow, A. M., C. L. Stucky, C. A. Hillery, R. G. Hoffmann, and J. A. Panepinto. 2013. Patients with sickle cell disease have increased sensitivity to cold and heat. American Journal of Hematology 88:37-43.
195. Natarajan, M., M. M. Udden, and L. McIntire. 1996. Adhesion of sickle red blood cells and damage to interleukin-1 beta stimulated endothelial cells under flow in vitro. Blood 87:4845-4852.
196. Sauntharajah, Y., C. A. Hillery, D. Lavelle, R. Molokie, L. Dorn, L. Bressler, S. Gavazova, Y.-H. Chen, R. Hoffman, and J. DeSimone. 2003. Effects of 5-aza-2′-deoxycytidine on fetal hemoglobin levels, red cell adhesion, and hematopoietic differentiation in patients with sickle cell disease. Blood 102:3865-3870.
197. Barabino, G., X. Liu, B. Ewenstein, and D. Kaul. 1999. Anionic polysaccharides inhibit adhesion of sickle erythrocytes to the vascular endothelium and result in improved hemodynamic behavior. Blood 93:1422-1429.
198. Hillery, C. A., J. P. Scott, and M. C. Du. 1999. The carboxy-terminal cell-binding domain of thrombospondin is essential for sickle red blood cell adhesion. Blood 94:302-309.
199. Stuart, J., P. Stone, N. Akinola, J. Gallimore, and M. Pepys. 1994. Monitoring the acute phase response to vaso-occlusive crisis in sickle cell disease. Journal of clinical pathology 47:166-169.
200. Croizat, H. 1994. Circulating cytokines in sickle cell patients during steady state. British Journal of Haematology 87:592-597.
201. Belcher, J. D., P. H. Marker, J. P. Weber, R. P. Hebbel, and G. M. Vercellotti. 2000. Activated monocytes in sickle cell disease: potential role in the activation of vascular endothelium and vaso-occlusion. Blood 96:2451-2459.
202. Ataga, K. I., M. D. Cappellini, and E. A. Rachmilewitz. 2007. β-Thalassaemia and sickle cell anaemia as paradigms of hypercoagulability. British Journal of Haematology 139:3-13.
203. Setty, B. Y., S. Kulkarni, A. K. Rao, and M. J. Stuart. 2000. Fetal hemoglobin in sickle cell disease: relationship to erythrocyte phosphatidylserine exposure and coagulation activation. Blood 96:1119-1124.
204. Ataga, K. I., C. G. Moore, C. A. Hillery, S. Jones, H. C. Whinna, D. Strayhorn, C. Sohier, A. Hinderliter, L. V. Parise, and E. P. Orringer. 2008. Coagulation activation and inflammation in sickle cell disease-associated pulmonary hypertension. Haematologica 93:20-26.
205. Manci, E. A., C. A. Hillery, C. A. Bodian, Z. G. Zhang, G. A. Lutty, and B. S. Coller. 2006. Pathology of Berkeley sickle cell mice: similarities and differences with human sickle cell disease. Blood 107:1651-1658.
206. Paszty, C., C. M. Brion, E. Manci, H. E. Witkowska, M. E. Stevens, N. Mohandas, and E. M. Rubin. 1997. Transgenic knockout mice with exclusively human sickle hemoglobin and sickle cell disease. Science 278:876-878.
207. Hillery, C. A., P. C. Kerstein, D. Vilceanu, M. E. Barabas, D. Retherford, A. M. Brandow, N. J. Wandersee, and C. L. Stucky. 2011. Transient receptor potential vanilloid 1 mediates pain in mice with severe sickle cell disease. Blood 118:3376-3383.
208. Kestin, M., P. Clifton, G. B. Belling, and P. Nestel. 1990. n-3 fatty acids of marine origin lower systolic blood pressure and triglycerides but raise LDL cholesterol compared with n-3 and n-6 fatty acids from plants. The American journal of clinical nutrition 51:1028-

1034.
209. Kinsella, J. E., B. Lokesh, and R. A. Stone. 1990. Dietary n-3 polyunsaturated fatty acids and amelioration of cardiovascular disease: possible mechanisms. The American journal of clinical nutrition 52:1-28.
210. Trebble, T., N. K. Arden, M. A. Stroud, S. A. Wootton, G. C. Burdge, E. A. Miles, A. B. Ballinger, R. L. Thompson, and P. C. Calder. 2003. Inhibition of tumour necrosis factor-α and interleukin 6 production by mononuclear cells following dietary fish-oil supplementation in healthy men and response to antioxidant co-supplementation. British Journal of Nutrition 90:405-412.
211. Harris, W. S. 2005. Extending the cardiovascular benefits of omega-3 fatty acids. Current atherosclerosis reports 7:375-380.
212. Mori, T. A. 2006. OMEGA-3 FATTY ACIDS AND HYPERTENSION IN HUMANS. Clinical and experimental pharmacology and physiology 33:842-846.
213. Lemaitre, R. N., I. B. King, D. Mozaffarian, L. H. Kuller, R. P. Tracy, and D. S. Siscovick. 2003. n− 3 Polyunsaturated fatty acids, fatal ischemic heart disease, and nonfatal myocardial infarction in older adults: the Cardiovascular Health Study. The American journal of clinical nutrition 77:319-325.
214. Ren, H., K. Ghebremeskel, I. Okpala, C. C. Ugochukwu, M. Crawford, and O. Ibegbulam. 2006. Abnormality of erythrocyte membrane n-3 long chain polyunsaturated fatty acids in sickle cell haemoglobin C (HbSC) disease is not as remarkable as in sickle cell anaemia (HbSS). Prostaglandins, leukotrienes and essential fatty acids 74:1-6.
215. Ren, H., I. Obike, I. Okpala, K. Ghebremeskel, C. Ugochukwu, and M. Crawford. 2005. Steady-state haemoglobin level in sickle cell anaemia increases with an increase in erythrocyte membrane n-3 fatty acids. Prostaglandins, leukotrienes and essential fatty acids 72:415-421.
216. Ren, H., I. Okpala, K. Ghebremeskel, C. C. Ugochukwu, O. Ibegbulam, and M. Crawford. 2005. Blood mononuclear cells and platelets have abnormal fatty acid composition in homozygous sickle cell disease. Annals of Hematology 84:578-583.
217. Daak, A. A., K. Ghebremeskel, Z. Hassan, B. Attallah, H. H. Azan, M. I. Elbashir, and M. Crawford. 2013. Effect of omega-3 (n− 3) fatty acid supplementation in patients with sickle cell anemia: randomized, double-blind, placebo-controlled trial. The American journal of clinical nutrition 97:37-44.
218. Okpala, I., O. Ibegbulam, A. Duru, S. Ocheni, I. Emodi, A. Ikefuna, G. Umar, I. Asinobi, A. Madu, and A. Okoye. 2011. Pilot study of omega-3 fatty acid supplements in sickle cell disease. Apmis 119:442-448.
219. Tomer, A., S. Kasey, W. E. Connor, S. Clark, L. A. Harker, and J. R. Eckman. 2001. Reduction of pain episodes and prothrombotic activity in sickle cell disease by dietary n-3 fatty acids. THROMBOSIS AND HAEMOSTASIS-STUTTGART- 85:966-974.
220. Cao, J., K. A. Schwichtenberg, N. Q. Hanson, and M. Y. Tsai. 2006. Incorporation and clearance of omega-3 fatty acids in erythrocyte membranes and plasma phospholipids. Clinical Chemistry 52:2265-2272.
221. Witte, T. R., A. J. Salazar, O. F. Ballester, and W. E. Hardman. 2010. RBC and WBC fatty acid composition following consumption of an omega 3 supplement: lessons for future clinical trials. Lipids in health and disease 9:31.
222. Hanson, M. S., H. Xu, T. C. Flewelen, S. L. Holzhauer, D. Retherford, D. W. Jones, A. C. Frei, K. A. Pritchard, C. A. Hillery, and N. Hogg. 2013. A novel hemoglobin-binding peptide reduces cell-free hemoglobin in murine hemolytic anemia. Am J Physiol-Heart C 304:H328-H336.
223. Wandersee, N. J., R. C. Punzalan, M. P. Rettig, M. D. Kennedy, N. M. Pajewski, R. L. Sabina, J. Paul Scott, P. S. Low, and C. A. Hillery. 2005. Erythrocyte adhesion is modified by alterations in cellular tonicity and volume. British Journal of Haematology

131:366-377.
224. Hanson, M. S., A. H. Stephenson, E. A. Bowles, M. Sridharan, S. Adderley, and R. S. Sprague. 2008. Phosphodiesterase 3 is present in rabbit and human erythrocytes and its inhibition potentiates iloprost-induced increases in cAMP. Am J Physiol-Heart C 295:H786-H793.
225. Brugnara, C. 1998. Use of reticulocyte cellular indices in the diagnosis and treatment of hematological disorders. International Journal of Clinical and Laboratory Research 28:1-11.
226. Chasis, J. A., and N. Mohandas. 1986. Erythrocyte membrane deformability and stability: two distinct membrane properties that are independently regulated by skeletal protein associations. The Journal of Cell Biology 103:343-350.
227. Rodgers, G. P., C. T. Noguchi, and A. N. Schechter. 1985. Irreversibly sickled erythrocytes in sickle cell anemia: a quantitative reappraisal. American Journal of Hematology 20:17-23.
228. Huang, Z., J. G. Louderback, S. B. King, S. K. Ballas, and D. B. Kim-Shapiro. 2001. In vitro exposure to hydroxyurea reduces sickle red blood cell deformability. American Journal of Hematology 67:151-156.
229. De Franceschi, L., D. Bachir, F. Galacteros, G. Tchernia, T. Cynober, S. Alper, O. Platt, Y. Beuzard, and C. Brugnara. 1997. Oral magnesium supplements reduce erythrocyte dehydration in patients with sickle cell disease. Journal of Clinical Investigation 100:1847.
230. Ballas, S. K., G. J. Dover, and S. Charache. 1989. Effect of hydroxyurea on the rheological properties of sickle erythrocytes in vivo. American Journal of Hematology 32:104-111.
231. Kuypers, F., D. Chiu, N. Mohandas, B. Roelofsen, J. O. den Kamp, and B. Lubin. 1987. The molecular species composition of phosphatidylcholine affects cellular properties in normal and sickle erythrocytes. Blood 70:1111-1118.
232. Gulley, M. L., D. W. Ross, C. Feo, and E. P. Orringer. 1982. The effect of cell hydration on the deformability of normal and sickle erythrocytes. American Journal of Hematology 13:283-291.
233. Vayá, A., S. Collado, M. A. Dasí, M. L. Pérez, J. L. Hernandez, and E. Barragán. 2013. Erythrocyte deformability and aggregation in homozygous sickle cell disease. Clinical Hemorheology and Microcirculation.
234. Manodori, A. B., G. A. Barabino, B. H. Lubin, and F. A. Kuypers. 2000. Adherence of phosphatidylserine-exposing erythrocytes to endothelial matrix thrombospondin. Blood 95:1293-1300.
235. Brittain, J. E., K. J. Mlinar, C. S. Anderson, E. P. Orringer, and L. V. Parise. 2001. Integrin-associated protein is an adhesion receptor on sickle red blood cells for immobilized thrombospondin. Blood 97:2159-2164.
236. Liu, S.-C., L. Derick, and J. Palek. 1993. Dependence of the permanent deformation of red blood cell membranes on spectrin dimer-tetramer equilibrium: implication for permanent membrane deformation of irreversibly sickled cells. Blood 81:522-528.
237. Mohandas, N., J. A. Chasis, and S. B. Shohet. 1983. The influence of membrane skeleton on red cell deformability, membrane material properties, and shape. In Seminars in Hematology. 225-242.
238. Popp-Snijders, C., J. Schouten, A. DeJong, and E. Van der Veen. 1984. Effect of dietary cod-liver oil on the lipid composition of human erythrocyte membranes. Scandinavian journal of clinical & laboratory investigation 44:39-46.
239. Kremmyda, L.-S., E. Tvrzicka, B. Stankova, and A. Zak. 2011. Fatty acids as biocompounds: their role in human metabolism, health and disease-a review. Part 2: Fatty acid physiological roles and applications in human health and disease. Biomedical

Papers 155:195-218.
240. Arai, H., T. Suzuki, K. Takama, and J. Terao. 1996. Reactivity of mammalian 15-lipoxygenase with phospholipids in large unilamellar liposomes. Biochemical and Biophysical Research Communications 228:675-682.
241. Géminard, C., A. de Gassart, and M. Vidal. 2002. Reticulocyte maturation: mitoptosis and exosome release. BIOCELL-MENDOZA- 26:205-216.
242. Iraz, M., H. Erdogan, B. Ozyurt, F. Ozugurlu, S. Ozgocmen, and E. Fadillioglu. 2005. Omega-3 essential fatty acid supplementation and erythrocyte oxidant/antioxidant status in rats. Annals of Clinical & Laboratory Science 35:169-173.
243. Pritchard, K. A., J. Ou, Z. Ou, Y. Shi, J. P. Franciosi, P. Signorino, S. Kaul, C. Ackland-Berglund, K. Witte, and S. Holzhauer. 2004. Hypoxia-induced acute lung injury in murine models of sickle cell disease. American Journal of Physiology-Lung Cellular and Molecular Physiology 286:L705-L714.
244. Belcher, J. D., H. Mahaseth, T. E. Welch, A. E. Vilback, K. M. Sonbol, V. S. Kalambur, P. R. Bowlin, J. C. Bischof, R. P. Hebbel, and G. M. Vercellotti. 2005. Critical role of endothelial cell activation in hypoxia-induced vasoocclusion in transgenic sickle mice. Am J Physiol-Heart C 288:H2715-H2725.
245. Daak, A. A., K. Ghebremeskel, K. Mariniello, B. Attallah, P. Clough, and M. I. Elbashir. 2013. Docosahexaenoic and eicosapentaenoic acid supplementation does not exacerbate oxidative stress or intravascular haemolysis in homozygous sickle cell patients. Prostaglandins, Leukotrienes and Essential Fatty Acids (PLEFA) 89:305-311.
246. Mitchell, B. L. 2007. Sickle cell trait and sudden death - Bringing it home. Journal of the National Medical Association 99:300-305.
247. Miller, F. A., M. Paynter, R. Z. Hayeems, J. Little, J. C. Carroll, B. J. Wilson, J. Allanson, J. P. Bytautas, and P. Chakraborty. 2010. Understanding sickle cell carrier status identified through newborn screening: a qualitative study. European Journal of Human Genetics 18:303-308.
248. Telen, M. J. 2007. Role of adhesion molecules and vascular endothelium in the pathogenesis of sickle cell disease. Hematology Am Soc Hematol Educ Program:84-90.
249. Zennadi, R., P. C. Hines, L. M. De Castro, J. P. Cartron, L. V. Parise, and M. J. Telen. 2004. Epinephrine acts through erythroid signaling pathways to activate sickle cell adhesion to endothelium via LW-alpha v beta 3 interactions. Blood 104:3774-3781.
250. Kjaer, M. 1998. Adrenal medulla and exercise training. European Journal of Applied Physiology and Occupational Physiology 77:195-199.
251. Kaul, D. K. 2004. "Stress" and sickle red cell adhesion. Blood 104:3425-3426.
252. Auletta, T., M. R. de Jong, A. Mulder, F. van Veggel, J. Huskens, D. N. Reinhoudt, S. Zou, S. Zapotoczny, H. Schonherr, G. J. Vancso, and L. Kuipers. 2004. beta-cyclodextrin host-guest complexes probed under thermodynamic equilibrium: Thermodynamics and AFM force spectroscopy. J. Am. Chem. Soc. 126:1577-1584.
253. Parsons, S. F., G. Lee, F. A. Spring, T. N. Willig, L. L. Peters, J. A. Gimm, M. J. A. Tanner, N. Mohandas, D. J. Anstee, and J. A. Chasis. 2001. Lutheran blood group glycoprotein and its newly characterized mouse homologue specifically bind alpha 5 chain-containing human laminin with high affinity. Blood 97:312-320.
254. An, X. L., E. Gauthier, X. H. Zhang, X. H. Guo, D. J. Anstee, N. Mohandas, and J. A. Chasis. 2008. Adhesive activity of Lu glycoproteins is regulated by interaction with spectrin. Blood 112:5212-5218.
255. Zennadi, R., B. J. Moeller, E. J. Whalen, M. Batchvarova, K. Xu, S. Q. Shan, M. Delahunty, M. W. Dewhirst, and M. J. Telen. 2007. Epinephrine-induced activation of LW-mediated sickle cell adhesion and vaso-occlusion in vivo. Blood 110:2708-2717.
256. Porzig, H., R. Gutknecht, G. Kostova, and K. Thalmeier. 1995. G-protein-coupled receptors in normal human erythroid progenitor cells. Naunyn-Schmiedebergs Archives

of Pharmacology 353:11-20.
257. Baumann, R., C. Blass, R. Gotz, and S. Dragon. 1999. Ontogeny of catecholamine and adenosine receptor-mediated cAMP signaling of embryonic red blood cells: Role of cGMP-inhibited phosphodiesterase 3 and hemoglobin. Blood 94:4314-4320.
258. Ebert, E. C., M. Nagar, and K. D. Hagspiel. 2010. Gastrointestinal and Hepatic Complications of Sickle Cell Disease. Clinical Gastroenterology and Hepatology 8:483-489.
259. Vacher, H., D. P. Mohapatra, and J. S. Trimmer. 2008. Localization and Targeting of Voltage-Dependent Ion Channels in Mammalian Central Neurons. Physiological Reviews 88:1407-1447.
260. Nusser, Z. 2009. Variability in the subcellular distribution of ion channels increases neuronal diversity. Trends in Neurosciences 32:267-274.
261. Toomre, D., and J. Bewersdorf. 2010. A New Wave of Cellular Imaging. Annual Review of Cell and Developmental Biology 26:285-314.
262. Nusser, Z. 2011. Differential subcellular distribution of ion channels and the diversity of neuronal function. Current Opinion in Neurobiology 22:1-6.
263. Muller, D. J., J. Helenius, D. Alsteens, and Y. F. Dufrene. 2009. Force probing surfaces of living cells to molecular resolution. Nat Chem Biol 5:383-390.
264. Ngo-Anh, T. J., B. L. Bloodgood, M. Lin, B. L. Sabatini, J. Maylie, and J. P. Adelman. 2005. SK channels and NMDA receptors form a Ca2+-mediated feedback loop in dendritic spines. Nat Neurosci 8:642-649.
265. Faber, E. S. L., A. J. Delaney, and P. Sah. 2005. SK channels regulate excitatory synaptic transmission and plasticity in the lateral amygdala. Nat Neurosci 8:635-641.
266. Bloodgood, B. L., and B. L. Sabatini. 2007. Nonlinear Regulation of Unitary Synaptic Signals by CaV2.3 Voltage-Sensitive Calcium Channels Located in Dendritic Spines. Neuron 53:249-260.
267. Adelman, J. P., J. Maylie, and P. Sah. 2012. Small-Conductance Ca2+-Activated K+ Channels: Form and Function. Annual Review of Physiology 74:245-269.
268. Ballesteros-Merino, C., M. Lin, W. W. Wu, C. Ferrandiz-Huertas, M. J. Cabañero, M. Watanabe, Y. Fukazawa, R. Shigemoto, J. Maylie, J. P. Adelman, and R. Luján. 2012. Developmental profile of SK2 channel expression and function in CA1 neurons. Hippocampus 6:1467-1480.
269. Lin, M. T., R. Lujan, M. Watanabe, J. P. Adelman, and J. Maylie. 2008. SK2 channel plasticity contributes to LTP at Schaffer collateral-CA1 synapses. Nat Neurosci 11:170-177.
270. Sailer, C. A., H. Hu, W. A. Kaufmann, M. Trieb, C. Schwarzer, J. F. Storm, and H.-G. Knaus. 2002. Regional Differences in Distribution and Functional Expression of Small-Conductance Ca2+-Activated K+ Channels in Rat Brain. The Journal of Neuroscience 22:9698-9707.
271. Sailer, C. A., W. A. Kaufmann, J. Marksteiner, and H.-G. Knaus. 2004. Comparative immunohistochemical distribution of three small-conductance Ca2+-activated potassium channel subunits, SK1, SK2, and SK3 in mouse brain. Molecular and Cellular Neuroscience 26:458-469.
272. Bowden, S. E. H., S. Fletcher, D. J. Loane, and N. V. Marrion. 2001. Somatic Colocalization of Rat SK1 and D class (Cav 1.2) L-type Calcium Channels in Rat CA1 Hippocampal Pyramidal Neurons. The Journal of Neuroscience 21:RC175.
273. Strassmaier, T., C. T. Bond, C. A. Sailer, H.-G. Knaus, J. Maylie, and J. P. Adelman. 2005. A Novel Isoform of SK2 Assembles with Other SK Subunits in Mouse Brain. Journal of Biological Chemistry 280:21231-21236.
274. Weatherall, K. L., S. J. Goodchild, D. E. Jane, and N. V. Marrion. 2010. Small conductance calcium-activated potassium channels: From structure to function.

Progress in Neurobiology 91:242-255.
275. Lim, C. S., and R. S. Walikonis. 2008. Hepatocyte growth factor and c-Met promote dendritic maturation during hippocampal neuron differentiation via the Akt pathway. Cellular Signalling 20:825-835.
276. Sokolova, O., L. Kolmakova-Partensky, and N. Grigorieff. 2001. Three-Dimensional Structure of a Voltage-Gated Potassium Channel at 2.5 nm Resolution. Structure 9:215-220.
277. Faber, E. S. L., A. J. Delaney, J. M. Power, P. L. Sedlak, J. W. Crane, and P. Sah. 2008. Modulation of SK Channel Trafficking by Beta Adrenoceptors Enhances Excitatory Synaptic Transmission and Plasticity in the Amygdala. The Journal of Neuroscience 28:10803-10813.
278. Ren, Y., L. F. Barnwell, J. C. Alexander, F. D. Lubin, J. P. Adelman, P. J. Pfaffinger, L. A. Schrader, and A. E. Anderson. 2006. Regulation of Surface Localization of the Small Conductance Ca2+-activated Potassium Channel, Sk2, through Direct Phosphorylation by cAMP-dependent Protein Kinase. Journal of Biological Chemistry 281:11769-11779.
279. Cai, X., C. W. Liang, S. Muralidharan, J. P. Y. Kao, C.-M. Tang, and S. M. Thompson. 2004. Unique Roles of SK and Kv4.2 Potassium Channels in Dendritic Integration. Neuron 44:351-364.
280. Fakler, B., and J. P. Adelman. 2008. Control of KCa Channels by Calcium Nano/Microdomains. Neuron 59:873-881.
281. Katz, B., and R. Miledi. 1973. The binding of acetylcholine to receptors and its removal from the synaptic cleft. The Journal of Physiology 231:549-574.
282. Terlau, H., and B. M. Olivera. 2004. Conus Venoms: A Rich Source of Novel Ion Channel-Targeted Peptides. Physiological Reviews 84:41-68.
283. Space, S. L., P. A. Lane, C. K. Pickett, and J. V. Weil. 2000. Nitric oxide attenuates normal and sickle red blood cell adherence to pulmonary endothelium. American Journal of Hematology 63:200-204.
284. Lee, S. P., M. L. Cunningham, P. C. Hines, C. C. Joneckis, E. P. Orringer, and L. V. Parise. 1998. Sickle Cell Adhesion to Laminin: Potential Role for the □5 Chain. Blood 92:2951-2958.
285. Müller, D. J., and Y. F. Dufrêne. 2011. Atomic force microscopy: a nanoscopic window on the cell surface. Trends in Cell Biology 21:461-469.
286. Maciaszek, J. L., H. Soh, R. S. Walikonis, A. V. Tzingounis, and G. Lykotrafitis. 2012. Topography of Native SK Channels Revealed by Force Nanoscopy in Living Neurons. The Journal of Neuroscience 32:11435-11440.
287. Dell'Acqua, M. L., and J. D. Scott. 1997. Protein Kinase A Anchoring. Journal of Biological Chemistry 272:12881-12884.
288. Odievre, M. H., V. Bony, M. Benkerro, C. Lapoumeroulie, C. Alberti, R. Ducrocq, E. Jacqz-Aigrain, J. Elion, and J. P. Cartron. 2008. Modulation of erythroid adhesion receptor expression by hydroxyurea in children with sickle cell disease. Haematologica-the Hematology Journal 93:502-510.
289. Walters, D. A., J. P. Cleveland, N. H. Thomson, P. K. Hansma, M. A. Wendman, G. Gurley, and V. Elings. 1996. Short cantilevers for atomic force microscopy. Review of Scientific Instruments 67:3583-3590.
290. Tzingounis, A. V., M. von Zastrow, and G. A. Yudowski. 2010. β-Blocker drugs mediate calcium signaling in native central nervous system neurons by β-arrestin–biased agonism. Proceedings of the National Academy of Sciences 107:21028-21033.
291. Fukayama, S., A. H. Tashjian, and F. R. Bringhurst. 1992. Forskolin-induced homologous desensitization via an adenosine 3',5'-monophosphate-dependent mechanism(s) in human osteoblast-like SaOS-2 cells. Endocrinology 131:1770-1776.
292. Ostrom, R., A. Bogard, R. Gros, and R. Feldman. 2012. Choreographing the adenylyl

cyclase signalosome: sorting out the partners and the steps. Naunyn-Schmiedeberg's Arch Pharmacol 385:5-12.
293. Adderley, S. P., R. S. Sprague, A. H. Stephenson, and M. S. Hanson. 2010. Regulation of cAMP by Phosphodiesterases in Erythrocytes. Pharmacological Reports 62:475-482.
294. Zaccolo, M., G. Di Benedetto, V. Lissandron, L. Mancuso, A. Terrin, and I. Zamparo. 2006. Restricted diffusion of a freely diffusible second messenger: mechanisms underlying compartmentalized cAMP signalling. Biochemical Society Transactions:495-497.
295. Lim, T. S., S. R. K. Vedula, W. Hunziker, and C. T. Lim. 2008. Kinetics of Adhesion Mediated by Extracellular Loops of Claudin-2 as Revealed by Single-Molecule Force Spectroscopy. Journal of Molecular Biology 381:681-691.
296. Grandbois, M., W. Dettmann, M. Benoit, and H. E. Gaub. 2000. Affinity imaging of red blood cells using an atomic force microscope. Journal of Histochemistry & Cytochemistry 48:719-724.
297. Maciaszek, J. L., H. Soh, R. S. Walikonis, A. V. Tzingounis, and G. Lykotrafitis. 2012. Topography of Native SK Channels Revealed by Force Nanoscopy in Living Neurons. The Journal of Neuroscience In Press.
298. Walton, E. B., S. Lee, and K. J. Van Vliet. 2008. Extending Bell's model: how force transducer stiffness alters measured unbinding forces and kinetics of molecular complexes. Biophysical Journal 94:2621-2630.
299. Puntheeranurak, T., L. Wildling, H. J. Gruber, R. K. Kinne, and P. Hinterdorfer. 2006. Ligands on the string: single-molecule AFM studies on the interaction of antibodies and substrates with the Na+-glucose co-transporter SGLT1 in living cells. Journal of Cell Science 119:2960-2967.
300. Maciaszek, J., B. Andemariam, and G. Lykotrafitis. 2013. AKAP-dependent modulation of BCAM/Lu adhesion on normal and sickle cell disease RBCs revealed by force nanoscopy. Biophysical Journal Under Review.
301. Sheetz, M. P. 1993. Glycoprotein motility and dynamic domains in fluid plasma membranes. Annu Rev Bioph Biom 22:417-431.
302. Eyler, C. E., and M. J. Telen. 2006. The Lutheran glycoprotein: a multifunctional adhesion receptor. Transfusion 46:668-677.
303. Beck, K., I. Hunter, and J. Engel. 1990. Structure and function of laminin: anatomy of a multidomain glycoprotein. The FASEB journal 4:148-160.
304. Milner, S. 1991. Polymer brushes. Science 251:905-914.
305. Zhao, B., and W. J. Brittain. 2000. Polymer brushes: surface-immobilized macromolecules. Progress in Polymer Science 25:677-710.
306. Brittain, W. J., and S. Minko. 2007. A structural definition of polymer brushes. Journal of Polymer Science Part A: Polymer Chemistry 45:3505-3512.
307. Makohliso, S. A., and S. Melchionna. 2001. Molecular characterization of a laminin-derived oligopeptide with implications in biomimetic applications. Biophysical Chemistry 89:129-144.
308. Giamblanco, N., E. Martines, and G. Marletta. 2013. Laminin Adsorption on Nanostructures: Switching the Molecular Orientation by Local Curvature Changes. Langmuir.
309. Bershadsky, A., M. Kozlov, and B. Geiger. 2006. Adhesion-mediated mechanosensitivity: a time to experiment, and a time to theorize. Current Opinion in Cell Biology 18:472-481.
310. Evans, E. A., and D. A. Calderwood. 2007. Forces and bond dynamics in cell adhesion. Science 316:1148-1153.
311. Sampson, L. J., Y. Hayabuchi, N. B. Standen, and C. Dart. 2004. Caveolae Localize Protein Kinase A Signaling to Arterial ATP-Sensitive Potassium Channels. Circulation

Research 95:1012-1018.
312. Chilcoat, C. D., Y. Sharief, and S. L. Jones. 2008. Tonic protein kinase A activity maintains inactive β2 integrins in unstimulated neutrophils by reducing myosin light-chain phosphorylation: role of myosin light-chain kinase and Rho kinase. Journal of Leukocyte Biology 83:964-971.

Chapter 12. List of Conference or Journal Publications

12.1. Journal Publications

Maciaszek, JL., Andemariam, B., Lykotrafitis, G., Single-cell force spectroscopy as a technique to quantify human red blood cell adhesion to subendothelial laminin. Under Review.

Wandersee, NJ., Maciaszek, JL., Giger, KM., Hanson, MS., Zheng, S., Guo, Y.,Mickelson, B., Hillery, CA., Lykotrafitis, G., Low, PS., Hogg, N., Dietary supplementation with docosohexanoic acid (DHA) increases red blood cell membrane flexibility in mice with sickle cell disease. Under Review.

Maciaszek, JL., Andemariam, B., Lykotrafitis, G., AKAP-dependent modulation of BCAM/Lu adhesion on normal and sickle cell disease RBCs revealed by force nanoscopy. Under Review.

Maciaszek, JL., Soh, H., Walikonis, RS., Tzingounis, AV., Lykotrafitis, G., “Topography of native SK channels revealed by force nanoscopy in living neurons”, *The Journal of Neuroscience*. 32, 11435-11440 (2012).

Maciaszek, JL., Andemariam, B., Huber, G., Lykotrafitis, G., Epinephrine Modulates BCAM/Lu and ICAM-4 Expression on the Sickle Cell Trait Red Blood Cell Membrane. *Biophysical Journal,* 102, 1137-1143 (2012).

Maciaszek, JL., Andemariam, B., Lykotrafitis, G., Microelasticity of red blood cells in sickle cell disease. *Journal of Strain Analysis for Engineering Design,* 46, 368-379 (2011).

Budyansky, M., Madormo, C., Maciaszek, JL., Lykotrafitis, G., Coherent gradient sensing microscopy (micro-CGS): A microscale curvature detection technique. *Optics and Lasers in Engineering*, 49, 874-879 (2011).

Maciaszek, JL., Lykotrafitis, G., Sickle cell trait human erythrocytes are significantly stiffer than normal, *Journal of Biomechanics*, 44, 657-661 (2011).

12.2. Personal Presentations At Conferences (* denotes oral presentation)

Maciaszek, JL., Andemariam, B., Lykotrafitis, G., "A-kinase anchoring proteins mediate healthy and sickle red blood cell adhesion to endothelial laminin-5", *55th American Society for Hematology Annual Meeting and Exposition*, New Orleans, LA, Dec 2013.

Maciaszek, JL., Andemariam, B., Lykotrafitis, G., "AKAPs mediate sickle cell disease erythrocyte adhesion via BCAM/Lu", *Biomedical Engineering Society 2013 Annual Meeting*, Seattle, WA, Sept 2013. *

Maciaszek, JL., Andemariam, B., Lykotrafitis, G., "Role of A-kinase anchoring proteins in activation of sickle cell disease red blood cell adhesion receptor BCAM/Lu", 50th Annual Technical Meeting of Society of Engineering Science, Providence, RI, July 2013. **

Maciaszek, JL., Lykotrafitis, G., "Epinephrine modulates sickle cell disease erythrocyte adhesion via ICAM-4 receptor overexpression", *Biomedical Engineering Society 2012 Annual Meeting*, Atlanta, GA, Oct 2012.

Maciaszek, JL., Soh, H., Kim, KS., Walikonis, RS., Tzingounis, AV., Lykotrafitis, G., "Spatial organization of calcium-activated SK channels revealed by atomic force microscopy in living neurons", *Society for Neuroscience 2011 Annual Meeting*, Washington, DC, Nov 2011.

Maciaszek, JL., Tzingounis, AV., Lykotrafitis, G., "Mapping Calcium-activated potassium channels (SK) in living neurons using single molecule force spectroscopy", *Biomedical Engineering Society 2011 Annual Meeting,* Hartford, CT, Oct 2011. *

Maciaszek, JL., Andemariam, B., Thrall, RS., Lykotrafitis, G., "Chemomechanics of the BCAM/Lu-laminin complex in Sickle Cell Disease: A Murine Model", *Biomedical Engineering Society 2011 Annual Meeting,* Hartford, CT, Oct 2011.

Maciaszek, JL., Andemariam, B., Lykotrafitis, G., "Adhesion and stiffness increases associated with sickle cell trait erythrocytes", *Society of Experimental Mechanics Annual*

Conference & Exposition on Experimental and Applied Mechanics, Student Paper Competition, Paper No. 542, Uncasville, CT, June 2011. *****

Maciaszek, J., Andemariam, B., Lykotrafitis, G., "Cytoadherence of Sickle Cell Trait Erythrocytes", *ASME 2010 International Mechanical Engineering Congress & Exposition,* NSF-Sponsored Student Poster Symposium, Vancouver, BC Canada, Nov 2010.

12.3. Conference Proceedings

Maciaszek, JL., Andemariam, B., Lykotrafitis, G., "A-kinase anchoring proteins mediate healthy and sickle red blood cell adhesion to endothelial laminin-5", *Blood*, 122, 968, (2013).

Wandersee, NJ., Hanson, MS., Maciaszek, JL., Larson, MC., Giger, KM., Zheng, S., Retherford, DM., Mickelson, B., Stucky, CL., Low, PS., Lykotrafitis, G., Hogg, N., Hillery, CA., "Dietary Supplementation with Docosahexanoic Acid (DHA) Improves RBC Flexibility and Reduces Cold Hypersensitivity in Mice with Sickle Cell Disease", *Blood*, 120, 2116 (2012).

Hanson, M., Maciaszek, JL., Larson, MC., Giger, KM., Zheng, S., Retherford, DM., Mickelson, B., Stucky, C., Low, PS., Lykotrafitis, G., Hogg, N., Hillery, CA., Wandersee, NJ., "Dietary Supplementation with Docosahexanoic Acid (DHA) Improves RBC Membrane Flexibility and Reduces Cold Hypersensitivity in Mice with Sickle Cell Disease", *Free Radical Biology and Medicine,* 53, S162 (2012).

Maciaszek, JL., Andemariam, B., Lykotrafitis, G., "Modulation of BCAM/Lu and ICAM-4 Expression on Red Blood Cell Membranes in Physiological Stress Conditions", *ASME 2011 International Mechanical Engineering Congress & Exposition,* Paper No. 62143, Denver, CO, November 2011.

Maciaszek, JL., Andemariam, B., Lykotrafitis, G., "Epinephrine Upregulates Sickle Cell Trait Erythrocyte Adhesion to Laminin and Integrins", *Mechanics of Biological Systems and*

Materials, 2, 159-162 (2011).

Maciaszek, J., Lykotrafitis, G., “Characterization of Erythrocytes in Sickle Cell Trait”, *Materials Research Society 2010 Fall Meeting*, Paper No. 912984, Boston, MA, November 2010.

Maciaszek, JL., Lykotrafitis, G. “Sickle Cell Trait Erythrocytes are Thrice as Stiff as Healthy Erythrocytes”, *ASME 2010 International Mechanical Engineering Congress & Exposition,* Paper No. 37779, Vancouver, BC Canada, November 2010.

Maciaszek, JL., Lykotrafitis, G. “Characterization of Erythrocytes from Healthy Individuals and from Patients with the Sickle Cell Trait”, *Proceedings of the 16th US National Congress of Theoretical and Applied Mechanics*, Paper No. 1161, College Park, PA, June 2010.

12.4. Conference Abstracts (* denotes oral presentation)

Maciaszek, JL., Andemariam, B., Lykotrafitis, G., “Regulation of the expression of adhesion receptor BCAM/LU in erythrocytes”, *ASME 2013 International Mechanical Engineering Congress & Exposition*, San Diego, CA, November 2013.

Maciaszek, JL., Andemariam, B., Lykotrafitis, G., “AKAPs mediate sickle cell disease erythrocyte adhesion via BCAM/Lu”, *Biomedical Engineering Society 2013 Annual Meeting*, Seattle, WA, September 2013.

Maciaszek, JL., Andemariam, B., Lykotrafitis, G., “Red Blood Cell Surface Receptor Expression Of BCAM/Lu Is Regulated By Protein Kinase A Activity”, *ASME 2013 Summer Bioengineering Conference*, Sunriver, OR, June 2013.

Wandersee, NJ., Hanson, MS., Maciaszek, JL., Larson, MC., Giger, KM., Zheng, S., Retherford, DM., Stucky, CL., Low, PS., Lykotrafitis, G., Hogg, N., Hillery, CA., “Dietary supplementation with docosahexanoic acid (DHA) improves RBC flexibility and reduces cold hypersensitivity in mice with sickle cell disease”, *2012 American Society of Hematology Annual Meeting and Exposition*, Atlanta, GA, Dec 2012.

Maciaszek, JL., Andemariam, B., Lykotrafitis, G., “Epinephrine Modulates BCAM/Lu and ICAM-4 Expression on Sickle Cell Trait Red Blood Cells”, *6th Annual Sickle Cell Disease Research & Educational Symposium & Annual Scientific Meeting*, Abstract 111, Hollywood, FL, Feb 2012. *

Maciaszek, JL., Lykotrafitis, G., “BCAM/Lu and ICAM-4 Expression on Sickle Cell Disease Red Blood Cell Membranes”, *48th Annual Technical Meeting of Society of Engineering Science*, Chicago, IL, Oct 2011. *

Kwang, K., Maciaszek, JL, Tzingounis, AV., Lykotrafitis, G. “Mapping Small-Conductance Calcium-Activated Potassium Channels (SK) in Neurons”, *Society of Experimental Mechanics Annual Conference & Exposition on Experimental and Applied Mechanics*, Uncasville, CT, June 2011. **

Maciaszek, JL., Andemariam, B., Lykotrafitis, G., “Modulation of BCAM/Lu and ICAM-4 Expression on Red Blood Cell Membranes in Physiological Stress Conditions”, *Connecticut Sickle Cell Translational Science Symposium*. Farmington, CT, June 2011. *

Maciaszek, J., Lykotrafitis, G., “Chemomechanical mapping of Lutheran/B-CAM interaction in erythrocytes of hemoglobin genotype AS”, *Biomedical Engineering Society 2010 Annual Meeting*, Austin, TX, Oct 2010.

Maciaszek, J., Lykotrafitis, G., “Mechanical and chemomechanical properties of HbAA and HbAS erythrocytes via AFM”, *47th Annual Technical Meeting of Society of Engineering Science*, Paper No. 10021662, Ames, IA, Oct 2010.